Ultra low-voltage low power backscatter communication and energy harvesting for long-range battery-free sensor tags

Alexander T. Hoang

A dissertation
submitted in partial fulfillment of the
requirements for the degree of

Doctor of Philosophy

University of Washington

2019

Reading Committee:

Matthew S. Reynolds, Chair

Joshua Smith

Brian Johnson

Program Authorized to Offer Degree:
Department of Electrical and Computer Engineering

University of Washington

Abstract

Ultra low-voltage low power backscatter communication and
energy harvesting for long-range battery-free sensor tags

Alexander T. Hoang

Chair of the Supervisory Committee:
Associate Professor Matthew S. Reynolds
Department of Electrical and Computer Engineering & Paul G. Allen School of Computer Science and Engineering

To achieve economic viability across wide area deployments, many smart cities and agricultural sensing applications require wireless sensing and communication devices with long operating ranges of hundreds of meters to kilometers. Ideally, such sensors would be battery-free to enable unlimited lifetime. Prior work in RF-powered sensor networks has generally focused on achieving either long-range communication, or battery-free operation, but generally not both at the same time. The key system level challenges are the need for efficient RF power capture from incident RF signals, efficient RF power harvesting, and a low-power sensing and communication approach such as backscatter communication that enables data collection at the minimum possible power consumption.

This thesis presents four systems that explore the key challenges in this space: (1) a 2.4 GHz RF energy harvesting system leveraging an ultra-low power timer to minimize the RF power required for a cold-start; (2) an efficient reduced-size metal-mount sensor tag antenna; (3) a secure microcontroller-based sensor tag with a fiber-optic anti-tamper loop; and finally (4) a 5.8 GHz battery-free sensor tag that is operational at 1km range, having an RF power level of only -23 dBm (5 μW) and a measured cold-start power-up voltage of only 15 mV. These systems each demonstrate innovative design elements that can be combined in different combinations to address challenging long-range, battery-free sensing and communication applications.

TABLE OF CONTENTS

Page

List of Tables iv

List of Figures v

Acknowledgments viii

Chapter 1: Introduction 1
1.1 Motivation 3
1.2 Original Contributions 8
1.3 Dissertation Organization 9
1.4 Publications 9

Chapter 2: Identification and Backscatter Communication 11
2.1 Tracking and Identification 11
2.2 Backscatter Communication 12

Chapter 3: A Timer Based 2.4 GHz Energy Harvester 16
3.1 Introduction 16
3.2 Related Work 18
3.3 Diode Based Harvester Characterization 18
3.4 Timer Circuit Characterization 19
3.5 System Evaluation 22
3.6 Chapter Conclusion 24

Chapter 4: Electrically small metal-mountable RFID antenna 25
4.1 Introduction 25
4.2 Related Work 25
4.2.1 Split Ring discussion 27

4.3 Electricall-small tag antenna design . . . 28
4.3.1 0.8mm Rogers RO4003 split ring . . . 28
4.3.2 1.6 mm Rogers RO4003 split ring . . . 29
4.3.3 4.7 mm Teflon split ring . . . 30
4.4 Link Budget . . . 31
4.4.1 Forward Link Budget . . . 31
4.4.2 Estimated tag RCS . . . 32
4.4.3 Return link budget . . . 33
4.5 Experiment . . . 34
4.6 Chapter Conclusion . . . 35

Chapter 5: A Battery Free Sensor Tag with Fiber Optic Tamper Detection . . . 37
5.1 Introduction . . . 37
5.2 Related Work . . . 38
5.3 Antenna and Mechanical design . . . 40
5.4 Custom Analog Front End ASIC . . . 41
5.5 Antenna Design and measurements . . . 43
5.6 Digital Security Section . . . 46
5.7 Range Measurements . . . 47
5.8 Chapter Conclusion . . . 48

Chapter 6: Kilometer-range Battery-Free backscatter sensor tag . . . 50
6.1 Introduction . . . 50
6.2 12 element antenna array Design . . . 53
6.2.1 Antenna measurement results . . . 57
6.3 Link Budget . . . 57
6.4 Backscatter Tag design and Characterization . . . 60
6.4.1 5.8 GHz Harvester design . . . 60
6.4.2 Low-power, low voltage oscillator . . . 69
6.4.3 Varactor diode modulator design . . . 72
6.4.4 Cabled measurements results . . . 73
6.4.5 Capacitive backscatter telemetry . . . 76
6.5 Over-the-air experimental measurements . . . 79

6.6 Chapter Conclusion 81

Chapter 7: Conclusion 82
7.1 Original Contributions 83
7.2 Future Work 84
7.2.1 Single-chip approach 84
7.2.2 Monostatic Configuration 84
7.2.3 Bistatic dislocated Configuration 84

Bibliography 86

LIST OF TABLES

Table Number Page

1.1 Power consumption change from 2009 to 2011 of different functions, [1] 4
1.2 Summary of Fig. 1.2 6
4.1 Comparison of Electrically Small Metal-Mountable RFID tags 26
4.2 Forward link budget Parameters 32
4.3 Radar cross section parameters 33
6.1 Comparison of several backscatter tags 52

LIST OF FIGURES

Figure Number Page

1.1 Passive backscatter tag employing energy harvesting and modulation through a communication link (includes antenna and communication medium) 2

1.2 Wireless communication standard power consumption comparison, references in Table 1.2 5

2.1 Backscatter signal flow chart 13

2.2 Backscatter impedance circuit 14

3.1 (a) Dual Polarized Patch Antenna (b) RF harvester and timer controlled boost converter 17

3.2 Block Diagram of Timer based harvester 18

3.3 (a) Open stub matching network diagram (b) Measured and Simulated S11 measurements 19

3.4 Boost Converter Circuit 20

3.5 Operating circuit measured by an Agilent MSO-X-3104A oscilloscope. – JFET source, – JFET drain, – $V_{C_{boost}}$. 21

3.6 Timer based boost converter voltage vs. input power 23

4.1 Tag Stackup side view. (a) 0.8 mm Rogers 4003. (b) 1.6 mm Rogers 4003. (c) 0.8 mm Rogers 4003 + 4.67 mm Teflon + 0.8 mm Rogers 4003. 26

4.2 Antenna top view (a) 0.8 mm Rogers 4003. (b) 1.6 mm Rogers 4003. (c) 0.8 mm Rogers 4003 + 4.67 mm Teflon + 0.8 mm Rogers 4003. 28

4.3 (a) Simulated return loss of the 0.8 mm Rogers 4003 RFID tag (b) Simulated radiation pattern of the 0.8 mm Rogers 4003 RFID tag 29

4.4 (a) Simulated return loss of the 1.6 mm Rogers 4003 RFID tag (b) Simulated radiation pattern of the 1.6 mm Rogers 4003 RFID tag 30

4.5 (a) Simulated return loss of the 4.7 mm Teflon sandwiched between two 0.08 mm Rogers R04003 substrate RFID tag (b) Simulated radiation pattern of the 4.7 mm Teflon sandwiched between two 0.08 mm Rogers R04003 substrate RFID tag . . . 31

4.6 Measured Read Rate vs. Range. (a) 0.8 mm Rogers RO3003. (b) 1.6 mm Rogers RO4003. (c) 4.7 mm Teflon sandwiched between two 0.8 mm Rogers RO4003. . . 35

5.1 Block diagram of UHF RFID tag . . . 38
5.2 Hazardous material tracking tag and its application . . . 39
5.3 Tag antenna and mechanical design . . . 40
5.4 ASIC die photo (1.5 mm x 1.5 mm). . . . 41
5.5 (a) Measured AFE ASIC Harvester efficiency vs. input power (b) Measured AFE ASIC V_{unreg} and V_{reg} vs. RF input power . . . 42
5.6 Measured Return loss of Matched AFE ASIC. . . . 43
5.7 Simulated Co-Polarized 3D Radiation pattern fed from Port 1. . . . 44
5.8 Simulated Co-Pol and Cross-Pol 1D radiation pattern. . . . 45
5.9 Measured and Simulated S-Parameters of UHF antenna. . . . 45
5.10 Reader GUI showing Authentication . . . 47
5.11 Measured reads per second with and without a battery present . . . 48

6.1 Block diagram of 5.8 GHz backscatter tag . . . 50
6.2 5.8 GHz quad patch antenna design . . . 53
6.3 Three-way planar type 2 Wilkonson power splitter . . . 53
6.4 Fabricated Antenna Stackup . . . 54
6.5 Simulated Antenna S-parameter (S11) . . . 55
6.6 Gain of 5.8 GHz quad patch array . . . 55
6.7 Wilkonson three way splitter simulated S-parameters . . . 56
6.8 (a) Anechoic chamber setup (b) Measured S21 of pair of quad patch arrays in anechoic chamber . . . 58
6.9 (a) Link Budget accounting for similar sized antennas and its maximum gains and propagation loss vs. Frequency (MHz) (b) Theoretical received power at tag end vs. Range (meters) . . . 59
6.10 1 km path loss antenna setup with handheld signal generator . . . 60
6.11 (a) Rectifier with matching network (b) Fabricated tag design including rectifier, oscillator, and modulator . . . 61
6.12 Circuit model of rectifier output including nonlinear source and load resistances . . . 62
6.13 (a) S11 measurements for the simulated and measured rectifier matching network at an input power of -20 dBm (b) Measured harvested voltage with open circuit and complete tag . . . 64
6.14 (a) Measured rectifier RF-DC efficiency vs. RF input power (dBm) (b) Simulated line losses (conduction and dielectric loss) with respect to frequency . . . 65
6.15 Diode equivalent SPICE model . . . 66

6.16 (a) Instantaneous current through R_s vs. time (b) Instantaneous power of R_s vs. time 67
6.17 Power consumption of each rectifier component as a percent of the total available power 68
6.18 (a) Low voltage, low power Colpitts oscillator schematic diagram (b) Small signal model of Colpitts Oscillator 69
6.19 (a) Varactor diode schematic diagram (b) Varactor capacitance (pF) vs reverse voltage (V) 72
6.20 Cabled backscatter test setup schematic 73
6.21 (a) Measured cabled experiment measuring backscatter power with varying carrier source power (b) Theoretical modulation loss as a function of input bias voltage as calculated from measured varactor diode impedances (Fig. 6.22) 74
6.22 Measured impedances at 5.8 GHz with -23 dBm input power and varying bias voltages 75
6.23 Cabled measured setup of capacitive weight sensor with tag 76
6.24 Measured capacitance vs. applied force of SingleTact S8-1N force sensor 77
6.25 Equivalent oscillator model with weight sensor capacitor 77
6.26 (a) Measured backscatter signal with respect to frequency offset of several weights (b) Theoretical and measured backscatter frequency offset vs. applied force (N) . . 78
6.27 (a) 517 meter outdoor experiment showing transmitter/receiver setup (b) Measured backscatter power at 517 meters 79
6.28 Aerial view of 517 meter outdoor experiment 80

ACKNOWLEDGMENTS

I am very fortunate and blessed to have gotten to this point in my life. I want to thank my advisor Matt Reynolds for taking me in when I was an undegrad at UW. All I wanted to do was help clean up his lab and equipment. I didn't expect that he would put me on my first research project, which would later turn out to be my first publication. I was shocked to hear Matt tell me one day that I should consider completing a PhD, as I never thought that I could achieve something like that. So thanks for being patient with me and helping me throughout these 5 years, it has meant so much to me for you to be there to help me grow and I couldn't have asked for a better advisor.

I also want to thank everyone that I've worked with in lab at the University of Washington – Daniel Arnitz, Kris Spaeth, Joshua Ensworth, Andreas Pedross-Engel, Apoorva Sharma, Eleftherios Kampianakis, Xiaojie Fu, Claire Watts, James Rosenthal, Sandamali Devadithya, Anissa Dad Thang Phu, Vandana Dhawan, and Wen-Yung Liao. You have all helped me in one way or another to get me to this point. I'm going to miss the gossips and laughs we had in lab when we were supposed to be working. I hope that wherever I end up after this, I'm able to work with people as good hearted and appreciative of me as all you were.

Thank you to all my funding sources that helped support my work throughout my years at the UW – Ricoh Innovations and Lawrence Livermore. Some notable collaboraters I would like to thank are Ken Gudan, Sergey Chemishkian, Shuai Shao, John Hull, Faranak Nekoogar, and Farid Dowla.

I want to thank the members of my dissertation committee - Josh Smith, Brian Johnson, and Sawyer Fuller. I appreciate the questions and comments from the committee, it really helped me create a more polished dissertation.

Lastly, I want to thank the ones that have been there throughout my whole life, watching me grow and become the man that I am today. My mom and dad, my brother Kevin, my sisters Ashley

and Alysha, and all my other relatives who have been keeping me strong throughout my time in college. All the hours spent in the gym with my brother and playing basketball has definitely helped me from going insane. Playing knowledge is power with Ashley and Alysha while getting glooped made me happy and those are times that I will never forget. And I really want to thank my girlfriend and future wife to be, Kelby, for showering me with love and support as I went through the last 2 years of my PhD. You're amazing and I can't wait to see what the future has in store for us! Thank you everyone for getting me to this point, I couldn't have done it without you all.

Chapter 1

INTRODUCTION

Wireless power harvesting is the collection of energy from RF sources and either storing it for future use or using it to power a device to perform an operation. Being able to wirelessly communicate from long ranges has dated back centuries ago. The world's first wireless telephone conversation occurred in 1880, where audio conversations were conducted over modulated light beams. Recently, research has shown that objects (like milk cartons) can have the ability to communicate to us to relay data [2, 3]. This type of technology is called backscatter communication. The premise is that the device can receive an incoming signal and modulate it to produce a message back to the receiver. Where this type of technology is most relevant in the market is with Radio Frequency Identification (RFID), a commercial backscatter device capable of being identified and tracked by an RFID reader. Backscatter communication can span anywhere from bus passes to Internet of things devices (smart home appliances, smart bulbs, apple watch). RFID comes in many form factors but can be split up into a few categories: active, passive, and semi-passive. Active tags use an external energy source to constantly power tags, such as batteries or a wall plug. These tags are great for long ranges, but suffer due to always having to be connected to an outlet or requiring batteries that would need to be replaced after a finite amount of time. A passive tag operates using the RF energy received from a transmitter. The energy is stored where it can be used to power circuitry and modulate a signal back to the reader. The advantage is that there is no need for batteries or any circuity to be replaced, but its disadvantage is its limited range. Semi-passive tags are the best of both worlds, where a tag can be passive closer to the source and active when its farther away.

This thesis explores novel design methodologies and architectures that address key challenges to realize wide area communication and sensing. By studying prior work and optimizing previous designs, we are able to present the first battery-free 5.8 GHz backscatter tag capable of kilometer range

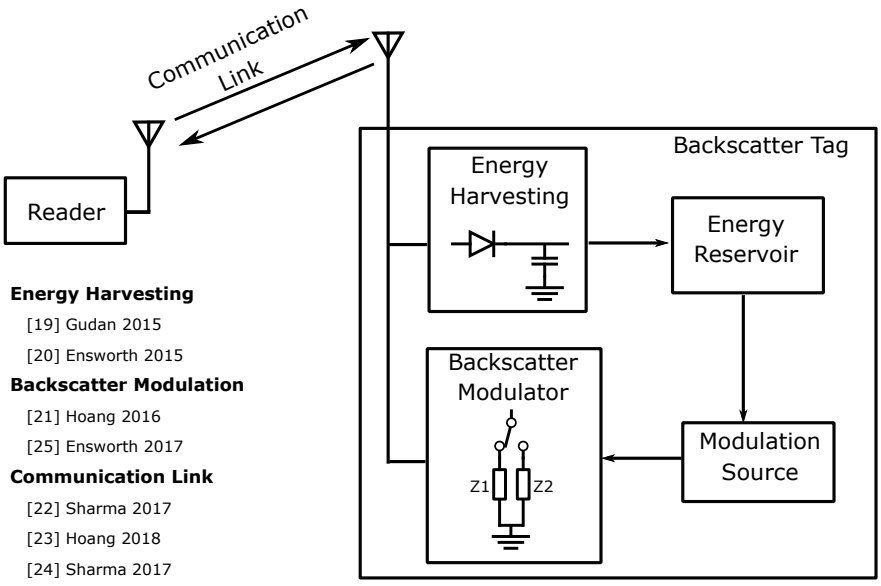

Figure 1.1: *Passive backscatter tag employing energy harvesting and modulation through a communication link (includes antenna and communication medium)*

communication and sensing. In this document, we first examine the feasibility of powering a relatively high power sensor using ambient RF energy harvesting. This document includes measurements and analysis of ambient RF energy harvesting at 2.4 GHz and storage using a timer based boost converter to boost incoming RF signals and storing it in an energy reservoir. This technology would allow for powering low power sensors without the use of batteries. The design methodologies for wireless power harvesting at 2.4 GHz, specifically the harvester can be adapted to work at 5.8 GHz. In the following chapter, an electrically small antenna design for metal mountable RFID is presented. This antenna design is implemented on a metal cylinder that is used to contain a sealed industrial radiation source. Being able to monitor inventory of these metal cylinders is crucial for preventing loss.

With the understanding of wireless power harvesting and antenna design from previous works, a battery free RFID tag is designed that includes a fiber optic loop for tamper detection and AES encryption, security features not seen in any commercial RFID tag. The RFID tag, with the addition

of external sensors, is designed for the purpose of monitoring hazardous material containers. We built an ASIC chip with the energy harvesting and rectification techniques familiarized from the boost converter and designed an air dielectric patch antenna that has a max realized gain of 8.5 dBi. The RFID tag's security functions are controlled by the TI MSP430 microcontroller, which is also used for streaming EPC data into the tag and outputs AES encrypted data back to the reader. It has a range of 5.5 meters in passive mode which is due to the energy consumption of the MSP430 and the LED fiber loop. Finally, we present an efficient method of wireless power harvesting and antenna design at 5.8 GHz. This system would allow an ultra-low power fully-passive backscatter sensor tag feasible, one that is capable of theoretical read ranges of up to 1 km in the co-located bistatic configuration. Designing an efficient rectifier, high gain antenna, and ultra-low power oscillator are vital components to the feasibility of a 1 km long range backscatter tag.

This thesis shows that long range low-power backscatter communication is possible and allows identification and monitoring from hundreds of meters away. This would open up opportunities for wide area connectivity such as long range agricultural monitoring and smart cities, the ability to share information from devices to the user. An example of this is smart meters, parking meters that use backscatter to communicate to a phone notifying them of how many parking spaces are unoccupied. Wide area connectivity will be important in improving the ease of life for citizens and the quality of government services.

1.1 Motivation

Wireless power transfer has been at the forefront of innovation since Nikola Tesla first discovered resonant coils in the late 1800s. His idea was to wirelessly deliver power worldwide from a transmitter to receiver in an efficient way. Fast forward to today and we have made advancements in wireless power delivery, like wireless Qi chargers for smartphones through commercial means. What we are not able to do is deliver power at longer ranges. Wireless Qi chargers can only charge phones that are placed right on the mat. Ongoing research is being conducted to design wireless long-range harvesting with the optimization of rectifiers or antennas. The fundamental setback of wireless power delivery is that power drops off in terms of R^4 in a monostatic backscatter communication

Table 1.1: Power consumption change from 2009 to 2011 of different functions, [1]

Function	**2009**	**2011**	**% Change**
Display	300 mW	900 mW	300%
Peripherals	400 mW	1500 mW	275%
Processor	800 mW	1620 mW	200%
Audio	300 mW	400 mW	30%
RF	1200 mW	1330 mW	11%
Total	3000 mW	5750 mW	92%

setup, so long ranges can only be achieved with efficient design and orders of magnitude of savings in power consumption.

Consumers rely on wireless communication for numerous things in day-to-day life. Smartphones are the number one contributer to wireless communication because we use them everyday, from listening to music to answering phone calls. The most produced active radios in the market for communication are Wi-Fi and Bluetooth. These standards have good range and data throughput to meet consumers needs, but the fundamental problem with conventional active radios, like WiFi and Bluetooth, are that they they consume a lot of power. This can be seen in our reduced phones battery life. These conventional communication methods are great in terms of reliability and signal strength, but does so at the expense of power.

To get a better understanding of the power consumption of a smartphone, we can breakdown the total power consumption into 5 main functions, the display, peripherals, processor, audio, and RF. The power consumption will vary with what the user is doing, for example, the phone could be asleep so the display won't consume as much energy, but this table is an average. Table 1.1 shows a comparison of the power consumption of each function on a smartphone in 2009 and 2011. As can be seen, the power consumption of a lot of these functions have increased by a considerable amount because of the addition of new functions on a phone. This means that our battery lives are shortened,

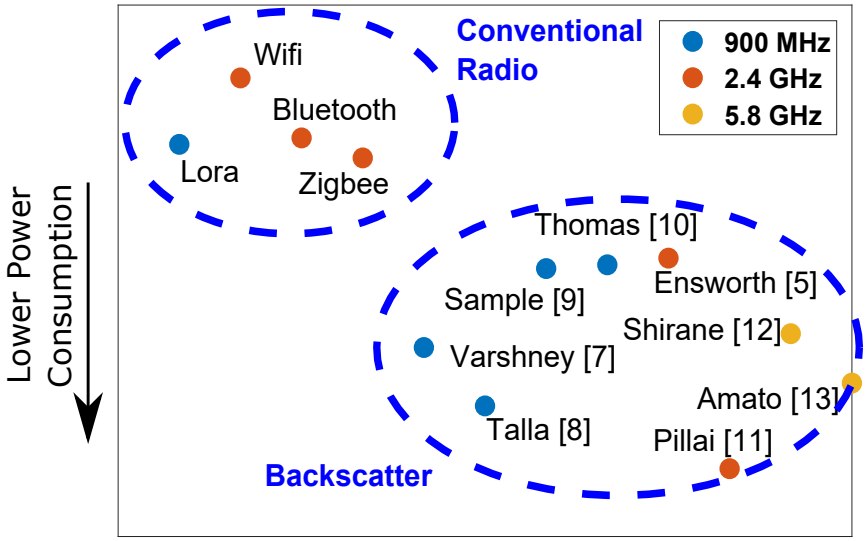

Figure 1.2: *Wireless communication standard power consumption comparison, references in Table 1.2*

but what I want to highlight is the fact that the RF function (which includes all the communications) has not changed much but also has not reduced either. Advances in technology has not been favorable for the communications side. Conventional radios just consume a considerable amount of power and there has been research into new communication methods. The biggest problem with these communication standards is that they require complex circuitry to produce a signal, with its PA's and frequency synthesizers. Currently, there is research being done on a solution that will remove this complexity burden from the device itself and moving it to another piece of hardware, this is the basis of backscatter communication.

Backscatter communication is now being researched as an alternative to the conventional communication methods, as it can combine the data rates of conventional radios but lowers the power consumption considerably. This would allow devices to operate for a longer period of time compared to its counterpart. There are many examples in literature that takes advantage of the conventional radio standards by using backscatter to reduce power consumption, like Wi-Fi backscatter [4, 5]

Table 1.2: Summary of Fig. 1.2

Reference	**Center Frequency**	**Power Consumption**	**Radio Type**
Varshney [8]	868 MHz	70 μW	Backscatter
Talla [9]	915 MHz	9.25 μW	Backscatter
Sample [10]	915 MHz	1.08 mW	Backscatter
Thomas [11]	915 MHz	1.23 mW	Backscatter
Ensworth [6]	2.4 GHz	1.55 mW	Backscatter
Pillai [12]	2.45 GHz	1.05 μW	Backscatter
Shirane [13]	5.8 GHz	113 μW	Backscatter
Amato [14]	5.8 GHz	20.4 μW	Backscatter
LoRa	915 MHz	80 mW	Conventional
Wifi	2.4 GHz	800 mW	Conventional
Bluetooth	2.4 GHz	100 mW	Conventional
Zigbee	2.4 GHz	50 mW	Conventional

and Bluetooth backscatter [6]. Fig. 1.2 shows the power consumption of wireless standards in the market and in literature. The conventional radios consume more than 10 mW's of power, which is considerably higher than most backscatter standards. This means that sensors and tags will have a longer lifetime than conventional radios. Backscatter was made popular because of the WISP designed by Intel [7]. This is a backscatter device that takes advantage of incoming transmitted data and reflects information back to the receiver. From that technology, RFID became popular as a device that could transmit a unique identification for tagging, but also for data.

RFID is a form of wireless communication that uses backscatter to modulate a transmitter signal and reflect it back to the receiver. This method has been studied throughout the past couple of years and has acquired a fair amount of interest until Google decided to back RFID technology and are looking for ways to innovate. Not only is the biggest tech giant interested in this technology, but

many other smaller businesses are looking towards RFID for tagging items to efficiently track items wherever they go, in an effort to compete with one of the largest online retailers, Amazon.

With the commercialization of RFID, further innovations have developed allowing more features to be added to the chip, such as security, power saving mode, battery assisted passive mode, programmability, and many others. One of the most fascinating innovations that's making a big push in RF communication is the ability to communicate and sense from kilometers away, which is the premise of this thesis document. One example of a tag capable of long distance backscatter communication is Xbee Zigbee S2C, with a reported range of 1.2 km at 2.4 GHz. This type of technology to backscatter information using low power components to communicate at long distances has been considered for agricultural monitoring. Agricultural fields can span hundreds of meters to kilometers with no way to easily detect if crops are malnourished in certain parts of the field other than physically going to the site. This is one reason why low power backscatter sensors have become popularized in this application field.

The problem with Zigbee and other related long range backscatter devices is that it requires a battery to function. What is the problem with being battery operated? One issue is that in a large field, replacing batteries for sensors becomes too costly, replacing possibly a thousand to a million tags just becomes too labor intensive even if the sensors have a long battery lifetime, they would have to be replaced eventually. Another reason why batteries are an issue is that they can harm the environment. Batteries contain toxic chemicals that can potentially harm the environment, specifically causing soil and water pollution [15]. The difficulty with battery free RF devices is that operational range is limited by the amount of power delivered to it. To achieve long range battery-free communication, designing a tag that is both antenna optimized and consumes ten times less power than the Xbee, but in a small form factor is important. Improving tags would require considerable savings in power consumption by optimizing circuit designs. The other method would be to increase the gain of the antenna. The problem is that most applications need small form factor tags, but to achieve a large gain would be to increase the size of the tag. One way to increase gain of a tag while keeping the form factor the same is increasing frequency.

There is not a sufficient amount of research being done for backscatter at frequencies above 2.4

GHz. The main reasons for the lack of research include increased propagation losses, increased circuit complexity, and cost. Diodes become less efficient the higher the frequency, which means rectifier become harder to design, a comparison of rectifier designs and efficiency can be seen in [16]. Less efficient power harvesters will cause maximum read range to decrease. Although there are many reasons not to increase frequency for backscatter applications, the positives to moving up to 5.8 GHz from 900 MHz or 2.4 GHz [17], include:

1. **Immune to conductive objects:** Ability to be placed on conductive objects without seeing a degradation in performance [18]

2. **Size:** Antenna can be much smaller with higher gain compared to 900 MHz antennas with the same gain

3. **Bandwidth:** There is more available bandwidth and less interference due to other devices

Recognizing that increasing frequency has its many benefits, the factors that need to be taken into consideration for 5.8 GHz tags are the design of the antenna, rectifier, and baseband generator. The goal is to design a high gain antenna in a small form factor with an efficient rectifier for maximum power transfer. This would allow for long-range wireless power harvesting at 5.8 GHz. By creating an efficient antenna and rectifier to harvest ample amounts of energy, a long range passive tag at 5.8 GHz with a low power consumption is possible. The rest of this thesis explores kilometer range communication at 5.8 GHz by efficient energy harvesting and circuit optimization.

1.2 Original Contributions

We will be presenting designs for long range communication and power harvesting, as well as tracking for backscatter devices. The original contributions discussed in this document include:

- Ultra-low power harvesting approaches at 2.4 GHz for powering sensors and external devices. Published in [19, 20].

- ISO1800-6C UHF RFID tags capable of being metal mountable. Published in [21, 22]

- Using a single wire transmission line as the communication channel for long range identification and distributed sensing. Published in [23, 24]

- A low power superheterodyne receiver architecture for wirelessly powered backscatter tags and sensors leveraging an external LO has been demonstrated using a bench top setup. Published in [25].

1.3 Dissertation Organization

This thesis will be organized as follows: Chapter 2 provides an overview of the importance of tracking and identification and will follow up with a background of low-power backscatter communication. Chapter 3 describes a method to harvest energy from the 2.4 GHz ISM band with the purpose of charging batteries on smartphones or for powering low power sensors and devices. Chapter 4 focuses on an electrically-small metal mountable UHF antenna. The antenna is tested in combination with a commercial RFID chip to determine its maximum read range. Chapter 5 focuses on a custom battery-free sensor UHF RFID tag with fiber optic tamper detection that utilizes a MSP430 microprocessor, a custom analog front-end ASIC, and fiber modules for tag tracking and security. Chapter 6 will discuss the feasibility of a long-range low-power fully passive sensor tag capable of wireless communication from one kilometer away. The focus is on an efficient rectifier and antenna design that would allow for a long-range backscatter communication for wide area connectivity.

1.4 Publications

A list of my publications that I have to date are included below:

[1] **A. T. Hoang**, A. Sharma, F. Nekoogar, F. Dowla and M. S. Reynolds, “An Electrically Small, 16.7 m Range, ISO18000-6C UHF RFID Tag for Metal Cylinder Mounting”, in IEEE Journal of Radio Frequency Identification, vol. 2, no. 2, pp.49-54, June 2018

[2] A. Sharma, **A. T. Hoang** and M. S. Reynolds, "Long-Range Battery-Free UHF RFID With a Single Wire Transmission Line," in IEEE Sensors Journal, vol. 17, no. 17, pp. 5687-5693, Sept.1, 1 2017.

[3] K. Gudan, S. Shao, J. J. Hull, **A. T. Hoang**, J. Ensworth and M. S. Reynolds, "Ultra-low power autonomous 2.4GHz RF energy harvesting and storage system," 2015 IEEE International Conference on RFID Technology and Applications (RFID-TA), Tokyo, 2015, pp. 176-181.

[4] A. Sharma, **A. T. Hoang** and M. S. Reynolds, "A Coplanar Vivaldi Style Launcher for Goubau Single Wire Transmission Lines," in IEEE Antennas and Wireless Propagation Letters, vol. PP, no. 99, pp. 1-1.

[5] J. F. Ensworth, **A. T. Hoang** and M. S. Reynolds, "A low power 2.4 GHz superheterodyne receiver architecture with external LO for wirelessly powered backscatter tags and sensors," 2017 IEEE International Conference on RFID (RFID), Phoenix, AZ, 2017, pp. 149-154.

[6] J. F. Ensworth, **A. T. Hoang**, T. Q. Phu and M. S. Reynolds, "Full-duplex Bluetooth Low Energy (BLE) compatible Backscatter communication system for mobile devices," 2017 IEEE Topical Conference on Wireless Sensors and Sensor Networks (WiSNet), Phoenix, AZ, 2017, pp. 45-48.

[7] **A. T. Hoang**, K. D. Coonley, F. Nekoogar and M. S. Reynolds, "A battery-free RFID sensor tag with fiber-optic tamper detection," 2016 IEEE SENSORS, Orlando, FL, 2016, pp. 1-3.

[8] J. F. Ensworth, **A. T. Hoang** and M. S. Reynolds, "A timer based boost converter for RF energy harvesting," 2015 IEEE Wireless Power Transfer Conference (WPTC), Boulder, CO, 2015, pp. 1-4.

Chapter 2

IDENTIFICATION AND BACKSCATTER COMMUNICATION

2.1 Tracking and Identification

Tracking and identification have gained a lot of interest over time as an application space for security. Through its early development, tracking position came in many forms with the purpose of navigation. This stretches all the way back to the 1st century in China where a ladle handle always pointed south, which later led to the development of the compass. By today's standards, we see compasses as a primitive source for tracking ones location, but that early development has led to advancements in tracking technology with the worldwide commercial adoption of global positioning system (GPS). Almost everyone has access to GPS, through their smartphones, which allows them to navigate through places that they have never been to before. The ability to track ones position plays an important role in todays society, not only for navigation but for security purposes.

Although GPS has its advantages of being able to detect objects and where they are located, it comes at an energy cost. Early research has shown that the GPS in a smartphone can consume upwards of 429 mW in active mode [26]. The main reason why these devices use up a lot of power, hence draining battery life is because base stations could be hundreds of kilometers away and to get a clear signal, more power is consumed to transmit a stronger signal. This system is ideal for applications where a battery is present and can be used with the device, but what about applications that require the same sort of localization without the need for batteries?

Passive RFID is a popular consumer product that is being used in a lot of places to track and identify objects. There is no need for batteries because all the power comes from the RF energy of the reader. One of the ways we're seeing passive RFID being used is in toll booths [27, 28, 29], an RFID sticker is applied to your car and when you drive through a toll both, you are automatically charged based on the unique identification of your RFID tag. This improves on the older methods

where cars would have to stop and pay for the toll manually. Another example of RFID in use today is for supply chain management in retail stores, [30]. Clothes in department stores are being bought and returned every day. To make retail store inventory management easier for employees, an RFID tag can be placed on every product. Then an RFID reader can scan the whole store for items in stock and store it in a database. This would allow store clerks to automatically track where each item is. These are only a few ways that tracking and identification has developed through technology. Improving upon these commercial products to allow for longer range communication can open up opportunities to do larger scale tracking and identification.

2.2 Backscatter Communication

One of the first examples of modulated backscatter dates back to 1948 by Stockman [31], with his invention of a voice communication system that used light as the backscatter source. This system comprised of focusing an ambient light source directly onto a mirror reflector. The sound waves coming from the microphone causes the mirror reflector to vibrate, which modulates the reflected ambient light source. The receiver then demodulates the reflected light using a partially enclosed phototube and an audio amplifier to play back the original sound on a speaker. This system was capable of playing back sound up to 90 meters.

The idea of communication by the reflection of power has developed further since then. Instead of using light source as the ambient carrier source, we have now transitioned to radio frequency waves. One of the earliest examples of telemetry by modulating an RF source was designed in the 1970s [32]. We have now reached a point where CMOS processes allows us to design single chip solutions to further develop backscatter communication. This has lead to commercialization of these backscatter devices which are now known as Radio Frequency Identification (RFID).

Traditionally backscatter communication relies on amplitude modulation (AM), where the carrier signals' amplitude is varied from a modulating signal, Fig. 2.1. Other methods of modulation for backscatter communication include frequency shift keying (FSK), where the carrier signals' frequency is modulated through discrete frequency changes, [33, 34]. Another method that's been researched is modulation using an ambient source, like television (TV) signal backscatter [35, 36].

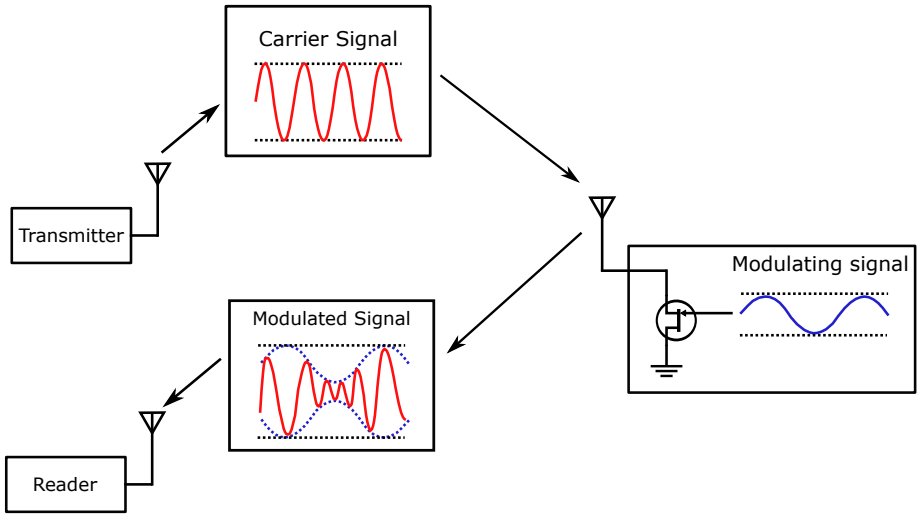

Figure 2.1: *Backscatter signal flow chart*

Liu et al, leveraged existing signals as the only energy source to power backscatter devices. The advantage that Liu et al's work has compared to others is that there is no need for a dedicated reader and the received power is much greater from a TV signal than a dedicated reader from hundreds of meters away. The TV broadcast channel is able to transmit 1 MW effective radiated power (ERP), which is much higher than conventional RFID readers can transmit, 4 W effective isotropic radiated power (EIRP). This would allow for effectively longer ranges to be achieved. In contrast, the work in this thesis aims to harvest a 5.8 GHz wireless signal from hundreds of meters away. This would expand to designing a low power passive backscatter tag for government purposes that will use an order of 100x lower transmit power than TV broadcast signals. Although the transmit power is much lower than TV broadcasts, we aim to have communication ranges of up to one kilometer.

One of the reasons why RFID and backscatter communication in general is being popularized is because it's orders of magnitude more power efficient than conventional radio communication because it offloads the main signal (carrier) generation onto the transmitter rather than the device. The only cost to power consumption is from the frequency synthesizer, to downconvert the carrier signal. To further reduce power consumption, one can remove and replace the on-board frequency synthesizer with a two port mixer, that takes in a carrier signal and an external local oscillator signal

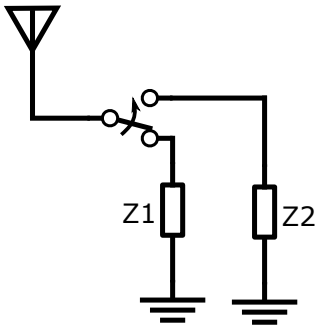

Figure 2.2: *Backscatter impedance circuit*

and downconverts that into an IF frequency, which can be demodulated and reflected back [25]. There are limitations to backscatter communication and one of them is communication range. Path loss is the reduction of an electromagnetic wave as it propogates through free space. The path loss due to the forward transmission of the electromagnetic signal can be modeled using the Friis transmission equation [37]

$$P_r = \frac{P_t G_t G_r \lambda^2}{(4\pi r)^2} \tag{2.1}$$

where P_r is the received power, P_t is the transmitted power, G_t is the gain of the transmitter antenna, G_r is the gain of the receiver antenna, λ is the wavelength, and r is the distance between the transmitter antenna and the receiver antenna. This equation describes the forward transmission power where the power at a receiver drops as a function of $1/r^2$.

In backscatter communication, we also need to account for the reverse path loss as well. The total round trip path loss (from reader to tag and tag to reader) for a bistatic co-located backscatter link can be described by the radar equation

$$P_r = \frac{P_t G_t G_r \lambda^2 \sigma}{(4\pi)^3 r^4} \tag{2.2}$$

where σ is the radar cross section (RCS) of the tag, which is the amount of power the tag is able to reflect back to the reader. It is evident now that the wireless communication range in backscatter

communication is severely hindered by the separation distance of the receiver to the tag, which is now a function of $1/r^4$.

The magnitude of the backscatter from the tag is dependent on the load impedances presented to the antenna [38]. In the case of backscatter, the load impedance is typically split into two parts, (1) the load at which the antenna is well-matched ("modulated state") and (2) the load at which the antenna is mismatched ("unmodulated state"), Fig. 2.2. To describe the magnitude change between the time varying loads, the differential RCS ($\Delta\sigma$) can be calculated

$$\Delta\sigma = \frac{\lambda^2}{4\pi} G_T^2 |\Gamma_1^* - \Gamma_2^*|^2 \tag{2.3}$$

where G_T is the gain of the tag, Γ_1^* is the complex power wave reflection coefficient for the tag antenna in the unmodulated state, and Γ_2^* is the complex power wave reflection coefficient of the tag antenna in the modulated state. The complex power wave reflection coefficient (Γ^*) can be derived from

$$\Gamma_{1,2}^* = \frac{Z_{L1,L2} - Z_a^*}{Z_{L1,L2} + Z_a} \tag{2.4}$$

where Z_a is the complex impedance of the tag antenna, $Z_{L1,L2}$ is the impedance of the tag in the modulated and unmodulated states respectively. The impedance difference in the modulated and unmodulated states is important to achieving a higher backscatter power at the receiver, which would translate to an increase in range.

Chapter 3

A TIMER BASED 2.4 GHZ ENERGY HARVESTER

* This chapter is an adapted version of [20].

3.1 Introduction

The goal of this work is to capture the ambient RF energy in the environment to continuously charge a capacitor, which can be used to power external sensors. The idea is to expend less energy than is stored, which will allow for continuous charging of an energy source or battery. The difficulty in harvesting ambient RF energy is that the amount of energy transmitted from the source is limited [39], so a low power boost converter is needed to boost the incoming signal. In this work, a low power timer is used to allow energy storage for a short period of time before turning off and holding the energy. In this initial proof of concept, the circuit is able to store more energy than expended at an input power level of -15 dBm at 2.45 GHz, which resulted in a harvested voltage of 460 mV and a boosted output voltage of 1.8 V.

Energy harvesting for low power applications has become a popular body of literature studies and for commercial applications. There is a variety of energy harvesting techniques including solar, RF, and vibration [40, 41, 42]. This work in particular focuses on RF harvesting. Many types of RF energy harvesters have been proposed to harvest uW's of energy [43, 44], but the significant problem is that there isn't enough rectified output voltage to turn on sub-millivolt sensors. Low power boost converters are being researched that can take sub-millivolt signals and boost them to a usable voltage level [45]. Boost converters that have shown to boost input voltages as low as 250 mV have been designed [46]. The struggle of boost converter harvesting is the cold-start issue, where there needs to be an initial charge to start the boost converter. In this design, a long interval timer is used, that is powered by an energy reservoir to control when the boost converter starts, Fig. 3.2. This allows the

boost converter to turn on and charge the energy reservoir, which in this case is a big capacitor.

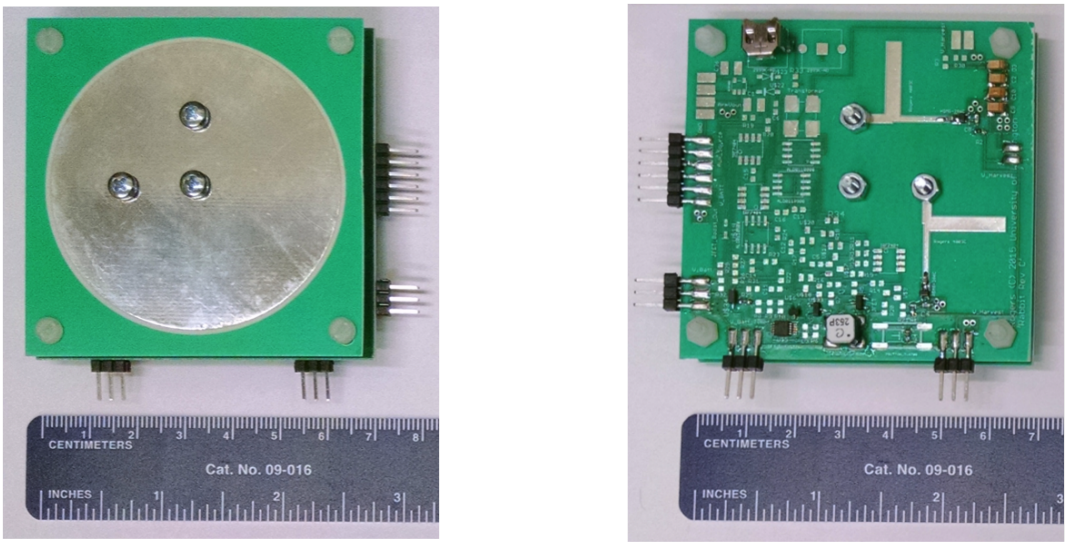

(a) **(b)**

Figure 3.1: *(a) Dual Polarized Patch Antenna (b) RF harvester and timer controlled boost converter*

The timer based harvester is built on two low-cost double sided FR4 printed circuit boards (PCB) measuring 7 cm x 7 cm and a thickness of 1.64 mm each. The "Antenna" PCB (Fig. 3.1a) contains a 6 mm diameter circular patch radiating element on both its top and bottom layers. The antenna is fed at two orthogonal feed points 1.5 cm from the center to achieve dual polarization. The center feedpoint is grounded to suppress unwanted mode coupling between the two feeds. This then feeds the "Circuit" PCB by 5 mm aluminum posts. The top copper layer on the Circuit PCB is an unbroken 2 oz. copper layer (except for clearance for the feed posts). This layer provides the ground plane for the antenna PCB, forming an air dielectric patch antenna. The bottom layer of the circuit PCB contains all the circuitry, including two RF harvesters, a large input capacitor, a low voltage boost converter, a low voltage timer, and an energy reservoir, Fig. 3.1b. In this proof of concept design, the energy reservoir is a large capacitor; this would be replaced by a battery in a realistic scenario to supply power when there is low or absent RF energy.

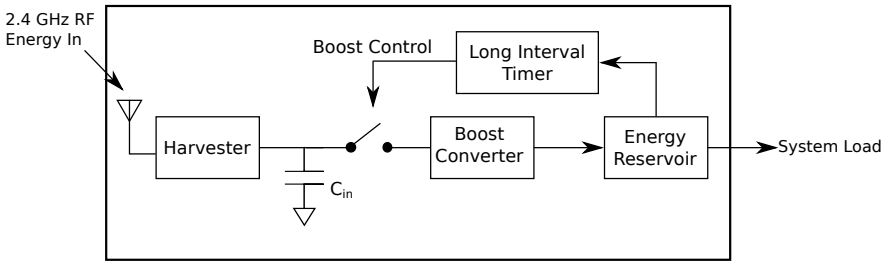

Figure 3.2: *Block Diagram of Timer based harvester*

3.2 Related Work

Many examples of trigger based low power boost converters have been proposed. The most difficult design challenge for low power boost converters is cold starting the circuitry, boosting the voltage from zero. Other work have tackled the cold start issue by using motion activation [47] or a ring oscillator with a clock doubler [48] to kick start their systems. The system described in this chapter does not focus on the cold start operation, but on extending battery life of systems by using available RF energy. Dynamically tuned circuitry for multiple different power levels have been proposed [49, 50] to maximize the harvested energy. In this work, the focus is on finding the minimum power level needed to power the long interval timer to start the boost converter. The drawback to working with low input powers is that at lower input powers efficiency drops.

3.3 Diode Based Harvester Characterization

A one stage diode rectifier using AVAGO HSMS286C Schottky diodes is used to convert the incoming RF signal to a DC output. The matching network consists of an open stub network to maximize power transfer from the antenna to the diode based harvester. The stub network structure was designed and simulated using AWR Microwave Office. Fig. 3.3a shows the structure of the open stub matching network with the sub-structures of the matching network labeled, A (1.81 mm x 5 mm), B (0.9 mm x 11.6 m), C (2.9 mm x 16 mm), and D (1.81 mm x 2 mm). The matching network is fabricated on a 31 mil low loss Rogers RO4003 substrate with an epsilon of 3.38. Measurements of the matching

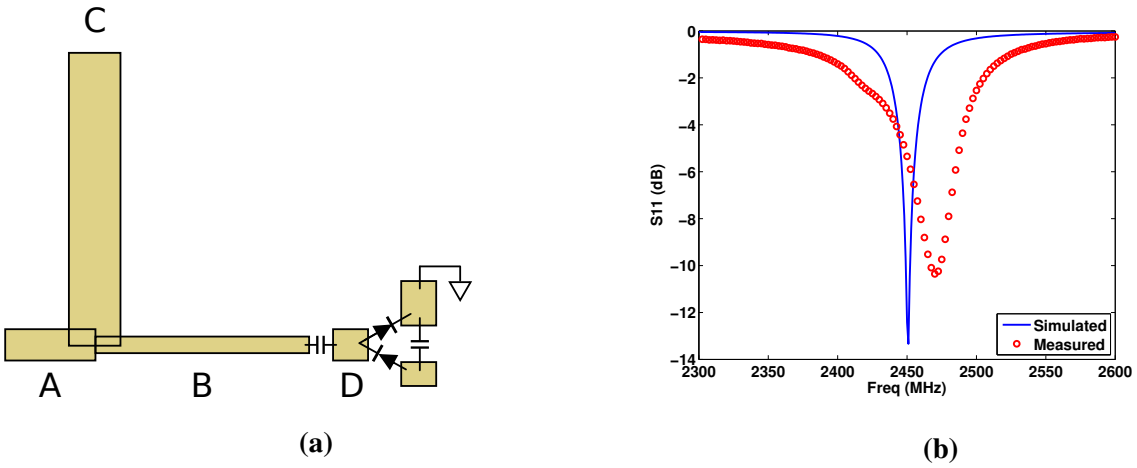

Figure 3.3: *(a) Open stub matching network diagram (b) Measured and Simulated S11 measurements*

network are done using an Agilent N5222A microwave network analyzer and shows the rectifier having good matching at 2475 MHz, which is a slightly off from simulation at 2450 MHz, Fig. 3.3b. This could be due to manufacturing tolerance or the substrate epsilon being a little off from simulation.

3.4 Timer Circuit Characterization

The timer based boost converter (TPL5100) being described in this chapter uses the rectified voltage and produces a 2.2 V output signal. This timer was chosen because of its low power consumption (nanoWatts) and optional programmability. The boost converter circuitry contains a transformer, CoilCraft LPR6235-253PMRB, and a P channel JFET, MMBFJ270, Fig. 3.4. A negative rectified DC voltage is stored into a large input capacitor C_{in} where it becomes the input to the boost converter. It then produces a positive boosted voltage onto C_{boost}. The voltage is then transferred to the energy reservoir where it can then charge a capacitor or a battery, that energy can then be used to power a low power sensor. The TI TPL5100 controls the boost converter operation by driving the P channel JFET, MMBFJ270 either to ground, for boost operation, or open node, for power accumulation on C_{in}. The timer is powered from a 1.8 V supply and consumes 30 nA of current for a total power

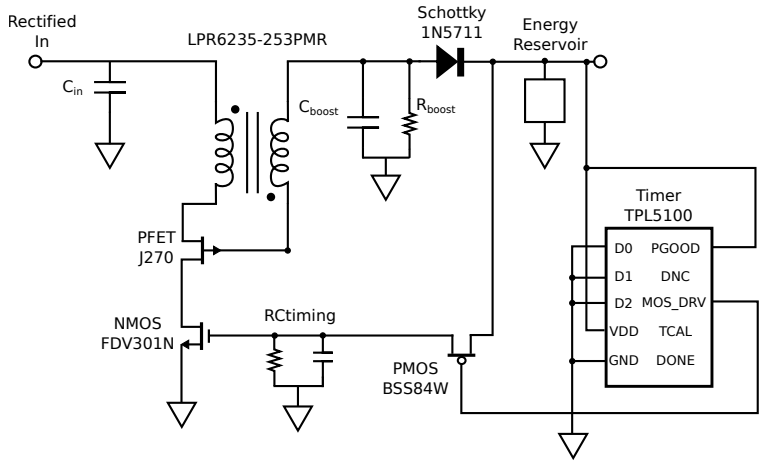

Figure 3.4: *Boost Converter Circuit*

consumption of 54 nW. Every 30 ms the timer outputs a square wave onto a PMOS BSS84W, when the switch is ON, the voltage from the energy reservoir is transferred to the NMOS FDV301N's gate. When the gate-source voltage is higher than its threshold (0.85 V), the NMOS then has a drain-source resistance (rds(on)) of 5 Ω. The rds(on) is an important value because it allows all the current to flow through the primary coil of the transformer, enabling full operation of the boost converter.

The TPL5100 operates at 30 ms pulses which is too short to fully discharge the input capacitor. To extend the time of the pulse, an RC circuit is placed at the gate of the NMOS FDV301N, to keep the NMOS ON (Saturation region) for a longer period of time, allowing the boost converter to operate longer. RC_{timing}, as seen in Fig. 3.4, is tuned to control the discharge time of C_{in}. A capacitor value of 4.7 nF and a resistor value of 940 MΩ are used in this setup. This combination of values allowed the boost converter to operate for roughly one second, which was enough time to drain the capacitor C_{in}, allowing C_{boost} to charge to its maximum voltage. The one second operation time we chose is important because it is enough time to operate the boost converter but not long enough to drain the input capacitor for the next boost operation. If the discharge time is too low, the input capacitor will have remaining energy that will not be utilized which could have been used

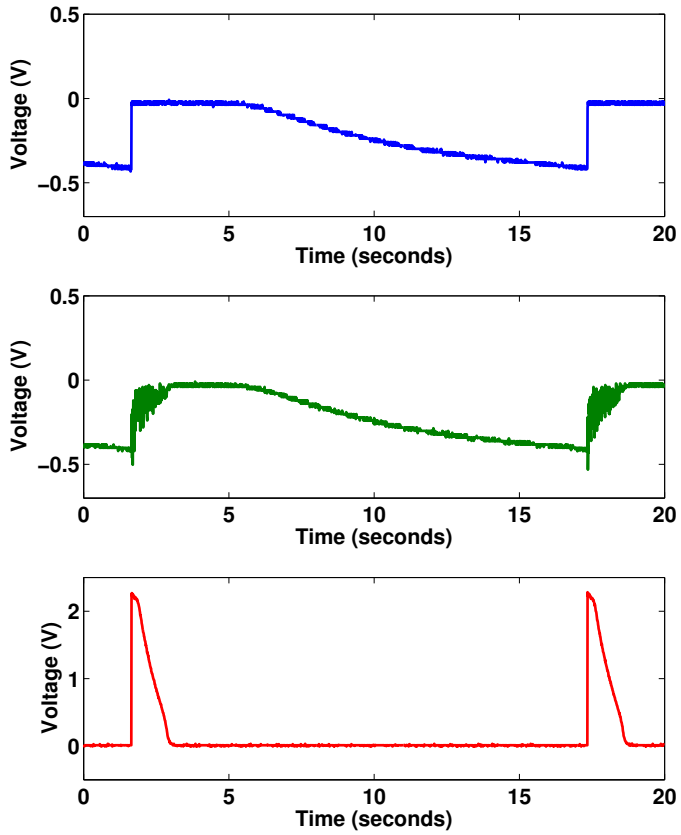

Figure 3.5: *Operating circuit measured by an Agilent MSO-X-3104A oscilloscope. – JFET source, – JFET drain, –* $V_{C_{boost}}$.

for the boost converter. If the discharge time is too high, the input capacitor will have all its energy drained and wasting the RF energy instead of being able to fully charge the input capacitor for the next boost operation.

RC_{boost} is another set of design parameters that is important and can be modified to decrease the energy consumption of the boost converter circuit. R_{boost} and C_{boost} are used together to drain the gate-source voltage of the P-channel JFET, allowing the JFET to reach the cutoff region, where the JFET then acts like an open circuit. This is important because it will halt operation of the

boost converter. Keeping the C_{boost} at 0.1 μF, R_{boost} can be configured to decrease the duration of wasted energy. If R_{boost} is set too high, the JFET will not be in saturation when the FDV301N is in saturation, resulting in no oscillations for multiple RC_{timing} pulses. If R_{boost} is set too low, the JFET will be in saturation before the FDV301N reaches saturation. This results in the source of the JFET not being grounded, causing a waste in energy since the boost converter isn't operating while energy is being used from the input capacitor. Optimizing R_{boost} to allow both the JFET and the FDV301N to reach saturation at the same time will insure that the duration of wasted energy is minimized while the boost converter activates after every timer pulse.

The boost converter node voltages are measured and the data is shown in Fig. 3.5. The drain of the JFET, source of the JFET, and C_{boost} voltages are measured using an oscilloscope. The plot shows that the boost converter starts oscillations when the source of the JFET is pulled down to ground. When the boost converter is off, the input capacitor charges up to -460 mV then is quickly discharged once the boost converter is on. The boosted output reaches 2.19 V, enough to charge the energy reservoir (large capacitor) and supply the minimum 1.8 V that is required of the TI TPL5100 timer. The measurement is done using a cabled RF input power of -15 dBm with the timer set for an interval of 16 seconds. The TI TPL5100 timer can be set to 16, 32, 64, 100, 128, 256, 512, or 1024 seconds depending on the connections to digital input pins (D0, D1, D2).

3.5 System Evaluation

In order to evaluate the performance of this proof-of-concept design, a set of experiments to verify that a net positive energy was being delivered to the energy reservoir was conducted. The first measurement was measuring the open loop output voltage of the harvester. This is a measure of the harvester performance independent of the boost converter. This value represents the upper limit of the input voltage to the boost converter for a given input power. For the second measurement, input and output voltages of the boost converter were measured with the harvester attached at the input. A 300 μF input capacitor C_{in} and a 0.1 μF boost capacitor C_{boost} was used for the boost converter circuit. The voltages of the capacitors were measured with harvester input powers ranging from -30 dBm to -10 dBm. The voltage at C_{in} supplies the input energy to the boost converter. After every

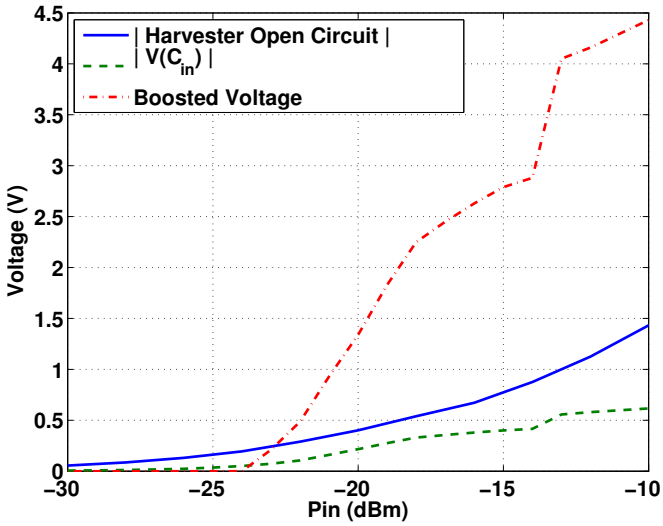

Figure 3.6: *Timer based boost converter voltage vs. input power*

trigger of the timer, the energy at the input capacitor is supplied to the boost converter. When the timer is in sleep mode, the input capacitor is charged to its maximum voltage, shown in Fig. 3.6. The maximum voltage of the input capacitor is reached prior to the boost converter being activated by the timer. The voltage will never be as high as the open loop harvested voltage due to the leakage in the capacitors and the intermittent load presented by the boost converter. To operate the TPL5100 timer, a minimum of -15 dBm input power is required. A voltage of 2.19 V is required because of the voltage drop across the 1N5711 diode (0.41 V) to power the TPL5100 timer (min. 1.8 V).

With an input power of -15 dbm, a break even point is achieved for harvested energy versus energy consumed by the timer circuit. This is the point at which the harvested energy and the energy consumed by the timer circuit is nominally equal. An initial voltage of 1.85 volts on the 400 μF capacitor acting as the energy reservoir is used to power the timer circuit. The harvested energy maintained a voltage of 1.85 V at the reservoir capacitor after over two hours of testing. The small amount of continuous power being consumed by the TPL5100 timer is offset by the bursts of input energy and boost converter every 16 seconds.

3.6 Chapter Conclusion

This chapter focused on the design methods and characterization of a timer based boost converter circuit. This proof-of-concept energy harvester shows that it is possible to capture ambient energy and expend less energy than is stored in order to continuously charge an energy source or battery. By using a low power timer (TI TPL5100) with fixed intervals of 16 seconds, a positive energy balance is achieved at a conducted RF input power level of -15 dBm at 2.45 GHz. The reservoir capacitor maintained a voltage of 1.85 V after over two hours of testing with an input harvested voltage of 460 mV. In a realistic deployment, the energy reservoir would be a battery instead of a large capacitor in order to continuously charge low power devices and sensors.

Chapter 4

ELECTRICALLY SMALL METAL-MOUNTABLE RFID ANTENNA

4.1 Introduction

Passive RFID is when an RFID device is powered primarily from an RF energy source. The amount of energy that can be harvested is determined by the amount of energy transmitted and the distance, as well as the gain of the antenna. An important aspect to increasing read range is the antenna. RFID tags are meant to be made small so that they can be placed anywhere and around hard to reach places. RFID tags in particular are being used to detect and locate numerous amount of products, metal objects being one of them. The difficulty in designing small RFID antennas for metallic objects is that the metal causes a change in antenna performance; parameters such as radiation pattern, input impedance, and center frequency can change dramatically when the tag is mounted on a conductive surface or object [51]. With the size constraint of the metallic object described in this chapter, achieving a high realized gain and directivity will be difficult.

This chapter will explore the design of three different RFID tag antennas that are metal mountable on a custom metal cylinder. The three tags incorporate a split ring resonator (SRR) design, which is used to reduce the antenna size and can be simpler to match to a commercial tag because of its many lines, which can be used to tune the inductance and capacitance. The tags will have different thicknesses and we will explore the maximum realized gain of each and their matching in the RFID frequency band of 902-928 MHz.

4.2 Related Work

This tag was specifically optimized for attachment to a metal cylinder, which is used to contain a sealed industrial radiation source. Monitoring these cylinders is important not only for worker safety but to prevent loss. With the use of these RFID tags, an accurate inventory management can happen.

Table 4.1: Comparison of Electrically Small Metal-Mountable RFID tags

	Ref. [52]	Ref. [53]	Ref. [54]	This Work
Frequency (MHz)	923	911	905	912.5
Dimensions (mm^3)	26 x 14 x 24	19 x 19 x 3	104 x 31 x 7.6	41.6 x 41.6 x 6.7
Tag Sensitivity (dBm)	-15	-20	-18.5	-18
Max Read Range (m)	5.5	3.5	14.6	25

The cylinder is 41.6 mm in diameter and 135 mm long and has a threaded port for a removable handling rod on the top. Since the cylinder is designed to have a rod inserted into it, the tag must fit atop the cylinder without extending beyond the edges. There are numerous studies on metal

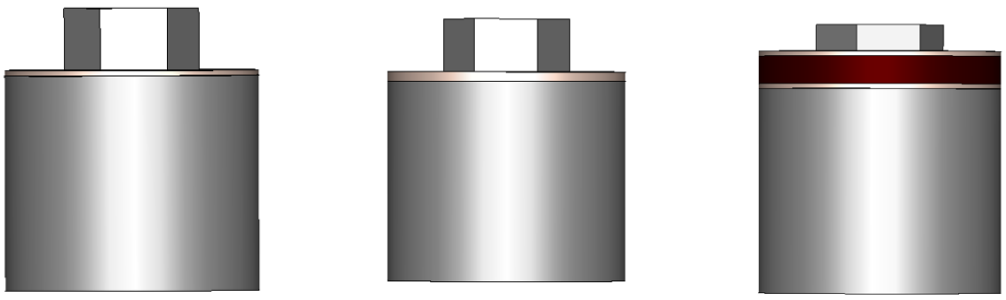

Figure 4.1: *Tag Stackup side view. (a) 0.8 mm Rogers 4003. (b) 1.6 mm Rogers 4003. (c) 0.8 mm Rogers 4003 + 4.67 mm Teflon + 0.8 mm Rogers 4003.*

mountable RFID tags, including [55, 56, 57, 58, 59, 60, 61, 62], with all having different antenna designs. In this work specifically, a split ring resonator for RFID mounted on a metal cylinder was designed. Other work have focused on design of a split ring resonator on different substrates to optimize function or cost [63].

4.2.1 Split Ring discussion

A double split ring design is a C-based ring with an outer C-ring, where the separation distance and ring gaps can be manipulated to achieve the performance needed. Resonant structures, like the split ring, are mainly used for electromagnetic applications where an array of them are put together to form a metamaterial surface. Metamaterials produce electromagnetic properties that cannot be easily obtained in nature. The combination of multiple split ring structures have opened up a variety of applications from new antenna designs to power harvesting applications [64, 65].

Split ring resonators have a gap or slit that prevents current to flow around any one ring. Although current cannot flow around a ring, there is a separation distance between the two rings that induces a capacitance, which will allow current to flow. A simple expression to approximate the resonant frequency (ω_0) of a double split ring resonator is presented in [66]:

$$\omega_0 = \sqrt{\frac{3dc^2}{\pi^2 r^3}} \tag{4.1}$$

where d is the separation distance between the radiuses of the outer and inner ring ($r_2 - r_1$), r is the average radius between the outer and inner ring $\left(\frac{r_1 + r_2}{2}\right)$, and c is the speed of light which is approximately $3 * 10^8$ meters per second.

Another split ring analytical model that relies on equivalent circuits was constructed on the basis that the structure can be simplified into lumped elements, like capacitance and inductance. The resonant frequency (ω_0) of the structure can then be simplified to an LC circuit as shown in [67]:

$$\omega_0 = \frac{1}{\sqrt{2\pi L(\frac{\pi C}{2} + C_{g1} + C_{g2})}} \tag{4.2}$$

where L is the average inductance between the inner ring and the outer ring $\left(\frac{L_1 + L_2}{2}\right)$, C is the capacitance of the inter ring or in other words, capacitance between the rings, C_{g1} is the gap capacitance of the inner ring, and C_{g2} is the gap capacitance of the outer ring.

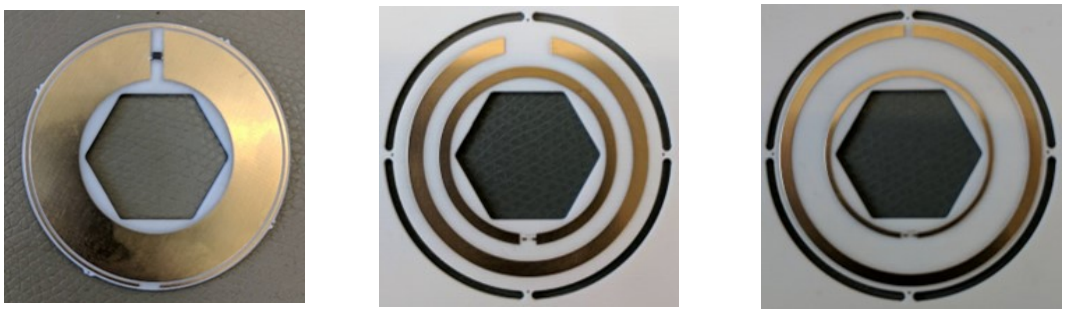

(a) **(b)** **(c)**

Figure 4.2: *Antenna top view (a) 0.8 mm Rogers 4003. (b) 1.6 mm Rogers 4003. (c) 0.8 mm Rogers 4003 + 4.67 mm Teflon + 0.8 mm Rogers 4003.*

4.3 Electricall-small tag antenna design

The antenna was designed using CST and was constrained to the dimensions of the metal cylinder, 41 mm in diameter with a hexagonal cutout. The tag antenna employs a split ring resonator, a design that can easily be tuned to match the impedance of the tag and can be designed to have high gain in a small form factor. The dimensions of the split ring varies depending on the tag antenna stack-up: a single 0.8mm Rogers substrate, 1.6mm substrate, and two single layer, 0.8 mm thick Rogers 4003 PCBs with a 4.7 mm thick teflon dielectric layer laminated between them, Fig. 4.1. Split ring resonator operate by having an outer C-ring and an inner C-ring, where both help tune the input impedance. The split ring, with its many internal capacitances and inductances, helped with matching the input impedance to the RFID chip (NXP SL3S1203FTB0) which has an impedance of 23-j224 Ω. The top view of the three configurations can be seen in Fig. 4.2, the bottom side of the tags are all comprised of full 0.07 mm copper, also known as the ground layer.

4.3.1 0.8mm Rogers RO4003 split ring

The first tag designed is a split ring configuration where a single 0.8mm Rogers RO4003 substrate was used in between the 0.07 mm copper layers. The bottom printed circuit board (PCB) contains

the ground plane which is composed entirely of 0.07 mm copper and the top PCB contains the split ring antenna design. This was designed to be thin and incorporate less materials for fabrication, which results in a cheaper tag. Simulations were done to determine the antennas behavior on the metal cylinder where the tag will be attached to.

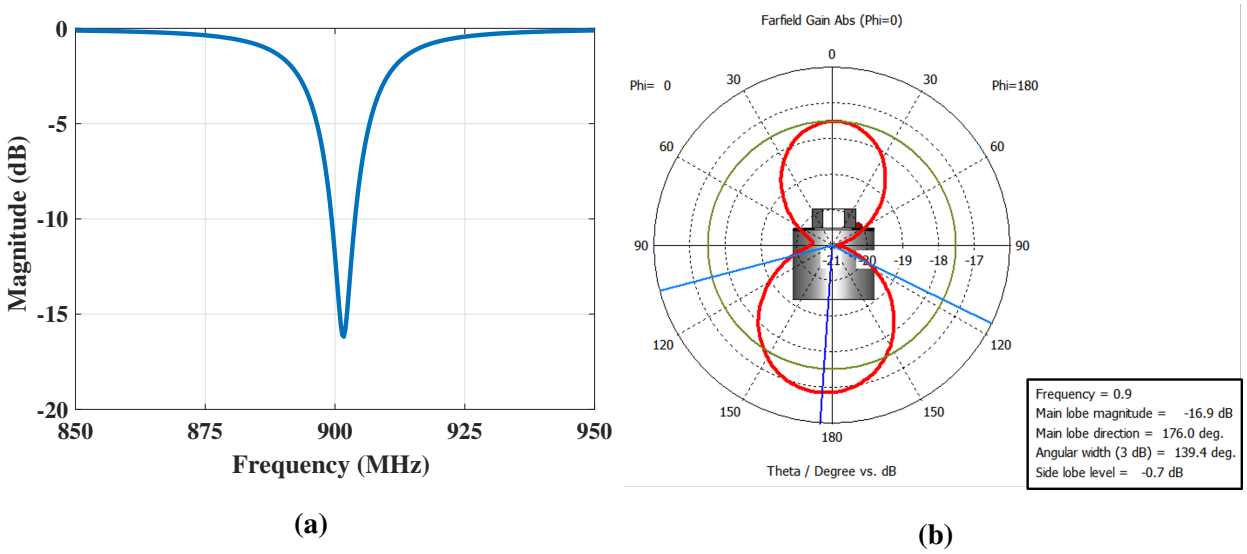

Figure 4.3: *(a) Simulated return loss of the 0.8 mm Rogers 4003 RFID tag (b) Simulated radiation pattern of the 0.8 mm Rogers 4003 RFID tag*

Simulation of the antenna design were done using the finite element method (FEM) solver built into CST Microwave Studio. Simulation suggests that the center frequency of the antenna is 901.7 MHz with a -10 dB bandwidth from 899.5 MHz to 903.9 MHz (4.4 MHz), Fig. 4.3a, with a simulated impedance of 16.5 + j222. The maximum realized gain of the antenna is -15.1 dBi at 900 MHz, which is the center frequency of the UHF RFID band.

4.3.2 1.6 mm Rogers RO4003 split ring

To determine the effect that a thicker material would provide for the tag, the thickness of the Rogers RO4003 substrate was doubled to 1.6 mm. With the thicker tag, the gap between the inner and outer

C-shaped loops is increased because of the change in capacitance due to the separation of the top metal layer to the bottom ground layer.

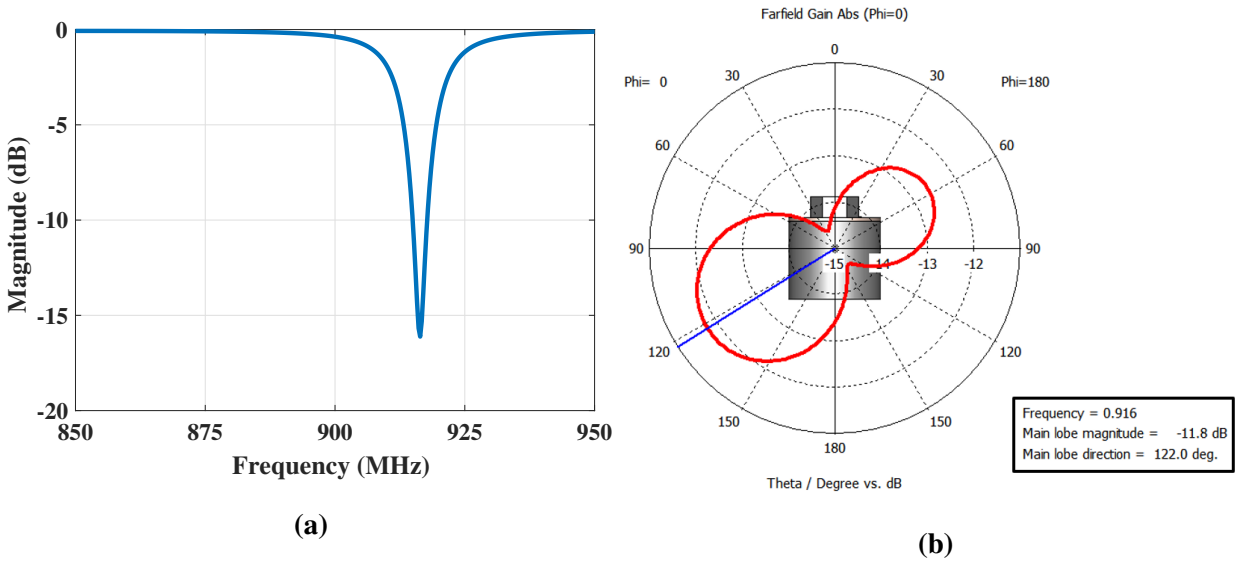

Figure 4.4: *(a) Simulated return loss of the 1.6 mm Rogers 4003 RFID tag (b) Simulated radiation pattern of the 1.6 mm Rogers 4003 RFID tag*

Through simulation, we were able to design a well-matched antenna at 916 MHz with a -10 dB bandwidth from 914.9 - 917.7 MHz (2.8 MHz). To obtain this matching, an external series 10 nH inductor was needed to get a simulated input impedance of 16.8 + j223.3. The realized gain of the antenna is -11.8 dBi at 916 MHz, Fig. 4.4.

4.3.3 4.7 mm Teflon split ring

The final antenna design incorporates a thick 4.7 mm Teflon sheet sandwiched between two 0.8mm low loss Rogers 4003 PCBs. Teflon was used because of its low loss material properties, only having a dielectric constant of 2.1. Teflon as a substrate instead of a thicker piece of Rogers RO4003 would not only save money on fabrication cost, but also reduce losses even further. Increasing the separation distance from the antenna to the ground layer even further would reduce the trace widths

of the antenna at these frequencies, but will allow for greater realized gain, [68, 69].

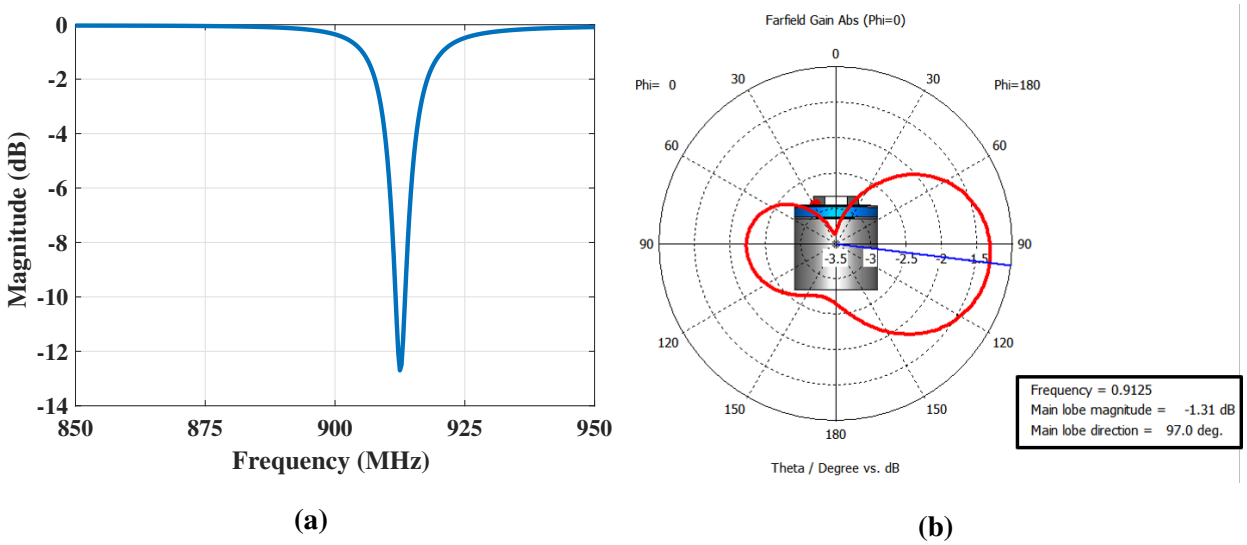

(a) **(b)**

Figure 4.5: *(a) Simulated return loss of the 4.7 mm Teflon sandwiched between two 0.08 mm Rogers R04003 substrate RFID tag (b) Simulated radiation pattern of the 4.7 mm Teflon sandwiched between two 0.08 mm Rogers R04003 substrate RFID tag*

Through simulation we were able to design a well-matched antenna at 912.5 MHz with a -10 dB bandwidth from 911.7 - 913.5 MHz (1.8 MHz). To obtain a well matched antenna, an external 27 nH inductor was placed in series to move the center frequency to the desired band with a simulated input impedance of 38.99 + j225.8. Simulation reports a -1.3 dBi realized gain at 915 MHz with this antenna stackup. Fig. 4.5 shows the simulation results for the Teflon tag.

4.4 Link Budget

4.4.1 Forward Link Budget

To get an idea of the read distance that can be achieved from using our tag setup, we can use the one way radar equation (or Friis transmission equation) [70] and the typical values for parameters like reader gain, tag gain, reader output power, and the threshold power needed to turn on the RFID

tag. All the values correspond to measurements of the Teflon tag. In an ideal scenario where all the power from the reader is transfered directly to the tag, we can estimate the maximum tag-to-reader distance R at which the RFID tag can be read

$$P_T = P_R + G_T + G_R + 20\log_{10}\left(\frac{\lambda}{4\pi R}\right) \tag{4.3}$$

where P_T is the RFID sensitivity in dBm, P_R is the maximum reader output power in dBm, G_T is the gain of the tag antenna in dBi, G_R is the reader antenna gain in dBi, and λ is the wavelength. Given the parameters from Table 4.2, the maximum theoretical reader-to-tag distance that the Teflon tag can be read is 21 meters. In an actual over-the-air experiment, the maximum distance will be lower due to multipath in the measurement environment and also pointing losses due to the misalignment of the reader antenna to the gain pattern of the tag antenna.

Table 4.2: Forward link budget Parameters

Parameter	**Typical Value**
Maximum reader output power (dBm)	32.5
Reader Antenna Gain (dBi)	8
Tag Antenna Gain (dBi)	-1.3
RFID power-up threshold (dBm)	-18
Estimated Tag Range (m)	18.9

4.4.2 Estimated tag RCS

Radar cross section (RCS) is an important factor in determining the amount of backscatter power that will be transmitted from the RFID tag. The radar cross section is a measure of effective area that the target can reflect the incoming radar signals in the direction of the transmit signal. The differential radar cross section equation [71, 72] can be written as

$$\Delta\sigma = \frac{\lambda^2}{4\pi} G_T^2 |\Gamma_1^* - \Gamma_2^*|^2 \tag{4.4}$$

where $\Delta\sigma$ is differential RCS, G_T is the gain of the Teflon tag antenna, Γ_1^* is the complex power wave reflection coefficient for the tag antenna in the unmodulated state, and Γ_2^* is the complex power wave reflection coefficient of the tag antenna in the modulated state. The complex power wave reflection coefficient (Γ^*) can be derived from

$$\Gamma_{1,2}^* = \frac{Z_{L1,L2} - Z_a^*}{Z_{L1,L2} + Z_a} \tag{4.5}$$

where Z_a is the complex impedance of the Teflon antenna, $Z_{L1,L2}$ is the impedance of the tag in the unmodulated state and modulated state respectively. We assume the modulated states impedance is a short or 0 Ω [72] because the impedance varies with distance and the received power at the tag which cannot be measured directly. Using Eq. 6.26 and the values from Table 4.3, the calculated RCS of the RFID tag and antenna combination is -23 dBsqm (0.1215 m^2).

Table 4.3: Radar cross section parameters

Parameter	**Typical Value**
λ (m)	0.328
G_T (dBi)	-1.3
Z_a (Ω)	39 + j 225.8
Z_{L1} (Ω)	23 - j 224
Z_{L2} (Ω)	0
$\Delta\sigma$ (dBsqm)	-23

4.4.3 Return link budget

To complete the link budget for the whole system, the backscatter power is examined. This will allow us to determine the lowest amount of energy that the reader needs in order to detect the signal (this is usually called sensitivity on the datasheet). In the test setup, an Impinj R420 reader was used, which has a default reader sensitivity of -70 dBm, which means that any signal below that power

level will not be detected by the reader. The backscattered power, P_R in dB at a certain distance R, can be determined, by using the calculated RCS ($\Delta\sigma$) and the two-way radar equation 4.6

$$P_R = P_{reader} + G_{tag} + G_{reader} + 10\log_{10}[\frac{\lambda^2\Delta\sigma}{(4\pi)^3R^4}] \tag{4.6}$$

For example, when the Teflon tag was placed 8 meters away, an RSSI of -65 from the Impinj reader GUI was measured. The theoretical value obtained by using eq. 4.6, shows that the received backscatter power is -67 dBm. The discrepancy between the measured and the theoretical value is that the theoretical doesn't take into account pointing losses, multipath, or cable losses.

4.5 Experiment

After verifying through simulation that the tags would perform well, we fabricated and measured the performance in our lab/office hallway. The tags were attached on the metal cylinder and placed on a cart at one end of the hallway. On the other end, there was an Impinj Speedway R420 ISO18000-6C RFID reader, a circularly polarized reader antenna with +8 dBi gain and a 3-dB beamwidth of 60deg, and a PC. Since there isn't a universal metric to measure RFID tag performance, we chose to measure read rate (numbers of reads per second) vs distance, as reported by the Impinj reader GUI.

In the over-the-air experiment, we placed the tag and metal container on top of a cart and varied the distance from the tag to the reader in fixed steps, 0.1 m, 0.5 m, and 1 m for the 0.8 mm Rogers RO4003 tag, 1.6 mm Rogers RO4003 tag, and the 4.7 mm Teflon core tag, respectively. At each location, the total number of reads in 30 seconds was recorded as shown in Fig. 4.6c. The thicker tag was able to achieve much farther read ranges (25 meters) as compared to the other two thinner tag because of its higher realized gain. The 1.6 mm Rogers RO4003 tag has a maximum read range of 6.5 meters with a 10 nH series inductor. The 0.8 mm Rogers RO4003 tag performed worse than the theoretical read range of 3.9 meters and we believe this was due to the manufacturing tolerances causing the center frequency to shift outside the UHF RFID frequency band. As shown in 4.1, the Teflon core tag was able to outperform other similarly sized electrically small metal mount RFID tags.

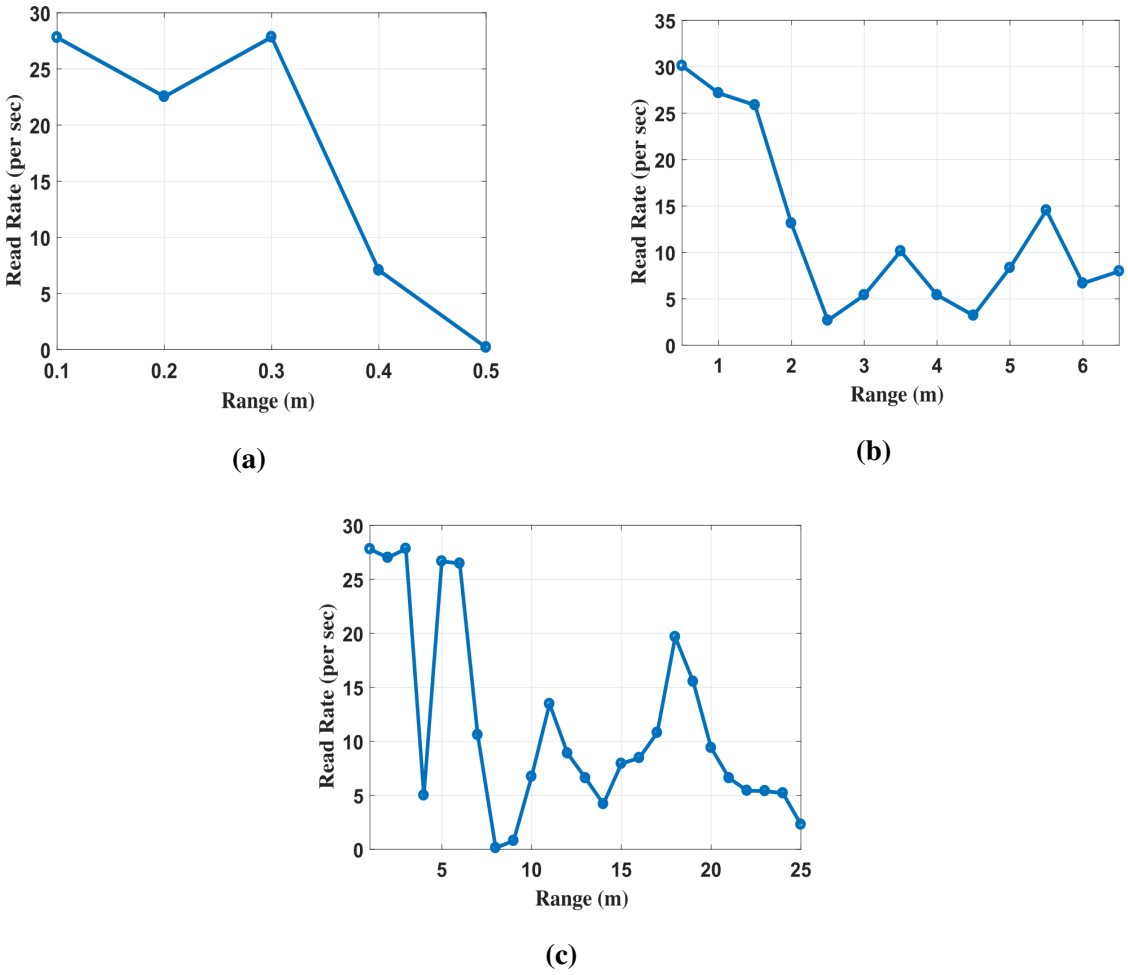

Figure 4.6: *Measured Read Rate vs. Range. (a) 0.8 mm Rogers RO3003. (b) 1.6 mm Rogers RO4003. (c) 4.7 mm Teflon sandwiched between two 0.8 mm Rogers RO4003.*

4.6 Chapter Conclusion

In conclusion, an RFID tag with a split ring antenna design was designed and can be mounted on a metal cylinder, which is used to contain a sealed industrial radiation source. Three separate antennas were designed using a split ring architecture but with different thicknesses. They comprised of a 0.8 mm Rogers 4003 substrate PCB, a 1.6 mm Rogers 4003 substrate PCB, and 4.7 mm Teflon core

sandwiched between two 0.8 mm Rogers 4003. All antennas were designed to match an NXP Inc. SL3S1203FTB0 RFID chip for optimal read range. Frequency domain simulations were presented using CST Microwave studio, the boards were fabricated and hallway read range experiments were done using a standard ISO18000-6C reader and a +8 dBi reader antenna.

The simulated bandwidth of each antenna was 4.4 MHz, 2.8 MHz, and 1.8 MHz, with realized gains of -15.1 dBi, -11.8 dBi, and -1.3 dBi, respectively. Measured read range data was shown and the Teflon had much farther read range (25 meters) than the other tags due to the tag being thicker at the expense of bandwidth. Overall, the thicker Teflon tag was able to outperform the rest of the tags in read range because it was less lossy due to the substrate used and the separation distance between the antenna and ground plane.

Chapter 5

A BATTERY FREE SENSOR TAG WITH FIBER OPTIC TAMPER DETECTION

* This chapter is an adapted version of [73].

5.1 Introduction

In this chapter, a focus on a passive radio-frequency identification (RFID) design that incorporates security features not seen in any commercial RFID chip with the purpose of monitoring hazardous materials is presented. The work described in Chapters 3-4 focused on efficient energy harvesting techniques and the design of an electrically small, high gain antenna. This chapter will explore the design methods of those previous chapters but integrating both the rectifier and antenna onto an RFID sensor tag with a fiber optic loop for tamper detection. This special purpose tag incorporates a custom analog front end (AFE) application-specific integrated circuit (ASIC) and a commercial MSP430 microcontroller to handle all security and RFID operations. Microcontroller-based EPC Generation 2 RFID tags originated with the WISP project, originally developed at Intel Corp. and modified for general release to the public [7]. The combination of low cost and easily modifiable WISP firmware has enabled a growing interest in RFID tags that implement various battery-free sensing and computing concepts [74, 75].

The hazardous material is stored in large containers whose mechanical seal must be continuously checked for indications of tampering. This requirement is addressed by threading a fiber optic loop through the mechanical seal. A random number generator algorithm running in the MSP430 microcontroller produces a continuous stream of random numbers (often called 'nonces'), which are transmitted by the tag into one end of the fiber loop by an infrared LED and checked at the other end with an infrared phototransistor. If the nonce is not detected because the communication link is

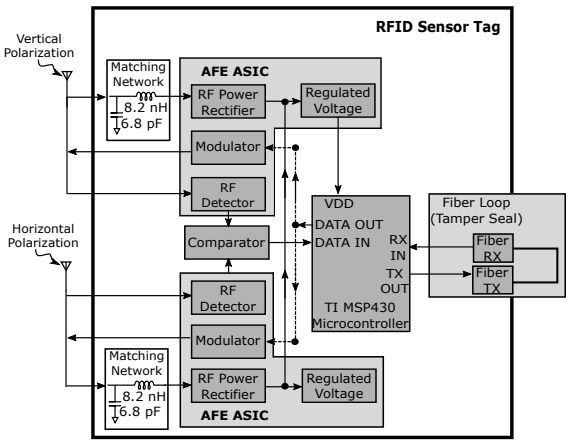

Figure 5.1: *Block diagram of UHF RFID tag*

interrupted, the tag's state (EPC) is changed to indicate a potential tamper event. Another critical feature in this application is battery-free operation. Because the hazardous material must be stored indefinitely in field conditions with widely varying temperature, battery lifetime is difficult to predict [76]. In order to avoid the cost and constant battery replacement, wireless power is an attractive option.

5.2 Related Work

We focused on creating a secure RFID tag for hazardous material tracking. In this application, readers are mounted in the storage area high above the containers, with directional antennas illuminating the containers from above, Fig. 5.2. Important examples of related hazardous material monitoring work are presented in [77, 78]. The Arg-US tag uses active (battery-powered) RFID in the form of bidirectional 433 MHz radio link between tags and base stations. In addition to the complexity and relatively large size of the ARG-US tags, the lithium thionyl chloride (Li-SOCl2) batteries present a significant disadvantage in this application. The ARG-US tag has a claimed battery lifetime of up to 10 years, much shorter than the lifetime of many hazardous materials. Furthermore, such batteries cannot be transported by aircraft, making battery replacement logistics challenging in some locations.

(a) Enclosed RFID Tag and fiber loop.

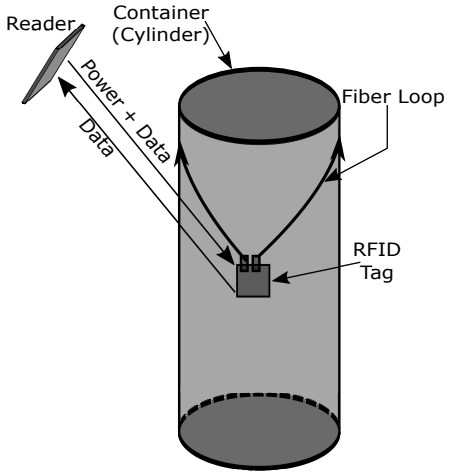

(b) Container installation.

Figure 5.2: *Hazardous material tracking tag and its application*

By comparison, the battery-free tag presented is much simpler, smaller, lower cost and has an unlimited lifetime with no shipping restrictions. Furthermore, when not powered by a reader the proposed battery-free tag is completely inert and does not emit any electromagnetic radiation, so it free of hazards of electromagnetic radiation to ordnance (HERO) [79] and can be moved into areas where explosives are present.

To monitor tampering, the ARG-US tag presented in [77] uses a flexible piezoresistive sensor squeezed between two of the containers attachment bolts and the metal flange of the container. The problem with that setup is that the sensor has to be customized to the specific bolt size. We have addressed this issue by attaching a fiber loop along the seal of the container. We can retrieve the status of the container by producing a digitally designed random number algorithm to outputs a continuous stream of numbers to one end of the fiber loop by an infrared LED, and checked at the other end with an infrared phototransistor. If the random number is not detected, the tag's state (EPC) will reflect an open loop state.

Another critical security feature of an RFID tag for hazardous material tracking is its ability to prevent hackers from hacking the tags. Other work have looked into this issue by implementing

some form of encryption [80, 81, 82]. Although [81] utilizes less hardware than the other encryption methods for passive RFID systems, they can be hacked easily as compared to the AES protocol. Because security is very important for this application, we chose to implement AES encryption into the digital logic portion of our tag design.

5.3 Antenna and Mechanical design

Passive RFID tags operate without the use of a battery or external power supply. The RF signal from an RFID reader is used to supply power to the analog and digital components of the tag. Common RFID tags contain a microprocessor, power rectifier, regulator, modulator, and demodulator. In our tag, we replaced the rectifier, regulator, and modulator with our own custom AFE ASIC, Fig. 5.1. Not only does this reduce the physical size of the tag, but also provides a savings in power

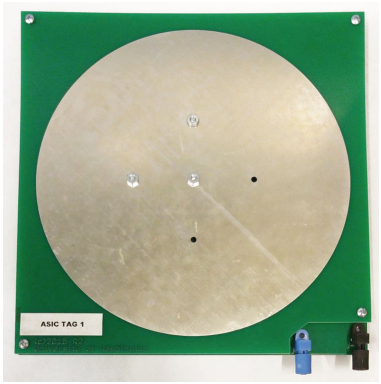

(a) Antenna PCB (top layer).

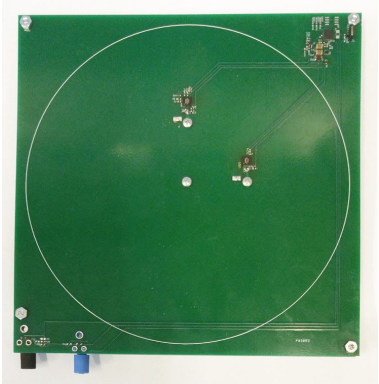

(b) Circuit PCB (bottom layer).

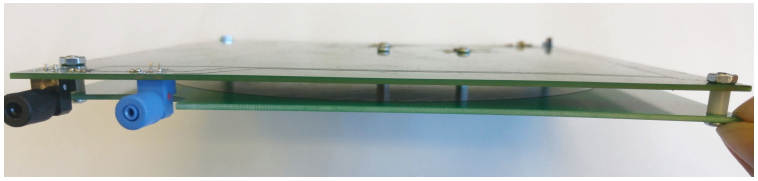

(c) Edge view showing feed and ground posts and fiber TX/RX.

Figure 5.3: *Tag antenna and mechanical design*

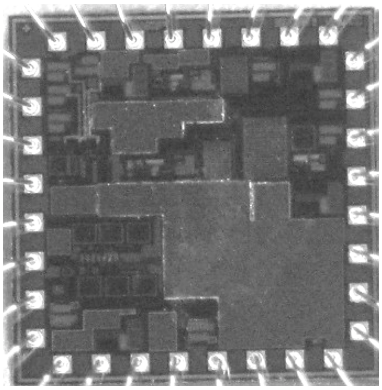

Figure 5.4: *ASIC die photo (1.5 mm x 1.5 mm).*

consumption. To test our custom ASIC, we combined it with an TI MSP430 microcontroller to create a complete microntroller-based UHF RFID sensor tag.

As shown in Fig. 6.11, the tag circuitry is contained on two low-cost double-sided FR4 printed circuit board (PCBs) measuring 19 cm x 19 cm and each board having a thickness of 1.64 mm. The "Antenna" PCB (Fig. 5.3a) contains a 170.8 mm diameter circular patch radiating element on both its top and bottom layers. This element is fed at two orthogonal feed points 32.55 mm from the center to achieve dual polarization. The center of the patch is grounded to suppress unwanted mode coupling between the two feeds. As shown in Fig. 5.3c, the feedpoints and center ground are carried via machine screws and 6.35 mm aluminum posts to the "Circuit" PCB. The top copper layer on the Circuit PCB is an unbroken 2 oz. copper layer (except for clearance for the feed posts). This layer provides the ground plane for the antenna element, forming an air dielectric patch antenna. The bottom layer of the circuit PCB contains all the tags circuitry, including the two RF AFE ASICs, one for each polarization, the MSP430 microcontroller, and the fiber ports, Fig. 5.3b.

5.4 Custom Analog Front End ASIC

As shown in the block diagram of Fig. 5.1, the tag's RF hardware is comprised of two identical AFE ASICs, one for each of the two-dual polarized antenna feed points. This allows a higher effective RF-DC efficiency because in a DC perspective, the chips are connected. The ASIC is implemented in

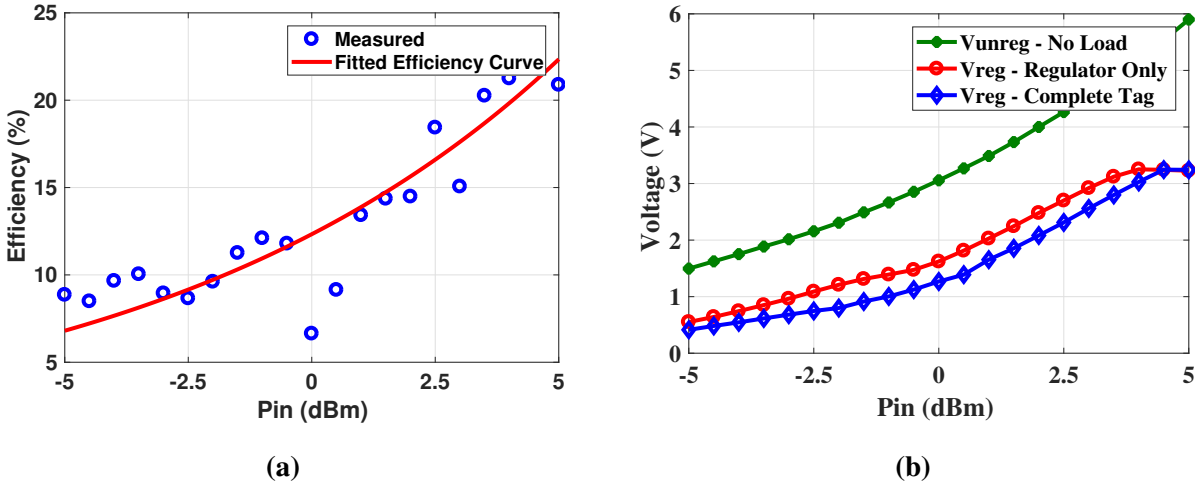

Figure 5.5: *(a) Measured AFE ASIC Harvester efficiency vs. input power (b) Measured AFE ASIC* V_{unreg} *and* V_{reg} *vs. RF input power*

the ON Semiconductor C5N 0.5μ CMOS process and it integrated a 5-stage Schottkey diode-based Villard harvester, a BPSK backscatter modulator, an ASK demodulator, and a voltage regulator. The only required external components are an external L-C matching network and a reservoir capacitor for the harvest DC. A die photo of the ASIC is shown in Fig. 5.4. The die area is 2.25 mm^2 and the chip is packaged in a standard QFN-32 package.

To maximize the amount of power transfer from the antenna to the energy harvester, an external L-C matching network was used. It consists of an 8.2 nH series inductor and a 6.8 pF shunt capacitor. The resulting return loss is shown in Fig. 5.6. The worst-case return loss is better than 20 dB over the 902-928 MHz UHF ISM band at 0 dBm input power. The measured harvester efficiency as a function of input power is presented in Fig. 5.5a. The efficiency of this harvester at 915 MHz and the target input power of +3dBm is around 17%, measured while al components were connected at the output of the rectifier; this includes diodes, capacitors, and the microcontroller. Measured harvester efficienct has come discontinuities because of the time varying nature of the MSP430 microcontroller and the non-linear components (diodes, capacitors). By comparison, to other state-of-the-art energy

harvesters [16], our harvester efficiency has room for improvement. This could be optimized by re-sizing the diodes and designing it for the specific tag load presented to it.

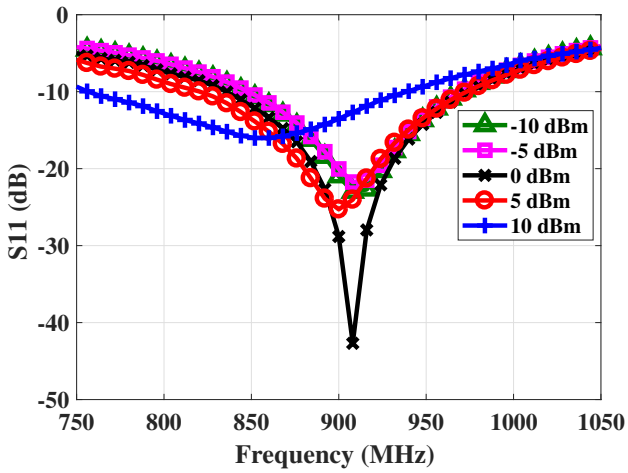

Figure 5.6: *Measured Return loss of Matched AFE ASIC.*

An internal 1.2 V bandgap voltage reference is used to drive an opamp-based shunt regulator with an output voltage of 3.1V. The voltage reference and regulator together draw around 10 μA during regulation. As the regulator enters regulation, there is a spike in regulator current consumption of around 28 μA which is due to unexpectedly high harvester source impedance. We expect that the revised diode sizing will also correct this issue. Fig. 5.5b shows the measured performance of the harvester, reference, and regulator combination as a function of RF input power at 915 MHz, with no load, just the regulator, and the complete tag circuity respectively. The finished tag enters and maintains regulation for RF input power over +3 dBm, as expected.

5.5 Antenna Design and measurements

An important factor in maximizing the read range of an RFID tag is the performance of the tag antenna. A simulation of the antenna was done in Computer Simulation Technology (CST) STUDIO SUITE to characterize the farfield radiation pattern and realized gain of the antenna. The 3D farfield simulation at 915 MHz is shown in Fig. 5.7, the antenna provides a maximum realized gain of 8.5

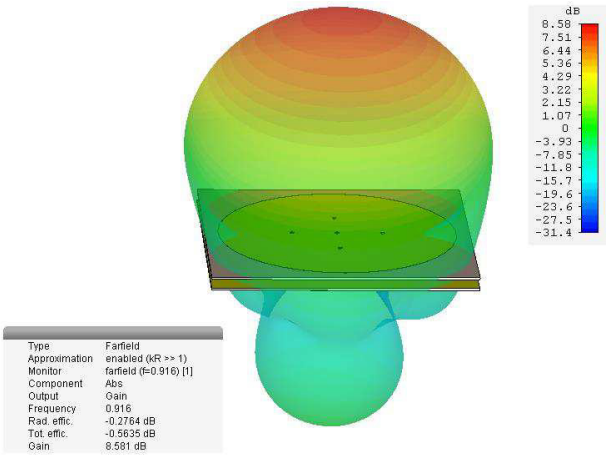

Figure 5.7: *Simulated Co-Polarized 3D Radiation pattern fed from Port 1.*

dBi. Fig. 5.8 provides the co and cross polarization of the antenna. The maximum gain of the tag is unaffected by the orientation while some of the side lobe gain is reduced by the different polarizations. The measured and simulated return and insertion loss of the design antenna is provided in Fig. 5.9. The measured bandwidth of port 2 of the antenna is 20 MHz at a center frequency of 915 MHz, which nearly covers the US FCC, UHF RFID Freq. band (902-928 MHz). Ports 1 and 2 of the antenna are well isolated as shown with a measured insertion loss of -25 dB at 915 MHz.

If we assume that tag read-range is limited by the available RF power from the reader (the so-called forward link limit), the Friis free-space path loss is used to estimate the available power at the tag P_t

$$P_t = P_r + G_t + G_r + 20\log_{10}\left(\frac{\lambda}{4\pi R}\right) - L \tag{5.1}$$

where P_r is the reader transmit power, $G_{t,r}$ are the gains of the tag and reader antennas, λ is the wavelength and R is the tag-to-reader distance. The factor L accounts for cable and connector losses.

By using the simulated realized gain of our designed antenna (8.5 dBi), gain of a commercial reader antenna (8 dBi), and the minimum turn on power of the AFE ASIC (3 dBm), we can estimate

that the theoretical range of this RFID tag would be approximately 5 meters. Measured data of the tag read rate vs range is presented in section 5.7.

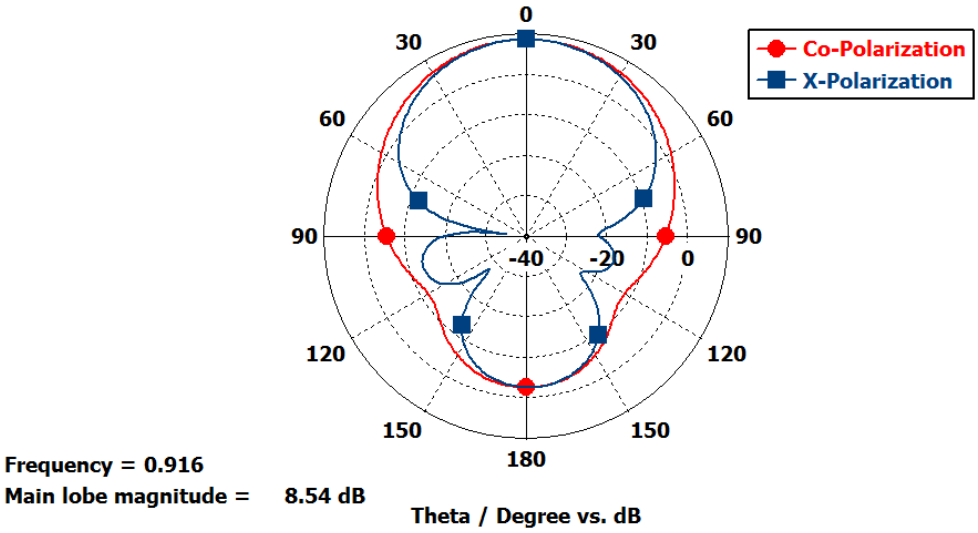

Figure 5.8: *Simulated Co-Pol and Cross-Pol 1D radiation pattern.*

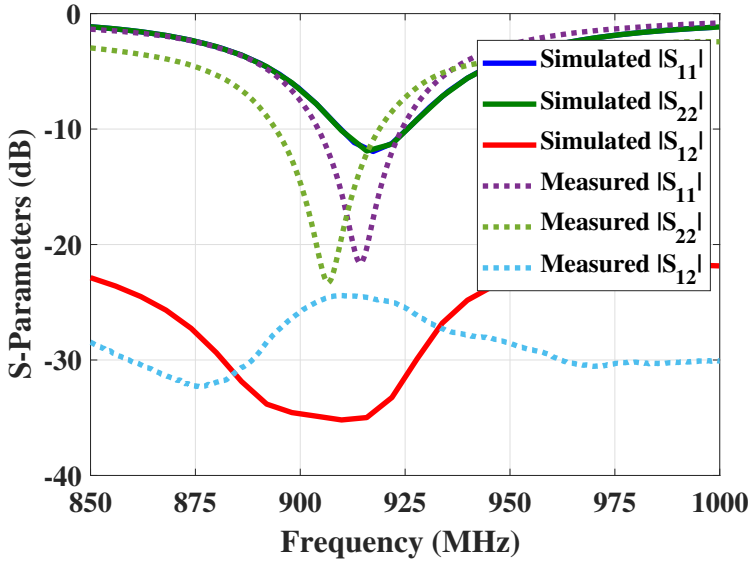

Figure 5.9: *Measured and Simulated S-Parameters of UHF antenna.*

5.6 Digital Security Section

The digital section of the tag consists of a TI MSP430F2132 microcontroller which has 8KB of Flash program storage, 512 bytes of RAM, and a 10-bit analog to digital converter (ADC). It performs all of the RFID and security functions (tamper detection using fiber loop and authentication using AES encryption). When the tag is stationed 1 meter away (+15 dBm input) from the reader, the MSP430 operates nearly continuously and consumes 787 μA average (2.3 mW). At greater distances, the duty cycle decreases leading to much lower average power consumption.

The fiber loop consists of an Industrial Fiber Optics IF-E97 660 nm emitter and IF-D92 detector. The fiber itself is a 1 mm plastic optical fiber rated for a temperature range of -40 C to +125 C. We can verify the fiber loop status (open or closed loop) by sending a stream of random numbers from one end of the fiber and verifying the random numbers at the other end, using the MSP430 microcontroller.

The fiber emitter and detector have an average power consumption of 59.74 μW (34.75 μA) and a max power consumption of 1.4mW. Resistive wires are an alternative tamper mechanism and an advantage that it has over the fiber loop is that it consumes much less power but at the expense of security. Resistive wires can be easily spliced and manipulated so that the tag wouldn't report a tampering event, a false negative. If the same tampering method were to be used with our fiber loop, it would have to take place in a matter of milliseconds because of the frequency at which the nonces are verified by the MSP430.

In this work we use a simple challenge-response authentication, to prevent tag cloning and eavesdropping. Our setup consists of a backend system (computer) that generates 16 challenge bits, which are sent from the reader to the tag. After the reader calls the 'select' GEN2 command, those 16 bits are stored in the memory of the microcontroller. Once the reader performs the 'ACK' GEN2 command, the tag sends an encrypted 16 challenge bits, tag ID, fiber loop status, and key. The data is then decrypted on the backend system to verify that both the key and tag ID that were sent from the tag are in the database and if the challenge bits that were generated and received are a matching valid pair. This database contains all verified tags that should be in the environment. If the tag is authentic,

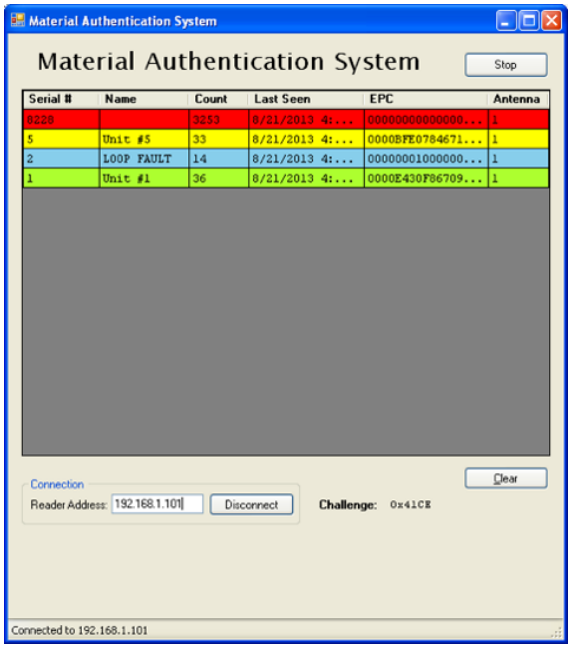

Figure 5.10: *Reader GUI showing Authentication*

the backend system GUI provides the Electronic Product Code (EPC) of the tag and a fiber loop status (open or closed loop), Fig. 5.10. The different authentication statuses are color coded on the custom GUI where red indicates an unknown tag, yellow means a previously authenticated tag timed out during the reading process and will be checked again, blue indicated there is an authenticated tag but the fiber loop has been broken, and lastly green means the tag is authentic and the fiber loop is in tact.

5.7 Range Measurements

We conducted a series of experiments focused on characterizing the real-world read rate vs range of both tag implementations described in this paper. Tag-rich environments benefit greatly from high read rates because the reader would be able to sequentially read all tags present in the environment in the shortest possible time.

In our over-the-air experiments, we had a computer set up with an Impinj Multi-reader Software,

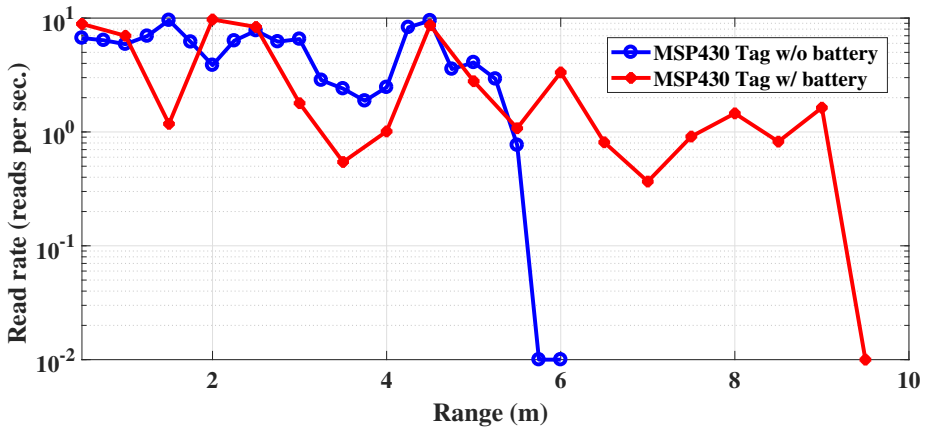

Figure 5.11: *Measured reads per second with and without a battery present*

a stationary Speedway R420 reader, our Analog UHF tag, and one circularly polarized reader antenna of +36 dBm with a gain of 8 dBi. To get our first set of data measurements, we mounted the reader and a circularly polarized reader antenna (Laird Technology S9028PCR) on top a cart at the end of the hallway. The microcontroller-based tag was mounted on another cart.

We then varied the distance from the reader to tag by 0.5 m steps at a starting distance of 0.5 m up to the tags max read distance. At each location, we recorded the total number of reads in 30 sec. As shown in Fig. 5.11, the microcontroller-based tag in passive and active mode was read more than once per second at up to 5.5 m and 9 m, repectively. The microcontroller-based tag's maximum read rate is limited by the available energy and the MSP430 microcontroller processing speed.

5.8 Chapter Conclusion

In this chapter, an ISO18000-6C (EPC Generation 2) battery free RFID sensor tag with fiber optic tamper detection for hazardous material monitoring and sensing was presented. We have successfully integrated two security features that are not seen in any commercial RFID tag, using firmware designed on a general purpose TI MSP430 microprocessor. With the use of a fiber wire, we can detect tampering of the tag by sending random 'nonces' through an LED and receiving it at the other end. We incorporated AES encryption through the RFID transmissions to prevent hackers

from intercepting the packets sent from the receiver to tag and vica versa.

The tag is housed in a ruggedized enclosure that incorporates a dual-polarized 6 dBi antenna for 902-928 MHz UHF RFID band. It integrates two custom UHF RF analog front end ASICs with a general purpose TI MSP430 microcontroller. The tag has a power-up threshold of +3 dBm due to the power requirements of the fiber-optic tamper detection loop. We designed a circular patch antenna with an air dielectric that has a simulated realized gain of 8.5 dBi. With this setup, we were able to achieve a measured operating range of over 5.5 meters in passive mode and 9 meters in active mode with a +36 dBm EIRP EPC Generation 2 reader.

Chapter 6

KILOMETER-RANGE BATTERY-FREE BACKSCATTER SENSOR TAG

6.1 Introduction

This chapter focuses on a new combination of approaches for battery-free wireless communication and sensing to maximize operational tag range. We present a passive battery-free backscatter tag topology that performs analog backscatter communication (not constrained by the power consumption of digital electronics) while having both ultra-low power and ultra-low voltage operation. Up to this point, we have explored methods of wireless power harvesting at 2.4 GHz using a timer based boost converter. We then designed an electrically small passive RFID tag capable of read ranges of 25 meters while attached to a metal cylinder. Here we explore an approach to significantly reduce the sensitivity of the passive backscatter tag by incorporating an efficient rectifier at low power levels, an ultra-low power baseband generator, and a high gain antenna. One of the difficulties of the design

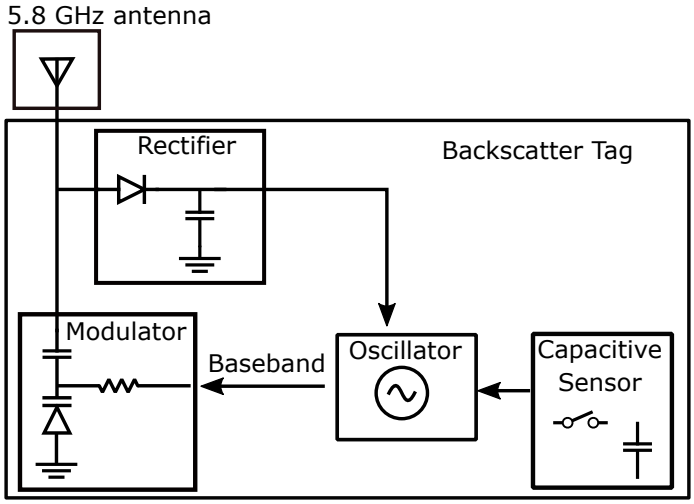

Figure 6.1: *Block diagram of 5.8 GHz backscatter tag*

of the tag is that it is constrained to a dollar sized bill area, which means the antenna and all the circuitry will need to fit on the board. In addition, a capacitive sensor is added to provide sensing capabilities and analog telemetry to further expand on analog frequency modulated backscatter sensing [83].

There are numerous backscatter tags in the ISM bands, specifically the 915 MHz band because of the popularity of RFID. The latest 915 MHz backscatter tag designed by Talla et al achieves 2.8 km backscatter by using chirp spread spectrum (CSS) modulation and low power circuitry [9]. The problem with their work is that they require a battery and they employ a bistatic dislocated configuration, where the tag is seperated from the transmitter by only 5 meters. In contrast, this work will be fully passive and operate in the bistatic co-located configuration. Emerging backscatter techniques in the 2.4 GHz band have been studied as well because of the availability to adhere to commercial products like WiFi and Bluetooth. Although there are many tags in these frequency bands, there is sparse research on backscatter tags in the 5.8 GHz band, [13, 84, 14, 85, 86, 87]. While most of the research has been focused on the application side at 5.8 GHz, there isn't sufficient research on extending range.

A comparison of this work, Table 6.1, shows that not only does this tag outperform other backscatter communication tags at 5.8 GHz [13, 14], but it also outperforms tags at other RF frequencies, 915 MHz and 2.4 GHz. In Amato et al's work, they focus on extending the range of a 5.8 GHz tag to kilometer read ranges by removing a lot of the unnecessary components in a transmitter like the amplifier. They employ a tunnel diode that is biased using a square wave generator that adjusts the impedance presented to the antenna. This creates a strong backscatter signal that can be detected from 1.2 km separation distance. The problem though is that this device requires a square wave generator that has a power consumption of 20 μW, if this same design were to be designed as a passive tag with 100% rectifier efficiency, the tag would have a sensitivity of -17 dBm, which is well below the -23 dBm we are able to achieve in this work. This is done by removing all the unnecessary components in a transmitter like the amplifier but also reducing the local oscillation frequency in which the power consumption of the tag is minimized.

The work presented here focuses on wide area communication and sensing at 5.8 GHz that

Table 6.1: Comparison of several backscatter tags

	Thomas [71]	Talla [9]	Sample [7]	Pillai [12]	Shirane [13]	Amato [14]	**This Work**
Frequency (MHz)	915	915	915	2400	5800	5800	**5800**
Power consumption (μW)	1230	9.25	9	1.05	125	20	**0.5**
Startup voltage (mV)	1300	1500	1800	200	600	60	**15**

focuses on optimizing the design of the rectifier, oscillator, and antenna design. This would allow us to design, to our knowledge, the first passive 5.8 GHz tag capable of operating down to 15 mV and -23 dBm, where conventional circuits are not operational. Conventional communication circuits typically require at least 1.8 V to power a frequency synthesizer, microcontroller, and/or RF amplifiers, reducing the operational range of a completely passive system. This system does not require an RF amplifier, and it removes the microcontroller for communication and replaces it with a low-power, low-voltage Colpitts oscillator.

A block diagram of the system is shown in Fig. 6.1. The important pieces to consider are the power consumption of the oscillator, the efficiency of the harvester, and the realized gain of the antenna. The backscatter tag fully operates with only the RF signal intercepting the tag. Characterization of the tag includes harvested start-up voltage and power consumption measurements of the analog components. A measured RF-DC efficiency of 5% at -23 dBm was observed with -23 dBm being the cold-start RF power (sensitivity) needed to both power the tag and perform communication. In a cabled benchtop test, a 100 kHz backscatter signal was detected that has -68 dBm of power. An outdoor 517 meter experiment provided additional validation that this tag is capable of backscatter from a kilometer separation distance.

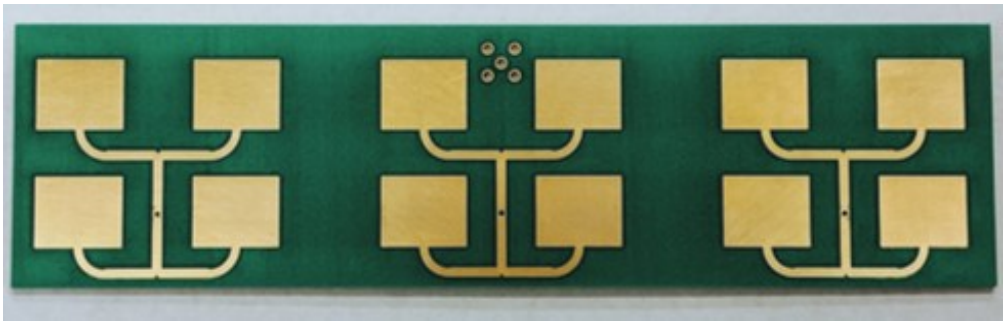

Figure 6.2: *5.8 GHz quad patch antenna design*

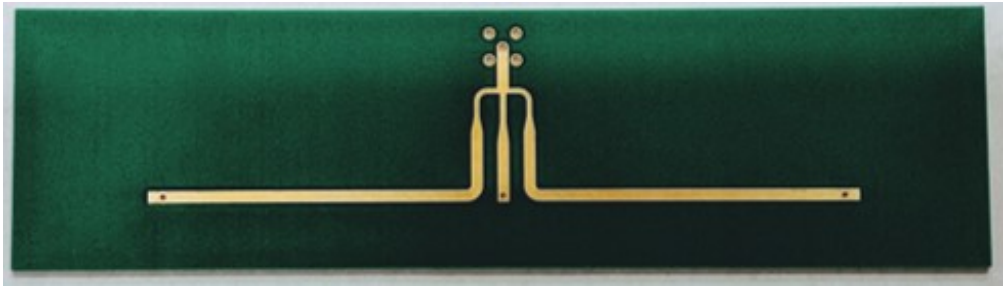

Figure 6.3: *Three-way planar type 2 Wilkonson power splitter*

6.2 12 element antenna array Design

One of the biggest constraints of this work is that the dimensions of the antenna, as well as the rest of the circuitry, needs to fit in the area of a dollar bill (155 mm x 66.3 mm). This limits the maximum gain that can be achieved of the antenna. A microstrip patch antenna design was used because it allowed us to design on a printed circuit board (PCB), while being low-cost, and having high gain. One of the disadvantages is that the bandwidth is considerably smaller than other antenna designs. In this application, bandwidth doesn't play a huge role because we are transmitting and receiving at a single frequency. We designed a 12 element array that constitutes three sets of a quad patch array to maximize gain within the space allowed. Each port of the array were attached using a three-way planar type 2 Wilkonson power splitter, Fig. 6.3. The splitter plays an important role since it combines the power equally from each array, which would allow for a larger main lobe.

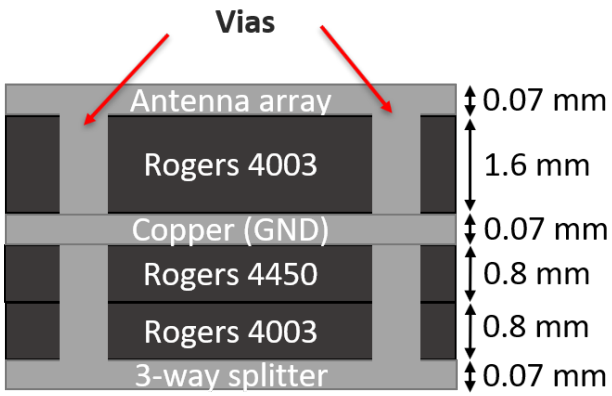

Figure 6.4: *Fabricated Antenna Stackup*

The antenna board has dimensions of 49 mm x 181 mm and is made on Rogers 4003 substrate. The antenna stack-up (Fig. 6.4) consists of three layers where the top layer contains 1 oz copper and 60 mil Rogers 4003, the middle layer contains 1 oz copper and Rogers 4450, and the bottom layer contains 1 oz copper. The top layer contains the antenna, as shown in Fig. 6.2. This design incorporates three sets of the quad patches ([88]), where each additional patch increases the gain by a factor called the array factor [89]. The array factor quantifies the effect of combining multiple arrays without taking into account the effect of the single antenna element. The total radiation pattern of the structure can be obtained by combining the array factor with the single antenna element. In this design, the normalized array factor for three sets of the quad patches can be written as

$$AF = \left| \frac{\sin(\frac{N\Phi}{2})}{N \sin(\frac{\Phi}{2})} \right| \tag{6.1}$$

$$\Phi = \frac{2\pi}{\lambda} d \cos(\theta) + \beta \tag{6.2}$$

where the normalized array factor is dependent on the number of elements (N), the element spacing (d), the polar angle (θ), and the phase difference between the arrays (β). The maximum array factor for three sets of the quad patches is 3 (4.77 dB). This is the additional gain that the antenna will have as compared to a single quad patch array. While simulating a single quad patch array, the total

realized gain was about 10.5 dBi, which means that the total maximum realized gain should be about 15.3 dBi, assuming that everything is matched and low losses.

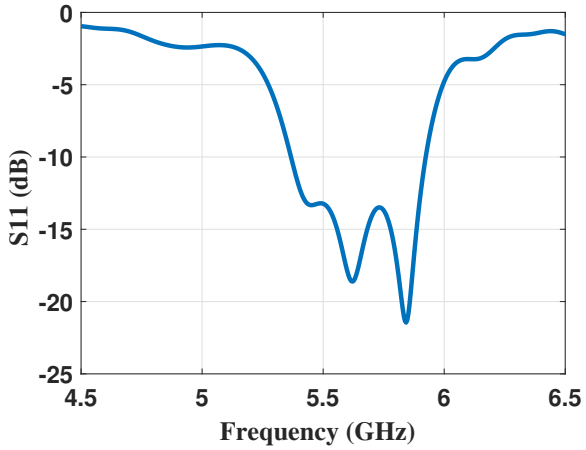

Figure 6.5: *Simulated Antenna S-parameter (S11)*

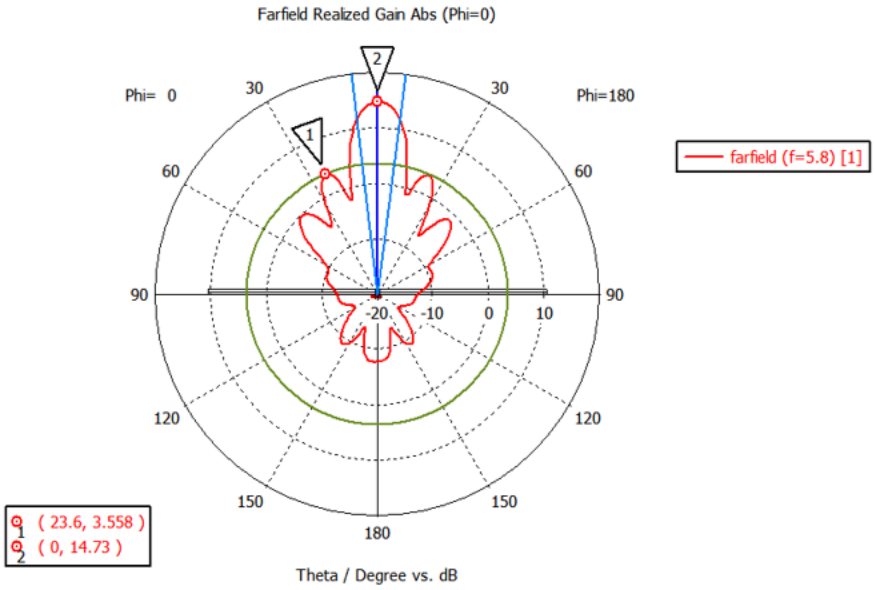

Figure 6.6: *Gain of 5.8 GHz quad patch array*

The bottom layer contains the three-way Wilkinson power splitter (Fig. 6.3), where the inputs to the splitter are connected to each of quad patch arrays by a via. The output of the spitter is then matched to 50 ohms. The simulated S-parameters for the splitter is shown in Fig. 6.7. Through optimization of line lengths and widths on CST Microwave Studio, we were able to achieve optimal matching over a wide bandwidth, with a simulated return loss (S11) of -15.3 dB at 5.8 GHz, S21 of -5.23 dB, S31 of -5.75 dB, and an S41 of -5.22 dB. The losses at each of the feed ports are marginally equal, this is important because it allows the antenna to achieve maximal gain and a more directed beam. The three-way splitter achieves almost the same amount of losses at each of the feed ports, resulting in higher gain and a more directed beam.

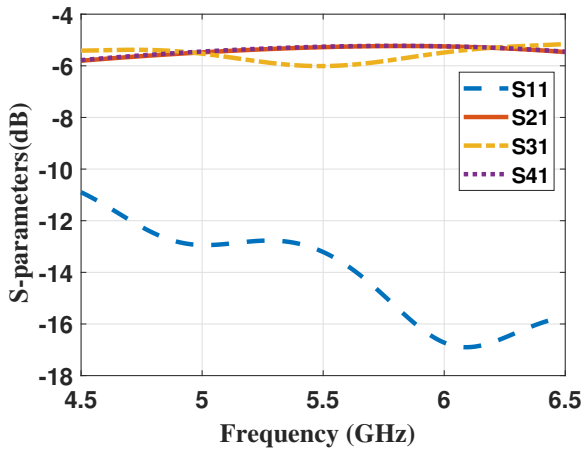

Figure 6.7: *Wilkonson three way splitter simulated S-parameters*

The time domain method (TEM) solver built into CST Microwave Studio was used for the design and optimization of the antenna. Simulation shows that the full antenna structure (quad patches and splitter) is well-matched with a -10 dB bandwidth from 5.368 to 5.923 GHz (550 MHz) and a return loss of -16.8 dB at 5.8 GHz, Fig. 6.5. The antenna has a maximum realized gain of 14.72 dbi along the ϕ = 90 direction, with a beamwidth of 23.6 degrees as shown in Fig. 6.6.

6.2.1 Antenna measurement results

To determine whether the fabricated antenna can efficiently capture power from an incident RF signal, measurements were done to determine the realized gain of the antenna. Measurements were performed in an anechoic chamber with a set of identical fabricated antennas each separated 3.25 meters away from each other, Fig. 6.8a.

The measured gain of the antenna was performed by using a vector network analyzer (VNA) to measure S_{21}, the power received at antenna 2 from the transmitted signal at antenna 1. With this setup, we can solve for the gain of the antenna by using a modified Friis equation

$$S_{21} = 20log(\frac{\lambda}{4\pi d}) + G_t + G_r \tag{6.3}$$

where S_{21} is the measured power received at port 2 from port 1 (Fig. 6.8b), λ is the wavelength, d is the antenna separation distance, G_t is the transmitter antenna gain, G_r is the receiver antenna gain. Since the transmitter and receiver antennas are identical, we can combine the expressions to solve for the gain of one of the antennas.

$$G = \frac{S_{21} - 20log(\frac{\lambda}{4\pi d})}{2} \tag{6.4}$$

The measured S21 of the pair of antennas at 5.8 GHz is -31.9 dB, the path loss at 3.25 meters is -57.95 dB, and this resulted in an antenna gain of 13.03 dB. This is about 2 dB off from the simulated and this might be due to manufacturing tolerances and slightly different substrate epsilon.

6.3 Link Budget

The goal of this work is to achieve backscatter communication and sensing from distances up to 1 kilometer. One of the greatest difficulties with designing a passive tag that is capable of communication from these distances is the free-space path loss (FSPL). Path loss can be calculated using

$$FSPL(dB) = 20\log(\frac{\lambda}{4\pi d}) \tag{6.5}$$

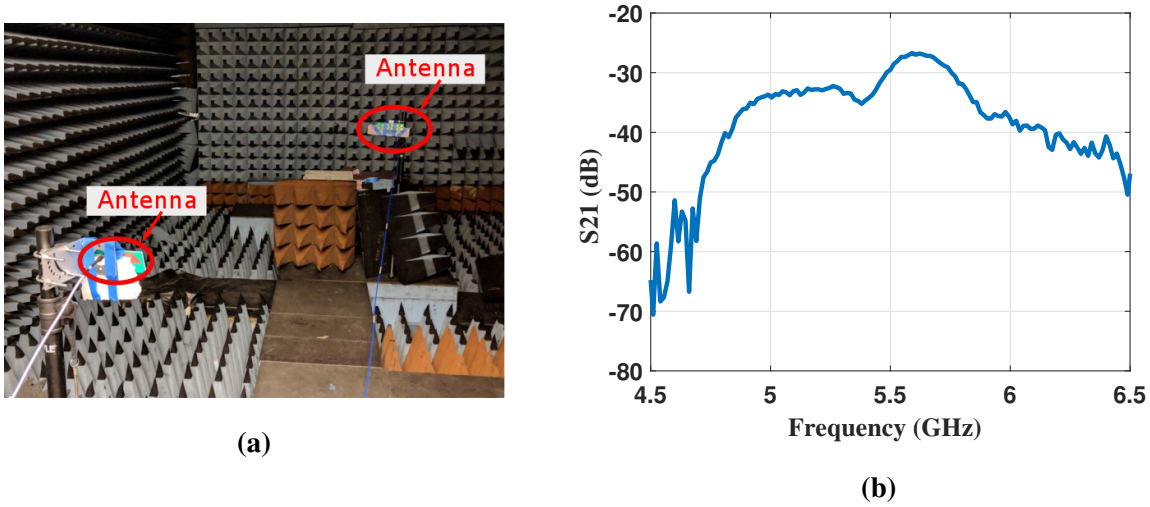

(a) **(b)**

Figure 6.8: *(a) Anechoic chamber setup (b) Measured S21 of pair of quad patch arrays in anechoic chamber*

where λ is the wavelength and d is the separation distance from the transmitter to the backscatter tag. By using this equation and using an operation frequency of 5.8 GHz, a path loss of -108 dB (not accounting for antenna gain) is observed at 1 kilometer. This is more than 34 dB greater than similar work that explores kilometer sensing and communication at 915 MHz [9].

The reason why we are exploring backscatter communication at a higher frequency compared to others in the literature is because it allows us to design a smaller antenna but with higher gain. This is important because if we were to create a backscatter communication system at 915 MHZ with the same transmitting, receiving, and tag antenna dimensions as this work, that system would have more losses. To get an idea of how this works, lets assume that the transmitting and receiving antenna both have a diameter of 1m and the tag antenna is the area of dollar bill. We can use the equation below to solve for the theoretical gain (G) of a parabolic dish

$$G(dB) = 10\log((\frac{D\pi}{\lambda})^2 * \eta) \tag{6.6}$$

where D is the diameter of the antenna in meters, λ is the wavelength, and η is the efficiency.

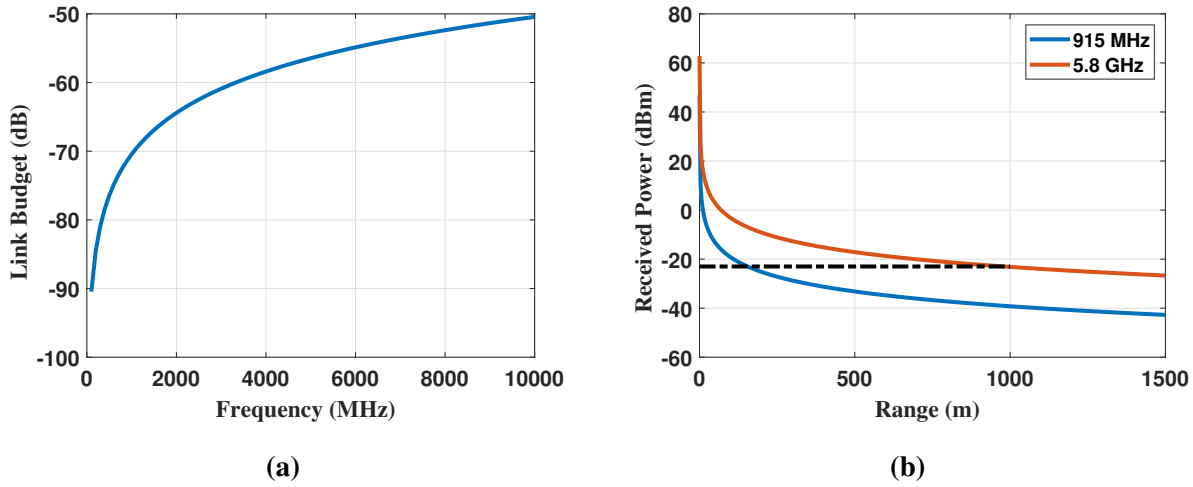

Figure 6.9: *(a) Link Budget accounting for similar sized antennas and its maximum gains and propagation loss vs. Frequency (MHz) (b) Theoretical received power at tag end vs. Range (meters)*

Fig. 6.9a is a plot of the link budget accounting for the theoretical gains of the antennas and the propagation loss in respect to frequency. As can be seen, with similarly sized antennas, the link budget is actually worse at lower frequencies. Comparing the ISM bands, 5.8 GHz is more than 16 dB better in the one way link budget compared to 915 MHz. If we were to transmit 32 dBm of power with a 915 MHz system and a 5.8 GHz system, to achieve 1 km communication, the 915 MHz tag would have to be 20 dB more sensitive, Fig. 6.9b. Although the next commercial ISM band is at 24 GHz, it is difficult to create backscatter circuitry (rectifier, oscillator, and modulator) at those frequencies which is why 5.8 GHz was the favorable option.

To get an idea of how much the real-world path loss is compared with the theoretical path loss, an outdoor experiment was performed. The experiment setup consisted of a spectrum analyzer and a 32.5 dBi dish antenna placed on a balcony pointed towards the tag antenna with a separation distance of 946 m. On the other end, a handheld signal generator is connected to the fabricated antenna, Fig. 6.10. The measured forward path loss with this setup is 106.5 dB, not accounting for antenna gains, which aligns well with the theoretical path loss. The 2 dB difference can be attributed to the

antenna separation not being exactly 1 km, the outdoor setup was 50 meters shorter. Also, there are trees, cars, and a water fountain obstructing the direct line of sight.

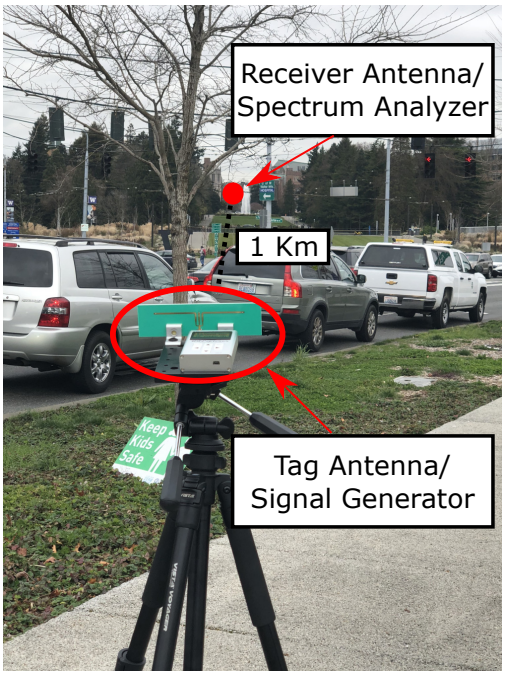

Figure 6.10: *1 km path loss antenna setup with handheld signal generator*

6.4 Backscatter Tag design and Characterization

The backscatter tag design focuses on low-power circuitry with an emphasis on low-voltage operation. With the tag being designed for kilometer range communication, it is difficult to harvest enough voltage necessary to start-up the circuit for backscatter operation. This section will explore the design and characterization of the rectifier, the low-voltage, low-power oscillator, and the modulator that is able to operate down to -23 dBm at 15 mV.

6.4.1 5.8 GHz Harvester design

Our system requires minimizing the amount of energy needed to operate the device. For a passive backscatter tag, the energy comes directly from the RF signal that's intercepting the tag. A harvester

is needed to capture the signal from an RF source to charge a capacitor, thus providing energy for communication. A harvester is composed of an RF-to-DC conversion (also known as rectifier) and an energy storage component (usually a capacitor). We can manipulate the amount of energy produced from the harvester by either: increasing the harvested voltage or increasing the energy reservoir capacitor value.

To increase the harvested voltage, a multi-stage rectifier can be employed which would provide voltage multiplication dependent on the number of stages [90]. The more voltage applied to the reservoir capacitor, the more energy stored in the capacitor. Increasing the capacitor value would also provide the same effect by increasing the maximum charge the capacitor can store, $Q_{max} = CV$. An unfortunate tradeoff to both of these approaches is that (1) increasing the rectifier stages, decreases efficiency due to parasitic capacitance [91] and (2) increasing the reservoir capacitor increases the charge time.

The reservoir capacitor is used to power an oscillator to provide the baseband operation, so determining the correct value is important as to not deplete the energy too soon. What exactly is the minimum reservoir capacitor needed to supply energy to the oscillator? A detailed analysis of

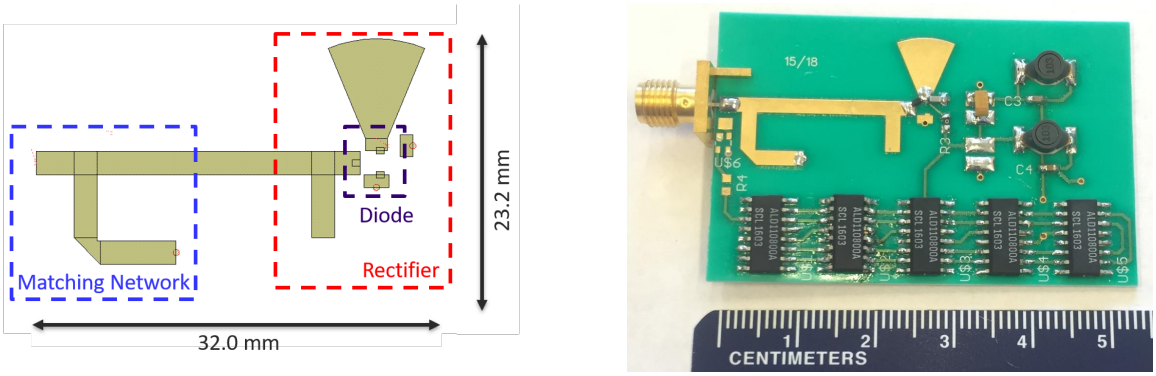

(a) **(b)**

Figure 6.11: *(a) Rectifier with matching network (b) Fabricated tag design including rectifier, oscillator, and modulator*

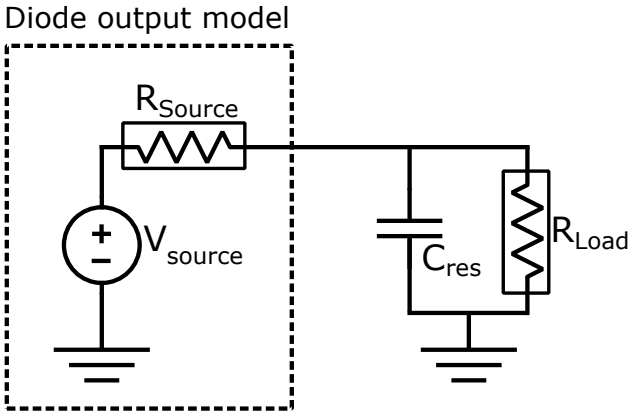

Figure 6.12: *Circuit model of rectifier output including nonlinear source and load resistances*

the oscillator will be described in the next section but the oscillator consumes 0.25 μW of power to function. This value is important in deciding the capacitance needed to not only drive the oscillator but to make sure that there isn't much energy lost every cycle.

To determine the amount of capacitance required to run the oscillator, one needs to know the amount of charge flowing into the capacitor when the oscillator is operational. Storing energy on a capacitor involves building up charges on each plate of the capacitor, inducing an electric potential energy. Work is required to transport each charge dq onto the capacitor and when the voltage increases, the work required to transfer these charges to the plate increases. The summation of these charges dq can be summarized as

$$E = \int_0^Q \frac{q}{C_{res}} dq \tag{6.7}$$

where E is the energy stored on the capacitor in Joules, q is the charge, and C is the capacitance. We can then solve for this integral to find the minimum capacitance needed given the power consumption of the oscillator and the maximum harvested voltage at a given power level. The energy stored on the reservoir capacitor C_{res} becomes

$$E = \frac{1}{2} C_{res} V^2 \tag{6.8}$$

where V is the voltage measured across C_{res}. The amount of stored energy is based on the voltage across the capacitor and the value of the capacitor. Since the capacitor is charging and discharging periodically, the useable energy stored on a capacitor is the difference between the stored energy of the capacitor after 1 charging period (V) and the stored energy of the capacitor when it is only charged to the threshold voltage (V_{th}) of the system (15 mV). The expression for useable energy becomes

$$E_{useable} = \frac{1}{2} C_{res} (V - V_{th})^2 \tag{6.9}$$

From the cabled measurements, we know that with -23 dBm (5uW) RF input, the efficiency was 5%, so the total power available at the reservoir capacitor is 0.25μW. The power (P) available at the tag is a function of energy and time

$$P = \frac{E}{t} \tag{6.10}$$

In our tag design, a 10 uF reservoir capacitor was used. With an RF input power of -23 dBm, the voltage across the capacitor is 18 mV. By using equations 6.8 and 6.9, we can solve for the amount of time it takes to charge the capacitor. The total energy stored in the capacitor is 0.495 nJ and the total time it takes to charge to 0.25 μW is 1.98 ms.

In our proposed harvester design, a single-stage diode based rectifier was used because the intercepted RF power is minimal at long ranges and rectifier efficiency becomes even more important. The Skyworks SMS7630 Schottky diode was used in the design because of its performance at high frequencies and its low threshold voltage, which is needed to achieve high efficiency at low input powers [92]. An open stub matching network was implemented to maximize the power transfer from the quad patch antenna to the single-stage diode based harvester. A radial stub is added to provide an RF short at the output, Fig. 6.11a. The rectifier was designed and optimized using AWR Microwave Office to achieve optimal matching at 5.8 GHz. It was designed on Rogers 4003 substrate with copper microstrip lines. The fabricated tag including the rectifier, oscillator, and modulator is shown in Fig. 6.11b.

Measurements of the rectifier and matching network were performed using an Agilent N5222A

network analyzer. A plot of the both the simulated and measured return loss at -20 dBm input power is shown in Fig. 6.13a. The fabricated rectifier is well matched at 5.8 GHz with a -10 dB bandwidth of 204 MHz (5696 MHz - 5900 MHz). As the input RF power decreases, the matching gets worse and this is due to the diodes change in impedance due to the non-linearity. The harvested output voltage with an open circuit and the complete tag (with oscillator and modulator as the load) of the tag is shown in Fig. 6.13b. A harvested efficiency of 4.7% was observed (Fig. 6.14a) at -23 dBm, which follows the trend for 5.8 GHz rectifier designs in the literature, [16]. To the best of our knowledge, this is the best rectifier efficiency given an input power of -23 dBm.

The source of the losses in the harvester can be obtained through simulation using AWR. With a an efficiency of 4.7% at -23 dBm, that means that 95.3% of the input power is lost. With the harvester, there are two dominant sources of loss, this includes the loss due to the Rogers substrate and the loss due to the diode. The loss due to the matching network transmission line from the input source to the diode can be simulated by de-embedding the diode from the transmission line and matching circuit then doing two simulations, 1) simulate the loss of the transmission line with a loss

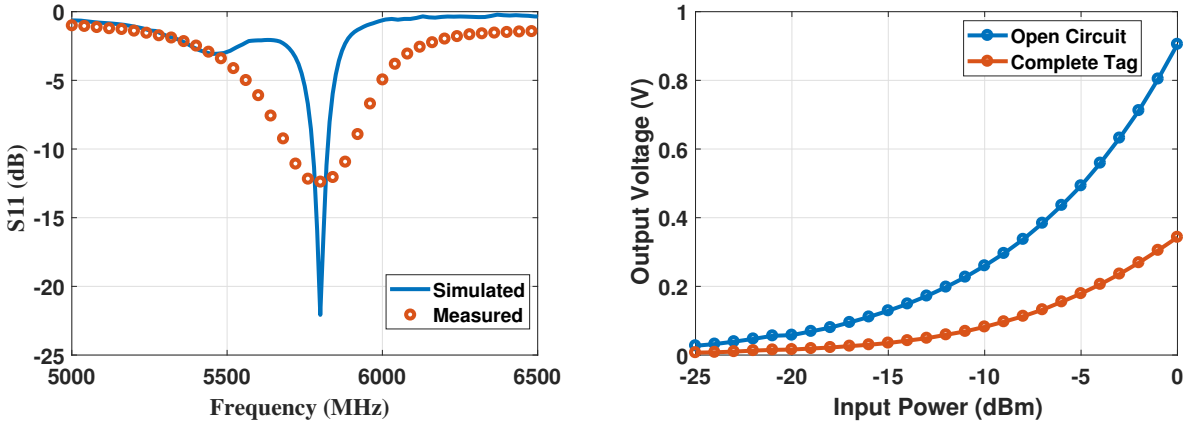

Figure 6.13: *(a) S11 measurements for the simulated and measured rectifier matching network at an input power of -20 dBm (b) Measured harvested voltage with open circuit and complete tag*

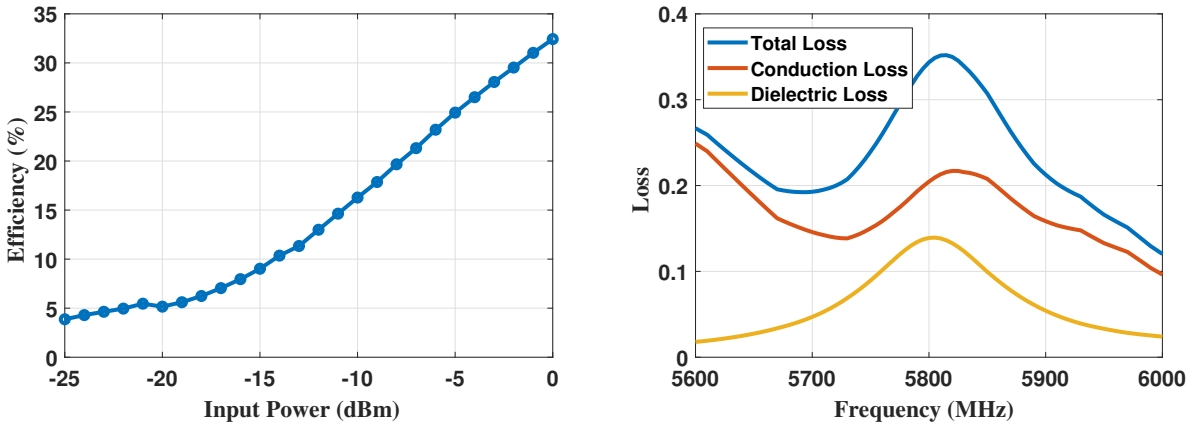

Figure 6.14: *(a) Measured rectifier RF-DC efficiency vs. RF input power (dBm) (b) Simulated line losses (conduction and dielectric loss) with respect to frequency*

tangent of Rogers 4003 substrate (0.0024), this simulates total loss of the line which includes the conduction loss and dielectric loss. 2) Simulate the loss of the transmission line with a loss tangent of 0, this simulates only the conduction loss. 3) Take the difference of the loss with Rogers substrate to the loss of the simulation with 0 loss tangent. This can be used to solve both losses. By simulating the total power accounted for in the S-parameters for the matching circuit line, the loss accounted for is 34.35% of the total losses, where 20.46% is due to conduction loss and 13.9% is due to dielectric loss, Fig. 6.14b .

The diode efficiency changes with a change in input power and because we are focused on low input power operations, most of the efficiency loss is due to the forward diode build-in potential (V_{bi}). When the input power is low, the reverse bias voltage (V_O), which comes from the load connected to the rectifier, is usually smaller than V_{bi}. In the low power region, the loss due to the diode can be approximated [93]:

$$Loss_{diode} = \frac{V_{bi}}{V_o + V_{bi}} \tag{6.11}$$

Using the equation above, we can predict the diode loss using the built in voltage of the SMS7630

(which can be found in the datasheet) which is 0.34 V and the 15 mV output voltage of the rectifier at -23 dBm input power, this turns into a diode loss of 95.77 % (3.13 μW). This is the loss of the diode but to get a complete analysis, including internal resistance, the diode model will be examined further.

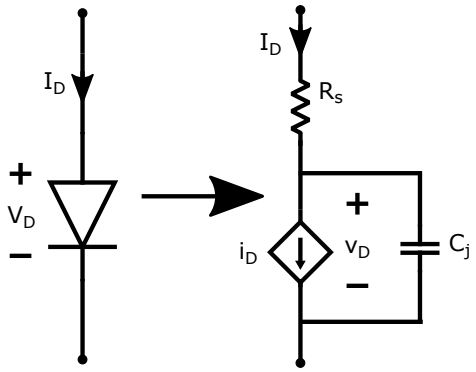

Figure 6.15: *Diode equivalent SPICE model*

The circuit in Fig. 6.15 provides the equivalent SPICE model for a diode. A diode consists of a series resistance R_s, a non-linear current source i_D, and a non-linear junction capacitor C_j. Resistance R_s is formed due to fabrication and the diode contacts to the package and requires a change in fabrication design to change its properties. The internal current source (i_D) represents the current flow through the diode as a function of applied voltage as described by

$$i_D = I_S \left[e^{\frac{v_D}{nV_T}} - 1 \right] \tag{6.12}$$

where I_S is the saturation current, v_D is the diode voltage, V_T is the thermal voltage which is 26 mV under room temperature, and n is the ideality factor. The junction capacitance is an important specification for diode choice as it has an effect on efficiency by changing the low-pass frequency response of the diode. This frequency response is due to the diode junction capacitance and the diode junction resistance (r_j)

$$r_j = \frac{8.33 * 10^{-}5nT}{I_b + I_s} \tag{6.13}$$

where n is the ideality factor, T is temperature in Kelvin, I_b is the externally applied bias current in

amps, and I_s is the saturation current. By lowering the junction capacitance, the corner frequency is increased, allowing the input signal to operate under the passband of the diode.

The diode power dissipation can be split into two parts, the series resistance and the diode itself (the current source and junction capacitance). The average power dissipation of the small internal series resistance R_s can be calculated using

$$P_{R_s} = \frac{1}{T}\int_0^T I_D^2(t) R_s dt \tag{6.14}$$

The series resistor (R_s) is 20Ω, as reported by the SMS7630 datasheet. The current through the diode was obtained through simulations in AWR, Fig. 6.16a. Evaluating the integral of the instantanous power (Fig. 6.16b) yields an average power consumption of 2.019 μW.

The average power dissipation of the remaining parts of the diode can be calculated using

$$P_D = \frac{1}{T}\int_0^T v_D(t) i_D(t) dt \tag{6.15}$$

where $v_D(t)$ is the diode voltage with respect to time and can be obtained through simulation. Using the expression, the average power consumption of the remaining parts of the diode turned out to

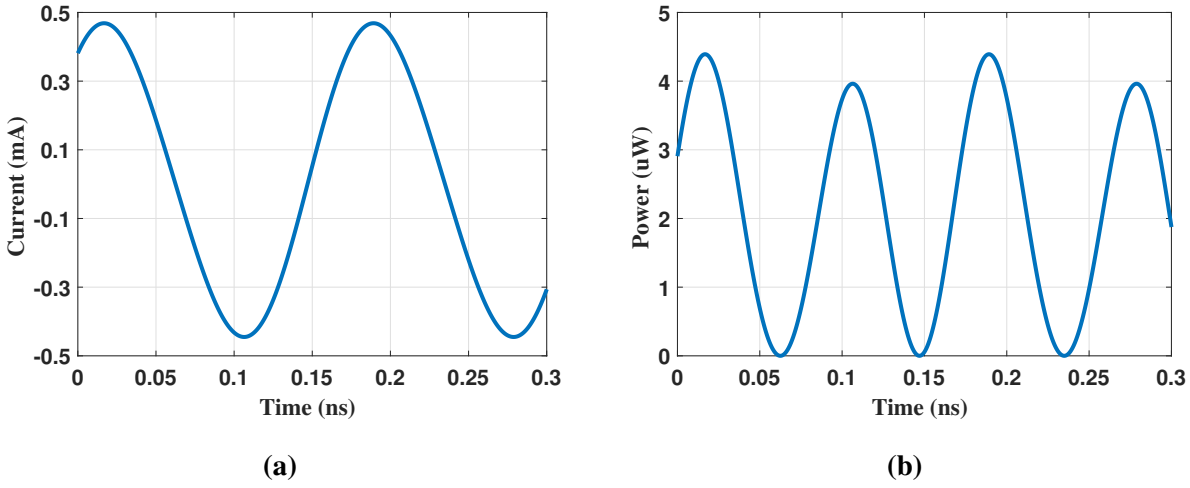

Figure 6.16: *(a) Instantaneous current through R_s vs. time (b) Instantaneous power of R_s vs. time*

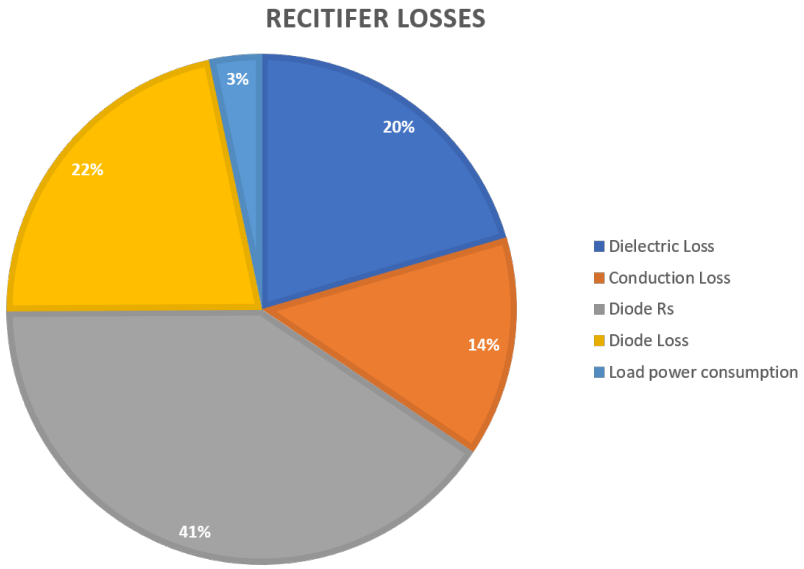

Figure 6.17: *Power consumption of each rectifier component as a percent of the total available power*

be 1.086 μW. Thus the total diode power consumption is the sum of the series resistor loss and the diode loss $P_T = P_{R_s} + P_D$, resulting in a total power consumption of 3.1 μW. This matches up well with eq. 6.10 where the diode loss from simulation is around 94.6% (loss from input of diode to output of diode, not including loss of transmission line). An overall view of the power consumption of each rectifier component is summarized in Fig. 6.17. One thing to note is that the rectifier can be improved by at least 10% just by creating a better matching circuit, which would add another 0.5 μW to the load or improve the sensitivity by 0.4 dB (with all other components staying the same). Though the largest source of loss is due to the diode, the intrinsic qualities of the diode cannot be changed so a different diode with a smaller series resistance is required, that I could not find in Digikey. A diode with a smaller series resistance is desired as that contributed 41% of the losses in the rectifier. To the best of my knowledge, this diode was the optimal diode choice for low power rectification with the lowest series resistance in the market.

6.4.2 Low-power, low voltage oscillator

The oscillator is important for modulating the incoming signal, not only does it need to consume almost zero power but output enough voltage to properly bias an RF modulator, a varactor diode in our case. The Colpitts oscillator design was based on Sousas' work [94], where only 20 mV was needed to provide 140 mV peak-to-peak oscillations. Other backscatter sensor designs in the literature are also looking towards using LC resonator designs as the clock generator for RFID, [95], but operates at 844 MHz. The benefit of using an LC resonator is that it can consume less power than RC resonators used in RFID. To the best of our knowledge, this is the first implementation of a colpitts oscillator for a practical backscatter application at 5.8 GHz.

Ultra-low voltage oscillators like this one requires serious consideration of the output admittance because the MOSFET will be operating under the triode-region where the real part of the output admittance (conductance) is higher than in the saturation region. This is important because the analysis of Colpitts oscillator's in the literature are under the saturation region [96].

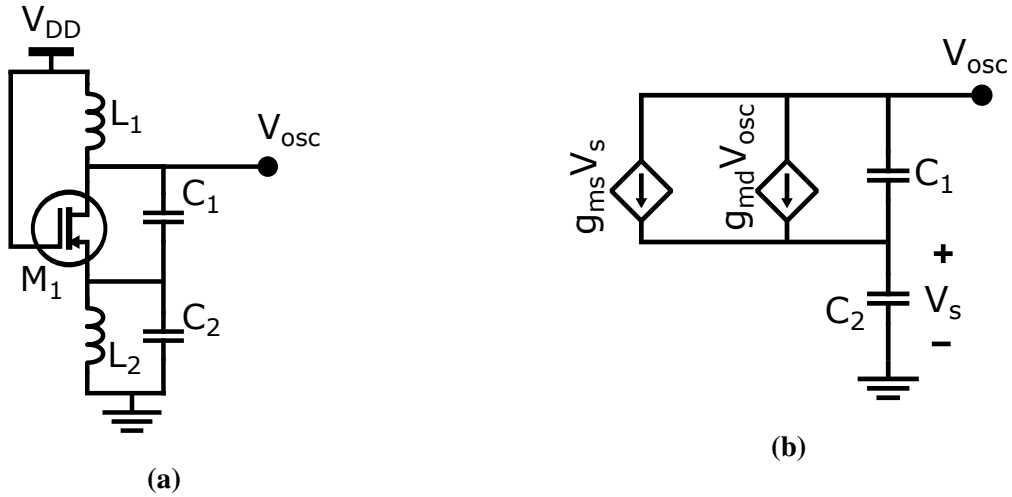

Figure 6.18: *(a) Low voltage, low power Colpitts oscillator schematic diagram (b) Small signal model of Colpitts Oscillator*

The obtain the expression for the minimum supply voltage needed to operate the colpitts oscillator,

Kirchoff's current law must be used on the AC equivalent model (Fig. 6.18b) of the ultra-low power, ultra-low voltage colpitts oscillator

$$i_{out} = v_{out}(j\omega C_1 + g_{md}) - v_s(j\omega C_1 + g_{ms}) \tag{6.16}$$

$$i_{out} = v_s j\omega C_2 \tag{6.17}$$

where v_s is the source voltage, g_{md} is the drain transconductance, and g_{ms} is the source transconductance. Equations Eq. 6.16 and 6.17 can be rearranged to get an expression for the output admittance (Y_{out}):

$$Y_{out} = \frac{g_{md}\left[1 + \frac{C_1}{C_2}\left(1 - \frac{g_{ms}}{g_{md}}\right)\right]}{\left(1 + \frac{C_1}{C_2}\right)^2 + \left(\frac{g_{ms}}{\omega C_2}\right)^2} + j\frac{\omega C_1\left(1 + \frac{C_1}{C_2}\right) + g_{md}\frac{g_{ms}}{\omega C_2}}{\left(1 + \frac{C_1}{C_2}\right)^2 + \left(\frac{g_{ms}}{\omega C_2}\right)^2} \tag{6.18}$$

Oscillations will start-up when the $Re\{Y_{out}\} < -G_P$, where G_P is the combined conductance of all circuit losses due to passive devices. In the AC equivalent, G_P is in parallel with L_1. The startup condition at which oscillations occur is summarized by Eq. 6.19, with the assumption that $g_{ms} \ll \omega(C_1 + C_2)$

$$g_{ms} > g_{md}\left(1 + \frac{C_2}{C_1}\right) + G_P\frac{C_1}{C_2}\left(1 + \frac{C_2}{C_1}\right)^2 \tag{6.19}$$

The drain-source voltage can be obtained by using the forward and reverse inversion levels and modified with the addition of the drain and source transconductance

$$V_{DD} = \Phi_t \ln(\frac{g_{ms}}{g_{md}}) + \frac{\Phi_t^2}{2I_S}(g_{ms} - g_{md}) \tag{6.20}$$

where Φ_t is the thermal voltage, and I_S is the specific current of the transistor. By identifying that the drain to source voltage is the same as the supply voltage (V_{DD}), we can combine Eq. 6.19 and 6.20, to attain the final expression for the minimum voltage supply needed to start up the Colpitts oscillator [94]

$$V_{DD} = \Phi_t \ln\left(1 + \frac{C_2}{C_1}\right) + \Phi_t \ln\left[1 + \frac{G_P}{g_{md}}\left(1 + \frac{C_1}{C_2}\right)\right] + g_{md}\frac{\Phi_t^2}{2I_S}\frac{C_2}{C_1}\left[1 + \frac{G_P}{g_{md}\left(1 + \frac{C_1}{C_2}\right)^2}\right] \tag{6.21}$$

The equation shows an importance in selecting the correct ratio of capacitor values (C_1 and C_2) and the combined conductance of all circuit losses (G_P). To minimize the start-up voltage, the ratio $\frac{C_2}{C_1}$ needs to be minimized, as well as the combined conductance of the losses.

In our design, we used 20 parallel ALD110902 [97] transistors in a common gate amplifier topology. By combining 20 parallel transistors, the transconductance will be low which is important for reducing the input voltage needed to produce oscillations. The frequency at which oscillations occur is shown in equation 6.22

$$f_0 = \frac{1}{2\pi\sqrt{(L_1 C_T)}} \tag{6.22}$$

where

$$C_T = \frac{C_1 C_2}{C_1 + C_2} \tag{6.23}$$

L_1 and L_2 were both selected to be 10 mH (SRE6603-103M) with Q = 50 at 100 kHz and C1 and C2 were selected to be 4.7 nF and 470 pF, respectively, to achieve a oscillation frequency of 100 kHz. This frequency was chosen because we were able to minimize power consumption while keeping the frequency large enough to create a backscatter signal that's distinguishable from the carrier signal.

Cabled measurements were performed combining the rectifier and the oscillator to determine the lowest input power required to start oscillations. The open circuit vs. complete tag rectified voltage is shown in Fig. 6.13b. Oscillations were produced at a threshold power of -23 dBm and a measured cold-start power-up voltage of 15 mV producing a peak-to-peak voltage of 140 mV. This signal will be used as the baseband signal to the modulator to modulate the impedance presented to the antenna. This change in impedance produces a backscatter signal with frequency components: $f_c \pm f_m$ where f_c is the carrier frequency, and f_m is the modulating signal frequency.

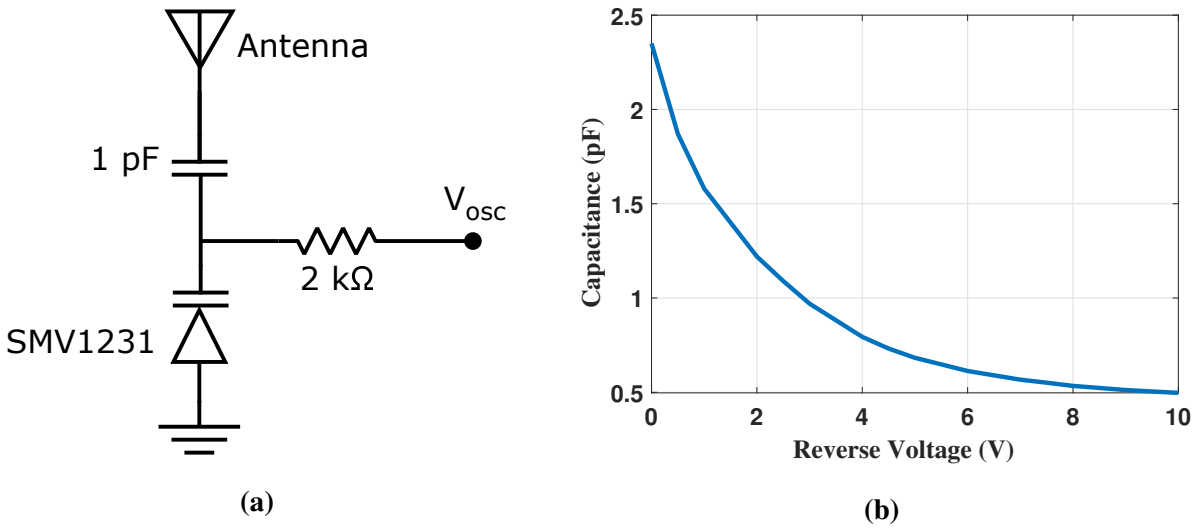

Figure 6.19: *(a) Varactor diode schematic diagram (b) Varactor capacitance (pF) vs reverse voltage (V)*

6.4.3 Varactor diode modulator design

A modulator is used to modulate the impedance presented to the tag antenna to produce a backscatter signal. In this work, a varactor diode (SMV1231) was used as the modulator because it acts as a variable capacitor under reverse bias where the capacitance (C_j) of the diode can be modeled as

$$C_j = \frac{CK}{(V_b - V)^m} \tag{6.24}$$

where C is the nominal capacitance when the diode is unbiased (when applied voltage is 0), K is a constant, V_b is the barrier voltage at junction, V is the applied reverse voltage, m is a constant that depends on the material properties of the diode. The change in reverse voltage induces a change in capacitance from the SMV1231, the performance characteristic of the SMV1231 varactor diode is summarized in the datasheet [98] and the capacitance as a function of reverse voltage is modeled in Fig. 6.19b. The advantage that a varactor diode has over conventional MOSFET modulators is that the varactor diode requires much less input voltage to generate a larger difference

in impedance. This is the first implementation of a varactor diode as an impedance modulator for backscatter communication. Typically varactor diodes are used for frequency generation, where the varactor diode is used for automatic frequency control [99]. Other work that incorporate a varactor diode in a way that closely resembles load manipulation is shown in [100] but the difference is that we are applying this to backscatter communication and not just examining its usefullness but actually applying it to an already low power communication standard. The oscillation signal that was generated from the Colpitts oscillator is used to drive the varactor diode, as shown in Fig. 6.19a. A 2 kΩ series resistor was used to limit the current going into the diode from the oscillator.

6.4.4 Cabled measurements results

The performance of the backscatter tag was first validated in a cabled monostatic benchtop setup shown in Fig. 6.20. A signal generator (Agilent N5181A) producing a carrier source at 5.8 GHz was used as the input (port 1) to the 20 dB directional coupler (Pasternack PE2204-20) with port 4 terminated with a 50 ohm stub. The tag is connected to port 2 and the backscatter signal is measured through port 3 using a spectrum analyzer (Agilent N9010A). The sensitivity of the tag was measured by inputting the lowest input RF power from the signal generator at which a backscatter signal was detected. A backscatter signal of -68 dBm was measured at a minimum input power of -23 dBm,

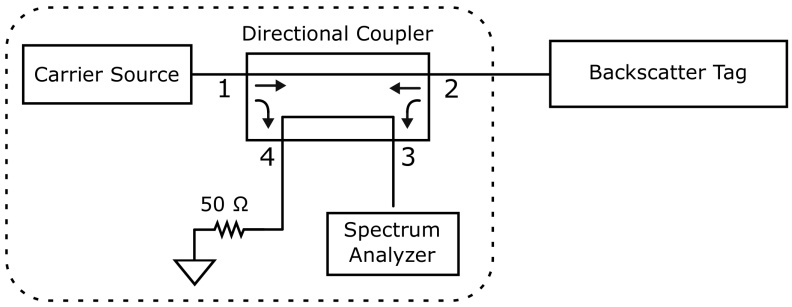

Figure 6.20: *Cabled backscatter test setup schematic*

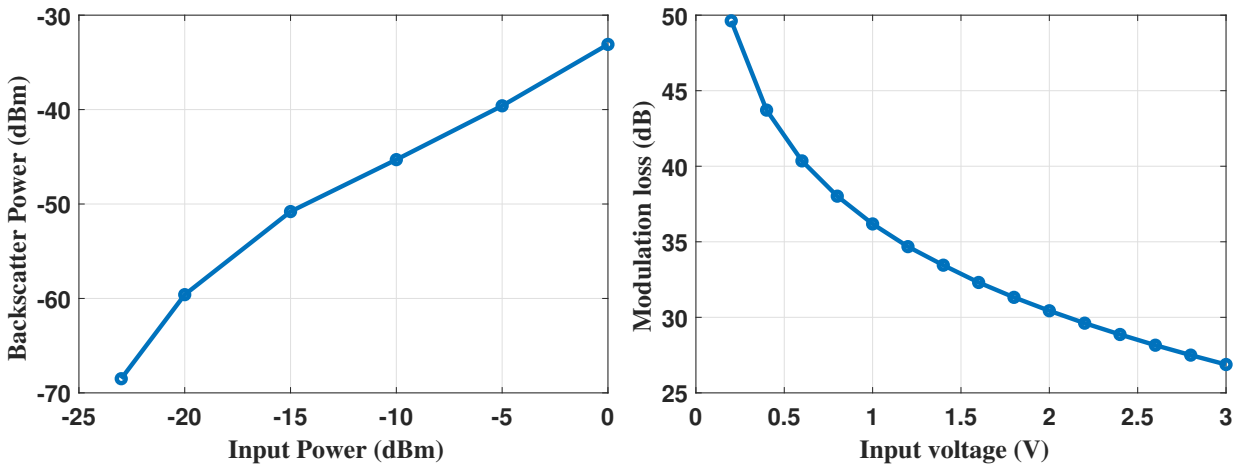

Figure 6.21: *(a) Measured cabled experiment measuring backscatter power with varying carrier source power (b) Theoretical modulation loss as a function of input bias voltage as calculated from measured varactor diode impedances (Fig. 6.22)*

which makes this tag the most sensitive passive backscatter tag operating at 5.8 GHz in the literature.

A plot of the measured backscatter power vs. input power is shown in Fig. 6.21a. As can be seen, the backscatter power is not a linear function of input power, the reason for this is due to the change in capacitance at lower reverse bias voltages, Fig. 6.19b. To measure the modulation loss as a factor of input voltage, the radar cross section of the tag needs to be calculated. To do this, a VNA was used to measure the impedance of the tag with a varying power supply connected to the varactor diode instead of the oscillator output. The modulation loss (in dB) can be obtained by taking the log of the RCS

$$M = 10 * \log_{10}(\Delta\sigma) \tag{6.25}$$

the differential RCS ($\Delta\sigma$) is given by

$$\Delta\sigma = \frac{\lambda^2}{4\pi} G_T^2 |\Gamma_1^* - \Gamma_2^*|^2 \tag{6.26}$$

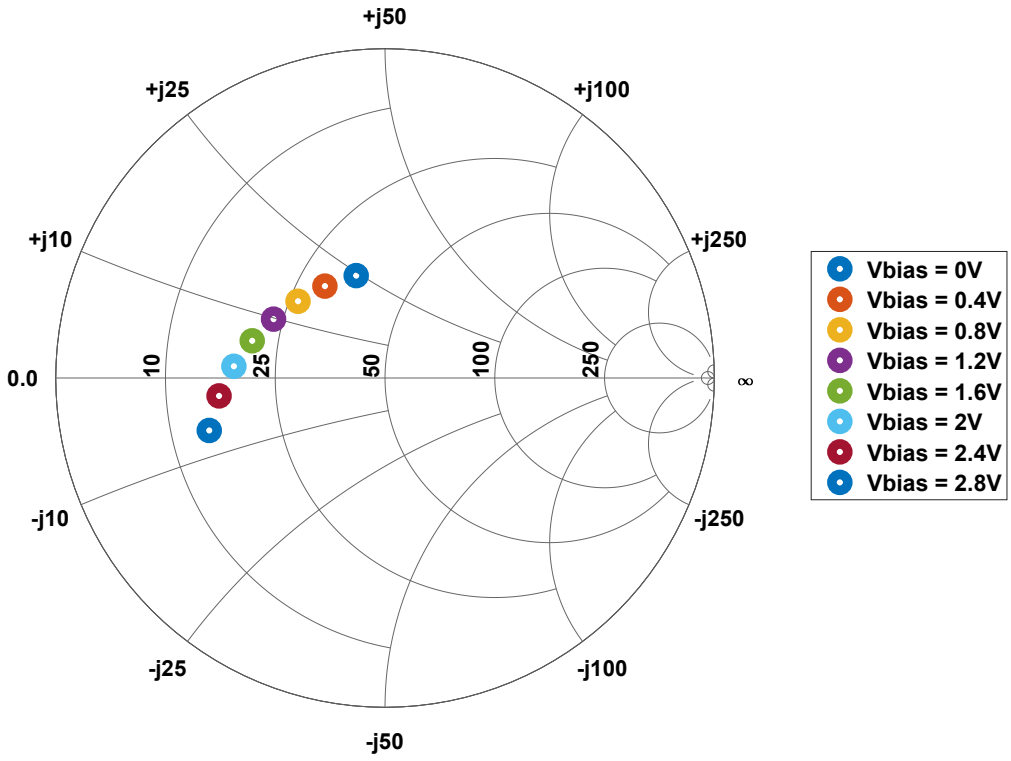

Figure 6.22: *Measured impedances at 5.8 GHz with -23 dBm input power and varying bias voltages*

where G_T is the tag antenna gain and $\Gamma_{1,2}$ is the conjugate match reflection coefficient

$$\Gamma_{1,2}^{*} = \frac{Z_{L1,L2} - Z_a^{*}}{Z_{L1,L2} + Z_a} \tag{6.27}$$

for an antenna impedance of Z_a and the complex load impedance Z_L. The complex load impedances with several bias voltages are shown on the smith chart in Fig. 6.22. The modulation loss with respect to reverse input voltage is summarized in Fig. 6.21b. When the input power to the tag is higher, the oscillator will produce a higher voltage, which means that the modulation loss will decrease, providing a higher backscatter power. In applications where a higher input power can be obtained, the performance of the tag will be much improved.

6.4.5 Capacitive backscatter telemetry

To fully realize the capabilities of backscatter communication, it is important to include come sensory information. Up to this point, the tag described in this chapter performs single tone backscatter, where only a single backscatter frequency is detected with no data information. There are many types of sensors that measure things like temperature, humidity, movement, sound, and many others. The problem with many of these sensors is that they usually consist of a power-hungry module that usually require some voltage source to operate. So we are limited in the types of sensors that can be used because the more power a sensor consumes, the shorter the operational range. In this work, a capacitive force sensor was used to implement sensing and create a fully realized tag without adding any more power consumption.

The capacitive force sensor used is the SingleTact force sensor S8-1N. The sensor changes its capacitance (C_{WS}) with a change in applied force. This sensor was placed in parallel with capacitor $C2$ on the Colpitts oscillator, a diagram of the oscillator model with the weight sensor capacitance is shown in Fig. 6.25. From the previous section, we know that capacitors C_1 and C_2 have a direct

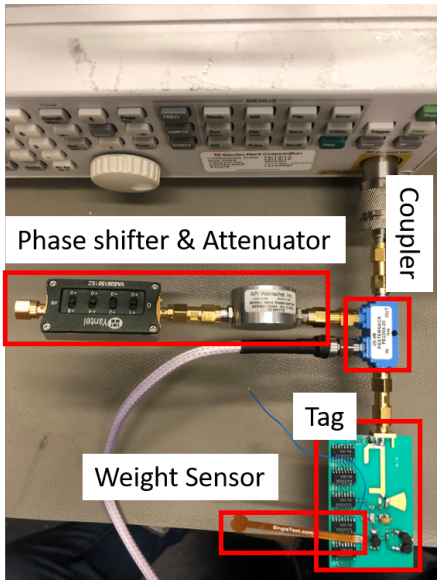

Figure 6.23: *Cabled measured setup of capacitive weight sensor with tag*

impact on the oscillation frequency, we can then use this fact coupled with the capacitance change from the sensor to manipulate the backscatter frequency. The frequency at which oscillations occur was shown in equation 6.21 but now the total capacitance C_T includes the capacitance of the sensor, as modeled by

$$C_T = \frac{C_1(C_2 + C_{WS})}{C_1 + (C_2 + C_{WS})} \tag{6.28}$$

where the sensor capacitance (C_{WS}) is the capacitance of the sensor which is dependent on the force

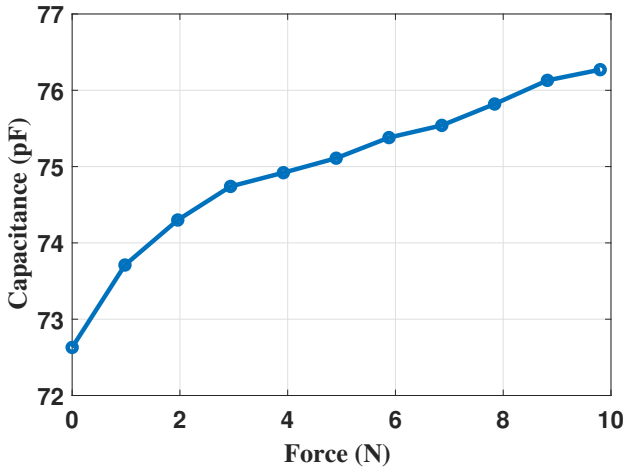

Figure 6.24: *Measured capacitance vs. applied force of SingleTact S8-1N force sensor*

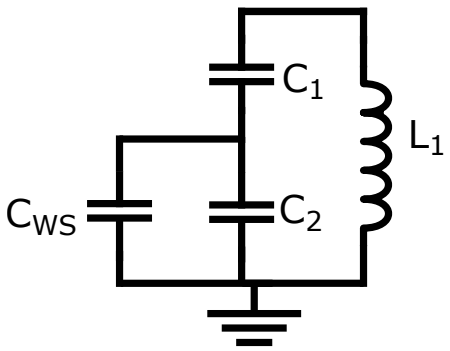

Figure 6.25: *Equivalent oscillator model with weight sensor capacitor*

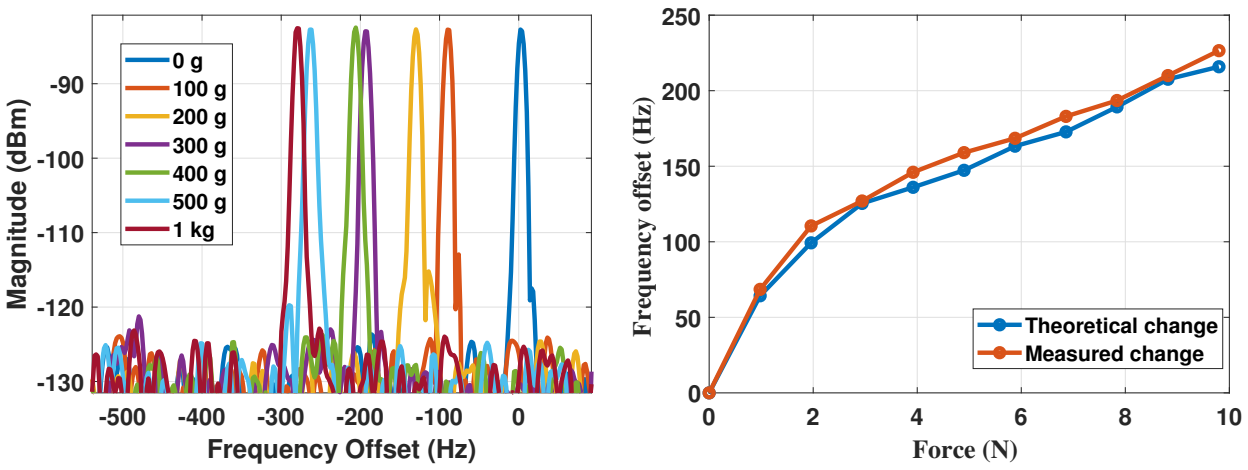

Figure 6.26: *(a) Measured backscatter signal with respect to frequency offset of several weights (b) Theoretical and measured backscatter frequency offset vs. applied force (N)*

applied. The datasheet did not provide a plot of capacitance vs. applied force, so a measurement was performed by probing the capacitive sensor using an LCR meter with several applied forces, Fig.6.24.

A cabled measurement was performed to measure the the effect that the weight sensor has on backscatter frequency. The measurement setup is similar to that used in the cabled backscatter experiment described in Chapter 6.4.4, except now, the sensor is attached to the circuit as shown in Fig. 6.23. Several different weights were applied to the sensor from 0 to 1 kg and the backscatter frequencies were measured using the spectrum analyzer, Fig. 6.26a. A plot of the theoretical and measured frequency offset vs. the force in Newtons as shown in Fig. 6.26. As can be seen, the measured offset from the backscatter signal matches up well with the theoretical offset obtained from using the frequency equation. One thing to note is that the frequency offset is only 226.5 Hz from 0 g to 1 kg of applied force. To get a larger frequency offset, the total capacitance across the oscillator needs to be smaller so that the weight sensor contributes more to the change in capacitance. Another way to create a larger offset is to decrease the inductor L_1, but a consequence to that is the

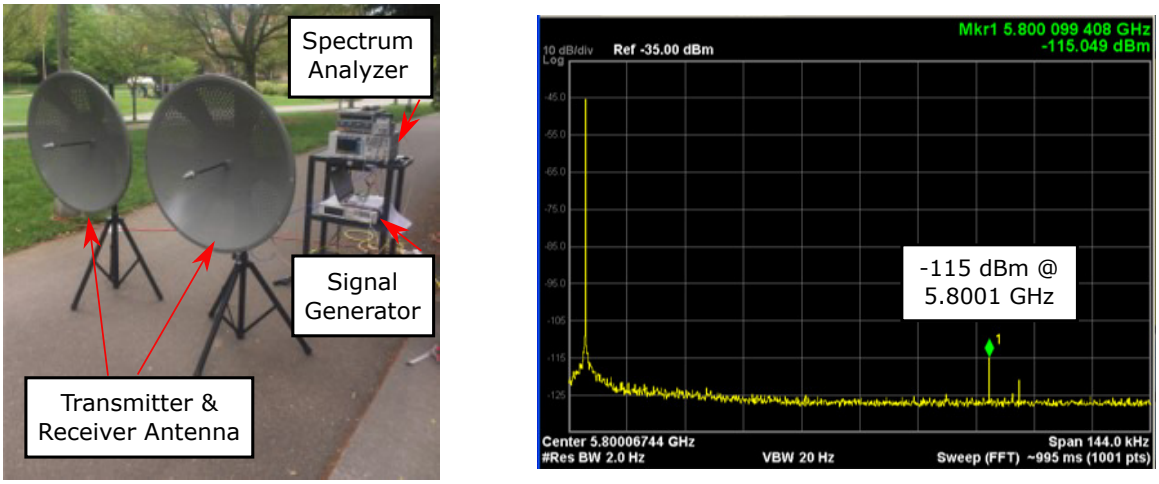

(a) **(b)**

Figure 6.27: *(a) 517 meter outdoor experiment showing transmitter/receiver setup (b) Measured backscatter power at 517 meters*

power consumption increases as a function of oscillation frequency, $P = f * (Vdd)^2$.

6.5 Over-the-air experimental measurements

By determining the sensitivity of the tag through a cabled setup, the Friis equation can be used to determine the range at which the tag will receive -23 dBm given the gain and carrier power. In the over-the-air results, a signal generator was used to produce the carrier signal and was amplified using a Pasternack PE15A5017 amplifier with 43 dB of gain. This signal was transmitted through a dish antenna with 32.5 dBi of gain and 5°of beamwidth. One thing to note is that because the beamwidth of each antenna are 5°, the experiment is more prone to pointing loss. This makes the experiment much more difficult to achieve results that are similar to the cabled benchtop setup. Concurrent to the transmitter is the receiver setup, which constituted of a spectrum analyzer and an identical dish antenna with 32.5 dBi of gain. The transmitter/receiver setup is also known as bistatic co-located mode, where both the transmitter and receiver are located the same distance away from the tag. A

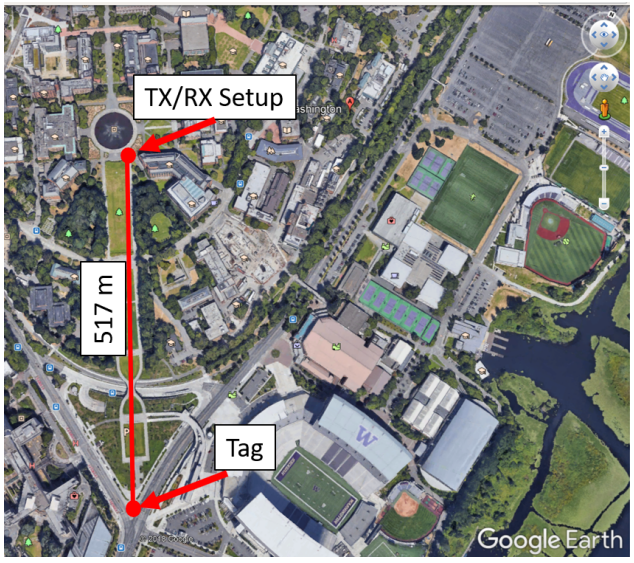

Figure 6.28: *Aerial view of 517 meter outdoor experiment*

photo of the setup if shown in Fig. 6.27a. The backscatter tag was placed 517 meters away from the transmitter and receiver, an aerial view is shown in Fig. 6.28.

A total carrier power emitting from the transmitter antenna was set to +38 dBm which would result in a theoretical carrier power of -19 dBm intercepting the tag at 517 meters away. The tag was able to backscatter a signal with a received power of -115 dBm, Fig. 6.27b. If we account for the cable loss and the path loss from 517 meters, the theoretical received backscatter power would be -113.5 dBm, which is a 1.5 dB difference from the cabled benchtop experiment. This shows that the over-the-air experiment results matched up well with the cabled results. The slight variation from the cabled and over-the-air experiments might be attributed to pointing loss effect. At these distances, it is very difficult to properly align the two antennas at their maximum peak radiation patterns. With this slight discrepancy though, we can be fairly confident that by using the Friis equation, we can approximately predict the maximum operating range of the backscatter tag at 1.1 km.

6.6 Chapter Conclusion

In this chapter, we presented a battery-free 5.8 GHz backscatter tag that can operate at voltages and an RF power level not seen by any battery-free tag. This tag architecture takes advantage of a low power, low voltage Colpitts oscillator to generate a baseband signal for modulation. It has a measured RF sensitivity of -23 dBm with a cold-start operating voltage of 15 mV input. A 517 meter bistatic co-located outdoor experiment validates the theoretical backscatter power of -57 dBm when -19 dBm is incident on the tag. With the addition of a capacitive force sensor, the tags are capable of communicating sensory information while still being low-power and low-voltage.

Chapter 7

CONCLUSION

This document has presented novel methods to wireless harvesting and antenna design for wireless sensing and communication. We considered the advantages that backscatter at high frequency has in the scaling of the a backscatter tag design, as well as limited interference at the 5.8 GHz band. To the best of our knowledge, this is the lowest power, 5.8 GHz wireless sensor tag with the lowest cold start voltage and RF sensitivity.

The harvesting of RF signals and boosting harvested voltage is considered in this document. A harvesting approach using a DC to DC boost converter to generate a usable voltage using a 2.4 GHz carrier source with an input of -15 dBm was presented. By using a timer, the boost converter was able to store enough energy to be boosted for each timer boost cycle. This allowed the continuous storage and charging of energy onto an energy reservoir. This was a proof of concept for an actual implementation to charge low power devices using ambient energy.

An important aspect in energy harvesting is the antenna design. We explored the methodology in designing an electrically small metal-mountable RFID tag. Metal mountable RFID are complicated to design for because metal is a reflector and can cause disruption in the field propagation. That's why powerful frequency domain solvers are needed to simulate the design of an antenna with metal. By using CST, a split ring antenna capable of 25 meter read range was built using a 4.7 mm Teflon core sandwiched between two 0.8 mm Rogers 4003 substrate PCBs.

Combining the fundamental knowledge and previous work on energy harvesting and antenna design, a battery free RFID tag with fiber optic tamper detection was created. To combat theft of hazardous materials from a container, a tag that can notify the user of a seal tamper was needed. We designed a passive tag that not only could send EPC data to the user, it could also send an open or closed loop status. To prevent hackers from changing the identification of the tags, we also

implemented AES encryption. These security features are not seen in any commercial RFID tag and it incorporates a dual patch air dielectric antenna that feeds to the circuitry board by metal spacers. This then feeds to the rectifier where the energy is stored in a capacitor to run an MSP430 microcontroller where the Gen 2 RFID functions are stored and executed. The tag is capable of read ranges of up to 5.5 meters in passive mode and 9 meters in active mode with a +36 dBm EIRP EPC Generation 2 reader.

A battery-free 5.8 GHz backscatter tag that is capable of 1 km sensing and communication has been validated through cabled and over-the-air experiments. The backscatter tag consists of a custom antenna with 13 dBi of gain, RF-DC harvester, a low-power, low-voltage Colpitts oscillator that provides the baseband signal to the varactor diode modulator, and a force sensor to provide force telemetry. This tag is capable of operating down to 15 mV with an RF sensitivity of -23 dBm, which has not been seen by any battery-free backscatter tag in the literature. A possible application for this tag would be in agricultural monitoring where the force sensor can be used to detect soil density to alert the farmer that more water is needed in certain parts of the field. This will reduce operation costs because you know where to water but this will also reduce the labor hours required by not having to physically go and check on all the plants.

7.1 Original Contributions

The original contributions discussed in this document include:

- Ultra-low power harvesting approaches at 2.4 GHz for powering sensors and external devices. Published in [19, 20].

- ISO1800-6C UHF RFID tags that have security features not seen in any commercial RFID tags, like AES encryption and a fiber loop. Published in [21]

- Using a single wire transmission line as the communication channel for long range identification and distributed sensing. Published in [23, 24]

- A low power superheterodyne receiver architecture for wirelessly powered backscatter tags and sensors leveraging an external LO has been demonstrated using a bench top setup. Published in [25].

7.2 Future Work

7.2.1 Single-chip approach

While the battery-free backscatter tag designed in Chapter 6 achieves an RF sensitivity and cold-start voltage not seen by any 5.8 GHz tag, it has the potential to improve even further. An integrated single-chip approach could improve the overall power consumption of the tag. Integrated CMOS oscillators have shown to consume significantly less power than its discrete counterparts. For example, in our backscatter tag, the Colpitts oscillator was designed using discrete ALD110800 MOSFETs. Additionally, integrating the backscatter modulator, the varactor diode (SMV1231), would further reduce the amount of power needed to drive the diode compared to the discrete diode soldered on a PCB. Essentially, the whole tag can be implemented on a chip, the only external components would be the large 10 mH inductors and possibly the matching circuit stub of the rectifier.

7.2.2 Monostatic Configuration

The ability to transmit and receive using the same antenna would greatly reduce the complexity of the system. One of the main difficulties is designing a carrier cancellation circuit that is capable of filtering out the signal carrier power without reducing the backscatter power. Narrowband 5.8 GHz carrier cancellation circuits that cancel out the carrier signal by more than 50 dB has been demonstrated [101]. This would open up a scenario where only a single antenna is needed for the experiments without reducing the backscatter signal itself.

7.2.3 Bistatic dislocated Configuration

The battery free 5.8 GHz tag described in Chapter 6 was tested under the condition that the transmitter and receiver would be located next to each other, in the bistatic co-located configuration. In some

applications, this configuration might not be the desired and or not practical, as could be the case where the transmitter is in close proximity to the tag, this is called bistatic dislocated. An example scenario is if the tags are placed on the outside edge of a field where they will be close to an outlet where the transmitter can be plugged in. In a theoretical scenario, the tag would be placed 5 meters away from the transmitter source, where the tag would have an RF input power of approximately 0 dBm. If the receiver antenna has 32.5 dBi of gain, the theoretical range would be approximately 15 km, assuming a receiver sensitivity of -120 dBm.

BIBLIOGRAPHY

[1] M. Hubbard, "Taming the smartphone power consumption vicious cycle," *Microwave Journal*, vol. 55, no. 11, pp. 92–96, 2012.

[2] R. A. Potyrailo, N. Nagraj, Z. Tang, F. J. Mondello, C. Surman, and W. Morris, "Battery-free radio frequency identification (rfid) sensors for food quality and safety," *Journal of Agricultural and Food Chemistry*, vol. 60, no. 35, pp. 8535–8543, 2012, pMID: 22881825. [Online]. Available: https://doi.org/10.1021/jf302416y

[3] D. J. Yeager, P. S. Powledge, R. Prasad, D. Wetherall, and J. R. Smith, "Wirelessly-charged uhf tags for sensor data collection," in *2008 IEEE International Conference on RFID*, April 2008, pp. 320–327.

[4] B. Kellogg, A. Parks, S. Gollakota, J. R. Smith, and D. Wetherall, "Wi-fi backscatter: Internet connectivity for rf-powered devices," in *ACM SIGCOMM Computer Communication Review*, vol. 44, no. 4. ACM, 2014, pp. 607–618.

[5] D. Bharadia, K. R. Joshi, M. Kotaru, and S. Katti, "Backfi: High throughput wifi backscatter," *ACM SIGCOMM Computer Communication Review*, vol. 45, no. 4, pp. 283–296, 2015.

[6] J. F. Ensworth and M. S. Reynolds, "Ble-backscatter: Ultralow-power iot nodes compatible with bluetooth 4.0 low energy (ble) smartphones and tablets," *IEEE Transactions on Microwave Theory and Techniques*, vol. 65, no. 9, pp. 3360–3368, Sept 2017.

[7] A. P. Sample, D. J. Yeager, P. S. Powledge, A. V. Mamishev, and J. R. Smith, "Design of an RFID-based battery-free programmable sensing platform," *IEEE Transactions on Instrumentation and Measurement*, vol. 57, no. 11, pp. 2608–2615, Nov 2008.

[8] A. Varshney, O. Harms, C.-P. Penichet, C. Rohner, F. Hermans, and T. Voigt, "Lorea: A backscatter architecture that achieves a long communication range," in *ACM SenSys 2017*. ACM Digital Library, 2017.

[9] V. Talla, M. Hessar, B. Kellogg, A. Najafi, J. R. Smith, and S. Gollakota, "Lora backscatter: Enabling the vision of ubiquitous connectivity," *Proceedings of the ACM on Interactive, Mobile, Wearable and Ubiquitous Technologies*, vol. 1, no. 3, p. 105, 2017.

[10] A. P. Sample, D. J. Yeager, P. S. Powledge, and J. R. Smith, "Design of a passively-powered, programmable sensing platform for uhf rfid systems," in *2007 IEEE International Conference on RFID*, March 2007, pp. 149–156.

[11] S. J. Thomas, T. Deyle, R. Harrison, and M. S. Reynolds, "Rich-media tags: Battery-free wireless multichannel digital audio and image transmission with uhf rfid techniques," in *2013 IEEE International Conference on RFID (RFID)*, April 2013, pp. 231–236.

[12] V. Pillai, H. Heinrich, D. Dieska, P. V. Nikitin, R. Martinez, and K. V. S. Rao, "An ultra-low-power long range battery/passive rfid tag for uhf and microwave bands with a current consumption of 700 na at 1.5 v," *IEEE Transactions on Circuits and Systems I: Regular Papers*, vol. 54, no. 7, pp. 1500–1512, July 2007.

[13] A. Shirane, Y. Fang, H. Tan, T. Ibe, H. Ito, N. Ishihara, and K. Masu, "Rf-powered transceiver with an energy- and spectral-efficient if-based quadrature backscattering transmitter," *IEEE Journal of Solid-State Circuits*, vol. 50, no. 12, pp. 2975–2987, Dec 2015.

[14] F. Amato, H. M. Torun, and G. Durgin, "Rfid backscattering in long-range scenarios," *IEEE Transactions on Wireless Communications*, vol. PP, no. 99, pp. 1–1, 2018.

[15] J. O. Duruibe, M. Ogwuegbu, J. Egwurugwu *et al.*, "Heavy metal pollution and human biotoxic effects," *International Journal of physical sciences*, vol. 2, no. 5, pp. 112–118, 2007.

[16] C. R. Valenta and G. D. Durgin, "Harvesting wireless power: Survey of energy-harvester conversion efficiency in far-field, wireless power transfer systems," *IEEE Microwave Magazine*, vol. 15, no. 4, pp. 108–120, June 2014.

[17] G. D. Durgin, "The hidden benefits of backscatter radio and rfid at 5.8 ghz."

[18] J. D. Griffin, G. D. Durgin, A. Haldi, and B. Kippelen, "Rf tag antenna performance on various materials using radio link budgets," *IEEE Antennas and Wireless Propagation Letters*, vol. 5, pp. 247–250, 2006.

[19] K. Gudan, S. Shao, J. J. Hull, A. Hoang, J. Ensworth, and M. S. Reynolds, "Ultra-low power autonomous 2.4GHz RF energy harvesting and storage system," in *2015 IEEE International Conference on RFID Technology and Applications (RFID-TA)*, Sept 2015, pp. 176–181.

[20] J. F. Ensworth, A. T. Hoang, and M. S. Reynolds, "A timer based boost converter for RF energy harvesting," in *2015 IEEE Wireless Power Transfer Conference (WPTC)*, May 2015, pp. 1–4.

[21] A. T. Hoang, K. D. Coonley, F. Nekoogar, and M. S. Reynolds, "A battery-free RFID sensor tag with fiber-optic tamper detection," in *IEEE SENSORS*, Oct 2016, pp. 1–3.

[22] A. Sharma, A. T. Hoang, and M. S. Reynolds, "An electrically small, 16.7 m range, iso18000-6c uhf rfid tag for metal cylinder mounting," *IEEE Journal of RFID*, May 2018 In Review.

[23] ——, "A coplanar vivaldi style launcher for goubau single wire transmission lines," *IEEE Antennas and Wireless Propagation Letters*, vol. PP, no. 99, pp. 1–1, 2017.

[24] ——, "Long-range battery-free UHF RFID with a single wire transmission line," *IEEE Sensors Journal*, vol. 17, no. 17, pp. 5687–5693, Sept 2017.

[25] J. F. Ensworth, A. T. Hoang, and M. S. Reynolds, "A low power 2.4 ghz superheterodyne receiver architecture with external lo for wirelessly powered backscatter tags and sensors," in *2017 IEEE International Conference on RFID (RFID)*, May 2017, pp. 149–154.

[26] L. Zhang, B. Tiwana, R. P. Dick, Z. Qian, Z. M. Mao, Z. Wang, and L. Yang, "Accurate online power estimation and automatic battery behavior based power model generation for smartphones," in *2010 IEEE/ACM/IFIP International Conference on Hardware/Software Codesign and System Synthesis (CODES+ISSS)*, Oct 2010, pp. 105–114.

[27] P. Blythe, "Rfid for road tolling, road-use pricing and vehicle access control," in *IEE Colloquium on RFID Technology (Ref. No. 1999/123)*, 1999, pp. 8/1–816.

[28] P. Manikonda, A. K. Yerrapragada, and S. S. Annasamudram, "Intelligent traffic management system," in *2011 IEEE Conference on Sustainable Utilization and Development in Engineering and Technology (STUDENT)*, Oct 2011, pp. 119–122.

[29] A. A. Khan, A. I. E. Yakzan, and M. Ali, "Radio frequency identification (rfid) based toll collection system," in *2011 Third International Conference on Computational Intelligence, Communication Systems and Networks*, July 2011, pp. 103–107.

[30] T. M. Choi, "Coordination and risk analysis of vmi supply chains with rfid technology," *IEEE Transactions on Industrial Informatics*, vol. 7, no. 3, pp. 497–504, Aug 2011.

[31] H. Stockman, "Communication by means of reflected power," *Proceedings of the IRE*, vol. 36, no. 10, pp. 1196–1204, Oct 1948.

[32] A. R. Koelle, S. W. Depp, and R. W. Freyman, "Short-range radio-telemetry for electronic identification, using modulated rf backscatter," *Proceedings of the IEEE*, vol. 63, no. 8, pp. 1260–1261, Aug 1975.

[33] J. Kimionis, A. Bletsas, and J. N. Sahalos, "Increased range bistatic scatter radio," *IEEE Transactions on Communications*, vol. 62, no. 3, pp. 1091–1104, March 2014.

[34] ——, "Bistatic backscatter radio for power-limited sensor networks," in *2013 IEEE Global Communications Conference (GLOBECOM)*, Dec 2013, pp. 353–358.

[35] V. Liu, A. Parks, V. Talla, S. Gollakota, D. Wetherall, and J. R. Smith, "Ambient backscatter: wireless communication out of thin air," in *ACM SIGCOMM Computer Communication Review*, vol. 43, no. 4. ACM, 2013, pp. 39–50.

[36] A. N. Parks, A. Liu, S. Gollakota, and J. R. Smith, "Turbocharging ambient backscatter communication," *ACM SIGCOMM Computer Communication Review*, vol. 44, no. 4, pp. 619–630, 2015.

[37] D. C. Hogg, "Fun with the friis free-space transmission formula," *IEEE Antennas and Propagation Magazine*, vol. 35, no. 4, pp. 33–35, Aug 1993.

[38] J. Schindler, R. Mack, and P. Blacksmith, "The control of electromagnetic scattering by impedance loading," *Proceedings of the IEEE*, vol. 53, no. 8, pp. 993–1004, 1965.

[39] J. F. Ensworth, S. J. Thomas, S. Y. Shin, and M. S. Reynolds, "Waveform-aware ambient rf energy harvesting," in *2014 IEEE International Conference on RFID (IEEE RFID)*, April 2014, pp. 67–73.

[40] M. Hassanalieragh, T. Soyata, A. Nadeau, and G. Sharma, "Ur-solarcap: An open source intelligent auto-wakeup solar energy harvesting system for supercapacitor-based energy buffering," *IEEE Access*, vol. 4, pp. 542–557, 2016.

[41] B. Li, X. Shao, N. Shahshahan, N. Goldsman, T. Salter, and G. M. Metze, "An antenna codesign dual band rf energy harvester," *IEEE Transactions on Circuits and Systems I: Regular Papers*, vol. 60, no. 12, pp. 3256–3266, Dec 2013.

[42] Y. Sang, X. Huang, H. Liu, and P. Jin, "A vibration-based hybrid energy harvester for wireless sensor systems," *IEEE Transactions on Magnetics*, vol. 48, no. 11, pp. 4495–4498, Nov 2012.

[43] M. S. Trotter, J. D. Griffin, and G. D. Durgin, "Power-optimized waveforms for improving the range and reliability of rfid systems," in *2009 IEEE International Conference on RFID*, April 2009, pp. 80–87.

[44] A. N. Parks, A. P. Sample, Y. Zhao, and J. R. Smith, "A wireless sensing platform utilizing ambient rf energy," in *2013 IEEE Topical Conference on Biomedical Wireless Technologies, Networks, and Sensing Systems*, Jan 2013, pp. 154–156.

[45] N. V. Desai, Y. K. Ramadass, and A. P. Chandrakasan, "A bipolar -40 mv self-starting boost converter with transformer reuse for thermoelectric energy harvesting," in *2014 IEEE/ACM International Symposium on Low Power Electronics and Design (ISLPED)*, Aug 2014, pp. 221–226.

[46] A. Bertacchini, S. Scorcioni, M. Cori, L. Larcher, and P. Pavan, "250mv input boost converter for low power applications," in *2010 IEEE International Symposium on Industrial Electronics*, July 2010, pp. 533–538.

[47] Y. K. Ramadass and A. P. Chandrakasan, "A battery-less thermoelectric energy harvesting interface circuit with 35 mv startup voltage," *IEEE Journal of Solid-State Circuits*, vol. 46, no. 1, pp. 333–341, Jan 2011.

[48] A. Shrivastava, N. E. Roberts, O. U. Khan, D. D. Wentzloff, and B. H. Calhoun, "A 10 mv-input boost converter with inductor peak current control and zero detection for thermoelectric and solar energy harvesting with 220 mv cold-start and -14.5 dbm, 915 mhz rf kick-start," *IEEE Journal of Solid-State Circuits*, vol. 50, no. 8, pp. 1820–1832, Aug 2015.

[49] A. Dolgov, R. Zane, and Z. Popovic, "Power management system for online low power rf energy harvesting optimization," *IEEE Transactions on Circuits and Systems I: Regular Papers*, vol. 57, no. 7, pp. 1802–1811, July 2010.

[50] O. Lopez-Lapena, M. T. Penella, and M. Gasulla, "A closed-loop maximum power point tracker for subwatt photovoltaic panels," *IEEE Transactions on Industrial Electronics*, vol. 59, no. 3, pp. 1588–1596, March 2012.

[51] D. M. Dobkin and S. M. Weigand, "Environmental effects on RFID tag antennas," in *IEEE MTT-S International Microwave Symposium Digest, 2005.*, June 2005, pp. 135–138.

[52] J. Zhang and Y. Long, "A novel metal-mountable electrically small antenna for rfid tag applications with practical guidelines for the antenna design," *IEEE Transactions on Antennas and Propagation*, vol. 62, no. 11, pp. 5820–5829, Nov 2014.

[53] W. Choi, J. Kim, J.-H. Bae, and G. Choi, "A small rfid tag antenna using proximity-coupling to identify metallic objects," *Microwave and Optical Technology Letters*, vol. 50, no. 11, pp. 2978–2981, 2008. [Online]. Available: http://dx.doi.org/10.1002/mop.23831

[54] A. Hamani, M. C. E. Yagoub, T. P. Vuong, and R. Touhami, "A novel broadband antenna design for uhf rfid tags on metallic surface environments," *IEEE Antennas and Wireless Propagation Letters*, vol. 16, pp. 91–94, 2017.

[55] S. L. Chen and K. H. Lin, "A slim RFID tag antenna design for metallic object applications," *IEEE Antennas and Wireless Propagation Letters*, vol. 7, pp. 729–732, 2008.

[56] J. Zhang and Y. Long, "A novel metal-mountable electrically small antenna for RFID tag applications with practical guidelines for the antenna design," *IEEE Transactions on Antennas and Propagation*, vol. 62, no. 11, pp. 5820–5829, Nov 2014.

[57] A. Sharma, A. Syed, and A. R. Harish, "Miniature slotted RFID tag antenna for metallic objects," in *2011 International Conference on Communications and Signal Processing*, Feb 2011, pp. 353–357.

[58] R. A. Ramirez, E. A. Rojas-Nastrucci, and T. M. Weller, "UHF RFID tags for on-/off-metal applications fabricated using additive manufacturing," *IEEE Antennas and Wireless Propagation Letters*, vol. 16, pp. 1635–1638, 2017.

[59] A. Hamani, M. C. E. Yagoub, T. P. Vuong, and R. Touhami, "A novel broadband antenna design for UHF RFID tags on metallic surface environments," *IEEE Antennas and Wireless Propagation Letters*, vol. 16, pp. 91–94, 2017.

[60] K. H. Lin, S. L. Chen, and R. Mittra, "A looped-bowtie RFID tag antenna design for metallic objects," *IEEE Transactions on Antennas and Propagation*, vol. 61, no. 2, pp. 499–505, 2013.

[61] H. D. Chen and Y. H. Tsao, "Low-profile PIFA array antennas for UHF band RFID tags mountable on metallic objects," *IEEE Transactions on Antennas and Propagation*, vol. 58, no. 4, pp. 1087–1092, April 2010.

[62] K. V. S. Rao, S. F. Lam, and P. V. Nikitin, "UHF RFID tag for metal containers," in *2010 Asia-Pacific Microwave Conference*, Dec 2010, pp. 179–182.

[63] P. Dangkham and C. Phongcharoenpanich, "A compact split ring resonator antenna on paper-based for uhf rfid passive tag," in *2015 IEEE Conference on Antenna Measurements Applications (CAMA)*, Nov 2015, pp. 1–4.

[64] B. Alavikia, T. S. Almoneef, and O. M. Ramahi, "Complementary split ring resonator arrays for electromagnetic energy harvesting," *Applied Physics Letters*, vol. 107, no. 3, p. 033902, 2015. [Online]. Available: https://doi.org/10.1063/1.4927238

[65] Z. Han, K. Kohno, H. Fujita, K. Hirakawa, and H. Toshiyoshi, "Tunable terahertz filter and modulator based on electrostatic mems reconfigurable srr array," *IEEE Journal of Selected Topics in Quantum Electronics*, vol. 21, no. 4, pp. 114–122, July 2015.

[66] J. B. Pendry, A. J. Holden, D. J. Robbins, and W. J. Stewart, "Magnetism from conductors and enhanced nonlinear phenomena," *IEEE Transactions on Microwave Theory and Techniques*, vol. 47, no. 11, pp. 2075–2084, Nov 1999.

[67] B. SAUVIAC, C. R. SIMOVSKI, and S. A. TRETYAKOV, "Double split-ring resonators: Analytical modeling and numerical simulations," *Electromagnetics*, vol. 24, no. 5, pp. 317–338, 2004. [Online]. Available: https://doi.org/10.1080/02726340490457890

[68] E. Nishiyama and M. Aikawa, "Wide-band and high-gain microstrip antenna with thick parasitic patch substrate," in *IEEE Antennas and Propagation Society Symposium, 2004.*, vol. 1, June 2004, pp. 273–276 Vol.1.

[69] H. Yang and N. Alexopoulos, "Gain enhancement methods for printed circuit antennas through multiple superstrates," *IEEE Transactions on Antennas and Propagation*, vol. 35, no. 7, pp. 860–863, Jul 1987.

[70] J. D. Griffin and G. D. Durgin, "Complete link budgets for backscatter-radio and RFID systems," *IEEE Antennas and Propagation Magazine*, vol. 51, no. 2, pp. 11–25, April 2009.

[71] S. J. Thomas, E. Wheeler, J. Teizer, and M. S. Reynolds, "Quadrature amplitude modulated backscatter in passive and semipassive uhf rfid systems," *IEEE Transactions on Microwave Theory and Techniques*, vol. 60, no. 4, pp. 1175–1182, April 2012.

[72] P. V. Nikitin, K. V. S. Rao, and R. D. Martinez, "Differential RCS of RFID tag," *Electronics Letters*, vol. 43, no. 8, pp. 431–432, April 2007.

[73] A. T. Hoang, K. D. Coonley, F. Nekoogar, and M. S. Reynolds, "A battery-free EPC Generation 2 computational RFID tag with fiber-optic tamper detection," in *Proceedings IEEE Sensors Conf.*, 2016.

[74] I. Zalbide, E. D'Entremont, A. Jiménez, H. Solar, A. Beriain, and R. Berenguer, "Battery-free wireless sensors for industrial applications based on UHF RFID technology," in *IEEE SENSORS 2014 Proceedings*, Nov 2014, pp. 1499–1502.

[75] S. Naderiparizi, A. N. Parks, Z. Kapetanovic, B. Ransford, and J. R. Smith, "Wispcam: A battery-free rfid camera," in *2015 IEEE International Conference on RFID (RFID)*, April 2015, pp. 166–173.

[76] A. A. Hussein, "Experimental modeling and analysis of lithium-ion battery temperature dependence," in *2015 IEEE Applied Power Electronics Conference and Exposition (APEC)*, March 2015, pp. 1084–1088.

[77] H. Tsai, J. H. Lee, P. D. Lurgio, J. Anderson, B. Craig, Y. Liu, and J. Shuler, "Comprehensive nuclear material surveillance with a radiation detector-equipped ARG-US RFID system," in *Proc. 54th INMM Annual Meeting, Palm Desert, CA*, 2013.

[78] P. R. Horton and I. G. Waddoups, "Active fiber optic technologies used as tamper-indicating devices," *Sandia National Laboratory, Tech. Rep. SAND95-2279*, Nov 1995.

[79] U. S. D. of Defense, "Interface standard: electromagnetic environmental effects, requirements for systems," in *MIL-STD-464C*, December 2010, pp. 1084–1088.

[80] D. Halperin, T. S. Heydt-Benjamin, B. Ransford, S. S. Clark, B. Defend, W. Morgan, K. Fu, T. Kohno, and W. H. Maisel, "Pacemakers and implantable cardiac defibrillators: Software radio attacks and zero-power defenses," in *2008 IEEE Symposium on Security and Privacy (sp 2008)*, May 2008, pp. 129–142.

[81] I. Vajda and L. Buttyán, "Lightweight authentication protocols for low-cost RFID tags," in *Second Workshop on Security in Ubiquitous Computing, in conjuction with Ubicomp 2003*, Aug 2003.

[82] B. Defend, K. Fu, and A. Juels, "Cryptanalysis of two lightweight rfid authentication schemes," in *Pervasive Computing and Communications Workshops, 2007. PerCom Workshops '07. Fifth Annual IEEE International Conference on*, March 2007, pp. 211–216.

[83] S. N. Daskalakis, S. D. Assimonis, E. Kampianakis, and A. Bletsas, "Soil moisture wireless sensing with analog scatter radio, low power, ultra-low cost and extended communication ranges," in *IEEE SENSORS 2014 Proceedings*, Nov 2014, pp. 122–125.

[84] B. S. and, "Passive 5.8-ghz radio-frequency identification tag for monitoring oil drill pipe," *IEEE Transactions on Microwave Theory and Techniques*, vol. 51, no. 2, pp. 356–363, Feb 2003.

[85] J. D. Griffin and G. D. Durgin, "Multipath fading measurements at 5.8 ghz for backscatter tags with multiple antennas," *IEEE Transactions on Antennas and Propagation*, vol. 58, no. 11, pp. 3693–3700, Nov 2010.

[86] C. R. Valenta, P. A. Graf, M. S. Trotter, G. A. Koo, G. D. Durgin, and B. J. Schafer, "Backscatter channel measurements at 5.8 ghz across high-voltage corona," in *Sensors, 2010 IEEE*. IEEE, 2010, pp. 2400–2404.

[87] A. Aleksieieva and M. Vossiek, "Design and optimization of amplitude-modulated microwave backscatter transponders," in *German Microwave Conference Digest of Papers*, March 2010, pp. 134–137.

[88] Kent electronics. [Online]. Available: http://www.wa5vjb.com/products6.html

[89] S. F. Maharimi, M. F. Jamlos, M. F. A. Malek, and S. C. Neoh, "Impact of number elements on array factor in linear arrays antenna," in *2012 IEEE 8th International Colloquium on Signal Processing and its Applications*, March 2012, pp. 296–299.

[90] J. Yi, W. Ki, and C. Tsui, "Analysis and design strategy of uhf micro-power cmos rectifiers for micro-sensor and rfid applications," *IEEE Transactions on Circuits and Systems I: Regular Papers*, vol. 54, no. 1, pp. 153–166, Jan 2007.

[91] T. Le, K. Mayaram, and T. Fiez, "Efficient far-field radio frequency energy harvesting for passively powered sensor networks," *IEEE Journal of Solid-State Circuits*, vol. 43, no. 5, pp. 1287–1302, May 2008.

[92] B. R. Marshall, M. M. Morys, and G. D. Durgin, "Parametric analysis and design guidelines of rf-to-dc dickson charge pumps for rfid energy harvesting," in *2015 IEEE International Conference on RFID (RFID)*, April 2015, pp. 32–39.

[93] J. Guo, H. Zhang, and X. Zhu, "Theoretical analysis of rf-dc conversion efficiency for class-f rectifiers," *IEEE Transactions on Microwave Theory and Techniques*, vol. 62, no. 4, pp. 977–985, April 2014.

[94] F. R. de Sousa, M. B. Machado, and C. Galup-Montoro, "A 20 mv colpitts oscillator powered by a thermoelectric generator," in *2012 IEEE International Symposium on Circuits and Systems*, May 2012, pp. 2035–2038.

[95] M. M. Islam, K. Rasilainen, and V. Viikari, "Implementation of sensor rfid: Carrying sensor information in the modulation frequency," *IEEE Transactions on Microwave Theory and Techniques*, vol. 63, no. 8, pp. 2672–2681, Aug 2015.

[96] G. M. Maggio, O. D. Feo, and M. P. Kennedy, "Nonlinear analysis of the colpitts oscillator and applications to design," *IEEE Transactions on Circuits and Systems I: Fundamental Theory and Applications*, vol. 46, no. 9, pp. 1118–1130, Sept 1999.

[97] A. L. D. Inc. (2018, February) Ald110902 datasheet.

[98] *Hyperabrupt Junction Tuning Varactors*, Skyworks Inc., 6 2012, rev. 1.

[99] Yoon-Deock Lee, Kwan-Kyu Nae, Eun-Jin Lee, Hyoung-Hwan Roh, Jin-Wook Jung, Young-Kou Han, Jin-Woo Jung, Seok-Cheon Baek, Myeong-Sub Jung, Hong-Goo Cho, Ha-Ryoung Oh, Young-Rak Seong, and Jun-Seok Park, "Ask modulator for rfid system using a novel variable dgs resonator," in *2007 European Radar Conference*, Oct 2007, pp. 381–384.

[100] C. Fager, H. Cao, T. Eriksson, R. Jos, H. Nemati, A. Soltani, and H. Zirath, "High efficiency transmitter using varactor based dynamic load modulation," in *2010 IEEE International Microwave Workshop Series on RF Front-ends for Software Defined and Cognitive Radio Solutions (IMWS)*, Feb 2010, pp. 1–4.

[101] S. Maddio, A. Cidronali, A. Palonghi, and G. Manes, "A reconfigurable leakage canceler at 5.8 ghz for dsrc applications," in *2013 IEEE MTT-S International Microwave Symposium Digest (MTT)*, June 2013, pp. 1–3.

VITA

Alexander T. Hoang was born in Vancouver, Washington USA. He received the Bachelor of Science in Electrical Engineering (BSEE) and Masters of Science (MS) degree at the University of Washington in 2015 and 2016, respectively. Alex then received his Ph.D degree from the University of Washington in 2019, and his dissertation titled *Ultra low-voltage low power backscatter communication and energy harvesting for long-range battery-free sensor tags*, was written under the direction of Dr. Matthew S. Reynolds.

During the course of this Ph.D degree, Alex and his partner Apoorva Sharma won the student award for their rectenna design for wireless brain power at the 2016 IEEE RFID conference. At the time of his dissertation, Alex holds 1 patent and authored in 2 published journals and 6 peer-reviewed conference proceedings articles. Alex has been a student member of the IEEE since 2015.